CROSS-SHORE NUMERICAL MODEL CSHORE 2022

FOR COASTAL SEDIMENTS AND STRUCTURES

BY

NOBUHISA KOBAYASHI AND TINGTING ZHU

RESEARCH REPORT NO. CACR-22-04
AUGUST 2022

CENTER FOR APPLIED COASTAL RESEARCH

University of Delaware
Newark, Delaware 19716

ACKNOWLEDGMENTS

The development of the cross-shore numerical model CSHORE was supported mostly by the U.S. Army Corps of Engineers, Coastal and Hydraulics Laboratory. The graduate students and researchers contributed to the development of CSHORE are acknowledged by quoting their publications in this report.

TABLE OF CONTENTS

CROSS-SHORE NUMERICAL MODEL CSHORE 2022 FOR COASTAL SEDIMENTS AND STRUCTURES

Nobuhisa Kobayashi[1] and Tingting Zhu

Abstract

The majority of the world shoreline is currently suffering from erosion. Beach erosion will become more serious if the mean sea level rise accelerates because of the greenhouse effect. Nourishment and maintenance of wide sand beaches for developed coastal communities will become more expensive unless the present nourishment design method is improved by the development of a reliable morphological model. Concurrently, the recent increase of coastal storm damage demands the development of numerical models for predicting the damage progression and breaching of coastal stone structures and earthen levees during extreme storms. Effort has been made to improve our quantitative understanding of beach morphology and structural damage progression with the goal to develop simple and robust models that are suited for engineering applications. Our effort for the last 20 years has produced the cross-shore numerical model CSHORE which is presently limited to the case of alongshore uniformity. CSHORE consists of the following components: a combined wave and current model based on time-averaged continuity, cross-shore and longshore momentum, wave energy or action, and roller energy equations; a sediment transport model for suspended sand and bedload; a permeable layer model to account for porous flow and energy dissipation; formulas for irregular wave runup; a probabilistic model for an intermittently wet and dry zone on impermeable and permeable bottoms for the purpose of predicting wave overwash of a dune and armor layer damage progression, respectively; a drag force model for piles interacting with waves and sand dunes; and a dike erosion model by irregular wave action; wave overtopping and bay flooding; sand transport on and inside porous structures; and intertidal mudflat profile evolution. The theories and formulas used in CSHORE are explained in order to facilitate the application of CSHORE to various coastal engineering problems that tend to occur in the vicinity of the shoreline.

1. Introduction

A sand beach with a wide berm and a high dune provides storm protection and damage reduction, recreational and economical benefits and biological habitats for plants and animals. Most sandy beaches are eroding partly due to sea level rise. Beach nourishment is widely adopted to maintain a wide beach for a developed coastal community if a suitable beachfill is available in the vicinity of an eroding beach. Empirical methods based on field data have been developed for the design of beach fills (Coastal Engineering Manual 2003). The design of the cross-shore beachfill profile is normally based on the concept of an equilibrium beach profile (Kriebel and Dean 1985). The alongshore spreading of the beachfill is generally predicted using a one-line model coupled with the CERC formula or the formula by Kamphuis (1991) for the longshore sediment transport rate. These simple beachfill design methods have been criticized and a number of more process based models have been proposed. However, the process-based models require much more computation time and may not necessarily be more accurate than the

[1] Center for Applied Coastal Research, University of Delaware, Newark, DE 19716, USA. nk@udel.edu

empirical methods calibrated for each project site in which the capability of field measurements has improved significantly for the last 30 years.

Sediment transport is caused by the combined action of waves and currents. Our capabilities of predicting wave and current fields have improved steadily for the last 30 years. However, the predictive capability of sediment transport on beaches has not improved much. The major reason for this discrepancy is that no dynamic equation is available to describe the motion of a large number of sediment particles. Consequently, sediment transport models are essentially empirical and dependent on reliable sediment transport data. Unfortunately, sediment dynamics on beaches are highly complex and involve wide ranges of morphological scales in time and space. Correspondingly, available sediment transport models have become more complex and less transparent. We have tried to synthesize available data and formulas in order to develop simple and transparent formulas for the cross-shore and longshore transport rates of suspended sand and bedload on beaches. The simple formulas need to include basic sediment dynamics sufficiently so that the formulas will be applicable to small-scale and large-scale laboratory beaches as well as natural beaches. Furthermore, the morphological model should be very efficient computationally because the model will need to be calibrated and verified using extensive data sets. The hydrodynamic input required for the morphological model should be limited to the quantities that can be predicted routinely and reliably. These considerations have guided our development of the cross-shore model CSHORE which is presently limited to the conditions of alongshore uniformity and uniform sediment.

Coastal storm damage has been increasing mostly due to the recent growth of coastal population and assets and possibly due to the intensification of hurricanes caused by global warming. Coastal structures including earthen levees (dikes) and rubble mound structures have been designed conventionally for no storm surge overflow and minor wave overtopping during a design storm. Empirical formulas for wave overtopping rates are used for a preliminary design (EurOtop Manual 2007). Physical model testing is normally conducted in a wave flume or basin for a detailed design. Various numerical models have also been developed to predict detailed hydrodynamics that are difficult to measure even in a laboratory (Kobayashi and Otta 1987; Kobayashi 1999; van Gent 2001). Advanced numerical models for hydrodynamics are reviewed by Losada et al. (2008) and Neves et al. (2008). However, our improved predictive capabilities for the hydrodynamics have not really improved our predictive capability for damage progression partly because damage to a coastal structure is cumulative (Melby and Kobayashi 1998). As a result, a performance or risk-based design of a coastal structure relies on empirical formulas for damage (e.g., Kobayashi et al. 2003; Melby and Kobayashi 2011). This practical difficulty is similar to that for sediment transport on beaches. Alternatively, the computationally-efficient CSHORE calibrated with extensive data sets has been developed for the design of inclined structures with relatively small wave reflection. Damage progression on the stone armor layer is predicted by modifying the sediment transport model (Kobayashi et al. 2010a). Cohesionless sediment transport formulas should be applicable to sand, gravel, and stone.

The models for the impermeable and permeable swash (wet and dry) zones are presented and connected

with the corresponding wet zone models. The connected model for the impermeable bottom is expanded to include the drag force acting on a cluster of piles on a sand beach and is also applied to predict dike erosion by wave action. Additional extensions include wave overtopping and bay flooding, sand transport inside porous structures, and intertidal mudflat profile evolution. The extended version of CSHORE up to 2022 is explained sufficiently so that other researchers may be able to improve the approximate models with the aid of future experiments and advanced numerical modeling.

2. History of CSHORE Development during 1998 – 2013

The history of the cross-shore model CSHORE is summarized to provide an overview of CSHORE and acknowledge a number of graduate students and visiting researchers who contributed to the development of CSHORE. The version of CSHORE 2013 included the various capabilities added to the initial CSHORE developed in 1998. The different stages of the CSHORE development are summarized in the following where the detail of each stage can be found in the listed publications.

The cross-shore model CSHORE was initially developed to predict the cross-shore transformation of irregular nonlinear waves using the time-averaged continuity, momentum, and wave energy equations together with a non-Gaussian probability distribution of the free surface elevation. However, empirical formulas of limited generality were required to parameterize the wave nonlinearity. The present version of CSHORE is based on linear wave theory and the Gaussian probability distribution to reduce the degree of empiricism.

- Kobayashi, N., Herrman, M.N., Johnson, B.D., and Orzech, M.D. (1998). "Probability distribution of surface elevation in surf and swash zones." J. Waterway, Port, Coastal and Ocean Eng., 124(3), 99-107.
- Kobayashi, N., and Johnson, B.D. (1998). "Computer program CSHORE for predicting cross-shore transformation of irregular breaking waves." Res. Rep. No. CACR-98-04, Center for Applied Coastal Research, Univ. of Delaware, Newark, Del.
- Johnson, B.D., and Kobayashi, N. (1998). "Nonlinear time-averaged model in surf and swash zones." Proc. 26th Coastal Eng. Conf., ASCE, 2785-2798.
- Kearney, P.G., and Kobayashi, N. (2000). "Time-averaged probabilistic model for irregular wave runup on coastal structures." Proc. 27th Coastal Eng. Conf., ASCE, 2004-2017.
- Johnson, B.D., and Kobayashi, N. (2000). "Free surface statistics and probabilities in surf zones on beaches." Proc. 27th Coastal Eng. Conf., ASCE, 1022-1035.

The next stage of the CSHORE development was motivated by the need of a computationally-efficient time-averaged model that can be used for the design of porous coastal structures. The linear-wave version of the initial CSHORE was modified to account for the effects of a permeable layer for the case of normally incident waves. The impermeable and permeable versions of CSHORE have been merged in the present CSHORE in order to expand the range of practical applications.

- Meigs, L.E., and Kobayashi, N. (2004). "Time-averaged model for irregular breaking waves on porous structures and beaches." Res. Rep. No. CACR-04-02, Center for Applied Coastal Res., Univ. of Delaware, Newark, Del.
- Meigs, L.E., Kobayashi, N., and Melby, J.A. (2004). "Cobble beaches and revetments." Proc. 29th Coastal Eng. Conf., World Scientific, 3865-3877.
- de los Santos, F.J., and Kobayashi, N. (2005). "Irregular wave setup and runup on cobble beaches and revetments." Res. Rep. No. CACR-05-06. Center for Applied Coastal Res., Univ. of Delaware, Newark, Del.
- Ota, T., Kobayashi, N., and Kimura, A. (2006). "Irregular wave transformation over deforming submerged structures." Proc. 30th Coastal Eng. Conf., World Scientific, 4945-4956.
- de los Santos, F.J., Kobayashi, N., and Losada, M. (2006). "Irregular wave runup and overtopping on revetments and cobble beaches." Proc. 30th Coastal Eng. Conf., World Scientific, 4667-4679.
- de los Santos, F.J., and Kobayashi, N. (2006). "Irregular wave seepage and overtopping of cobble beaches and revetments." Res. Rep. No. CACR-06-01, Center for Applied Coastal Res., Univ. of Delaware, Newark, Del.
- Kobayashi, N., Meigs, L.E., Ota, T., and Melby, J.A. (2007). "Irregular breaking wave transmission over submerged porous breakwaters." J. Waterway, Port, Coastal, Ocean Eng., 133(2), 104-116.
- Kobayashi, N., and de los Santos, F.J. (2007). "Irregular wave seepage and overtopping of permeable slopes." J. Waterway, Port, Coastal, Ocean Eng., 133(4), 245-254.
- Ota, T., Matsumi, Y., Kobayashi, N., and Kimura, A. (2007). "Influence of damage progression on performance of rubble mound breakwaters." Proc. Coastal Structures'2007, Venice, Italy, 1806-1817.
- Kobayashi, N., de los Santos, F.J., and Kearney, P.G. (2008). "Time-averaged probabilistic model for irregular wave runup on permeable slopes." J. Waterway, Port, Coastal, Ocean Eng., 134(2), 88-96.

Concurrently, the impermeable version of CSHORE was extended to predict the cross-shore and longshore transport rates of suspended sand and bedload on beaches as a part of the MORPHOS project of the U.S. Army Engineer Research and Development Center. MORPHOS is the world's first attempt at developing an open-source, physics-based computer model of coastal storms and their impact that can be used by the broad coastal community. A series of extensions were made in the following publications to make CSHORE more versatile and better verified.

- Zhao, H., and Kobayashi, N. (2005). "Suspended sand transport in surf zones on equilibrium beaches." Res. Rep. No. CACR-05-01, Center for Applied Coastal Res., Univ. of Delaware, Newark, Del.
- Kobayashi, N., Zhao, H., and Tega, Y. (2005). "Suspended sand transport in surf zone." J. Geophys. Res., 110, C12009, doi:10.1029/2004JC002853.
- Agarwal, A., and Kobayashi, N. (2005). "Time-averaged model for longshore current and sediment transport in surf and swash zones." Res. Rep. No. CACR-05-07, Center for Applied Coastal Res., Univ. of Delaware, Newark, Del.
- Schmied, L., Kobayashi, N., Payo, A., and Puleo, J.A. (2006). "Cross-shore sediment transport and beach profile change." Res. Rep. No. CACR-06-03, Center for Applied Coastal Res., Univ. of

Delaware, Newark, Del.
- Schmied, L.D., Kobayashi, N., Puleo, J.A., and Payo, A. (2006). "Cross-shore suspended sand transport on beaches." Proc. 30th Coastal Eng. Conf., World Scientific, 2511-2523.
- Agarwal, A., Kobayashi, N., and Johnson, B.D. (2006). "Longshore suspended sediment transport in surf and swash zones." Proc. 30th Coastal Eng. Conf., World Scientific, 2498-2510.
- Payo, A., Kobayashi, N., and Kim, K.H. (2006). "Beach nourishment strategies." Proc. 30th Coastal Eng. Conf., World Scientific, 4129-4140.
- Kobayashi, N., Agarwal, A., and Johnson, B.D. (2007). "Longshore current and sediment transport on beaches." J. Waterway, Port, Coastal, Ocean Eng., 133(4), 296-304.
- Buck, M., Kobayashi, N., Payo, A., and Johnson, B.D. (2007). "Experiments and numerical model for berm and dune erosion." Res. Rep. No. CACR-07-03, Center for Applied Coastal Res., Univ. of Delaware, Newark, Del.
- Gencarelli, R., Johnson, B.D., Kobayashi, N. and Tomasicchio, G.R. (2007). "Dune erosion and breaching." Proc. Coastal Structures'2007, Venice, Italy, 502-513.
- Kobayashi, N., Payo, A., and Schmied, L. (2008). "Cross-shore suspended sand and bedload transport on beaches." J. Geophys. Res., 113, C07001, doi:10.1029/2007JC004203.
- Kobayashi, N., Buck, M., Payo, A., and Johnson, B.D. (2009). "Berm and dune erosion during a storm." J. Waterway, Port, Coastal, Ocean Eng., 135(1), 1-10.
- Kobayashi, N., Payo, A., and Johnson, B.D. (2009). "Suspended sand and bedload transport on beaches." Handbook of Coastal and Ocean Engineering, World Scientific, Singapore, Chapter 28, 807-823.
- Payo, A., Kobayashi, N., and Yamada, F. (2009). "Suspended sand transport along pier depression." J. Waterway, Port, Coastal, Ocean Eng., 135(5), 245-249.
- Buck, M., Kobayashi, N., Payo, A., and Johnson, B.D. (2008). "Berm and dune erosion." Proc. 31th Coastal Eng. Conf., World Scientific, 1749-1761.
- Gencarelli, R., Tomasicchio, G.R., Kobayashi, N., and Johnson, B.D. (2008). "Beach profile evolution and dune erosion due to the impact of Hurricane Isabel." Proc. 31th Coastal Eng. Conf., World Scientific, 1697-1709.
- Gencarelli, R., Tomasicchio, G.R., Kobayashi, N., and Johnson, B.D. (2008). "Effects of Hurricane Isabel along the North Carolina coastline: Beach profile evolution and dune erosion." Proc. 3rd International Short Conf. on Applied Coastal Res., Lecce, Italy, 200-210.

The following papers summarized the progress of the CSHORE development up to 2009.

- Kobayashi, N. (2006). "Time-averaged wave models for coastal structures and sediments." Proc. 2nd International Short Course and Workshop on Coastal Processes and Port Eng., Cosenza, Italy, 61-75.
- Kobayashi, N. (2009). "Efficient wave and current models for coastal structures and sediments." Nonlinear Wave Dynamics. World Scientific, Singapore, 67-87.
- Kobayashi, N., Figlus, J., and Buck, M. (2009). "Beach nourishment and dune erosion." Proc. 3rd Internal Short Conf. on Applied Coastal Res., Lecce, Italy, 71-98.
- Kobayashi, N. (2009). "Documentation of cross-shore numerical model CSHORE2009." Res. Rep.

No. CACR-09-06, Center for Applied Coastal Res., Univ. of Delaware, Newark, Del.

The publications above were based on the earlier version of CSHORE limited to the wet zone below the mean water level. In order to extend CSHORE to the zone which is intermittently wet and dry, laboratory experiments were conducted for wave overtopping and overflow on fixed levees. The laboratory data was used for the development of a probabilistic model for the wet and dry zone on an impermeable bottom. This hydrodynamic model coupled with the sediment transport model in CSHORE has been used to predict wave overwash of dunes. Johnson et al. (2012) calibrated and verified the public domain CSHORE using extensive field data of storm-induced foreshore and dune erosion. The hydrodynamic model has also been extended to the wet and dry zone on a permeable bottom for the prediction of wave overtopping of rubble mound structures. This model coupled with the CSHORE bedload formula modified for stone and gravel has been shown to be capable of predicting the evolution of damaged stone armor layers and gravel beaches.

- Farhadzadeh, A., Kobayashi, N., Melby, J.A., and Ricottilli, C. (2007). "Experiments and numerical modeling of wave overtopping and overflow on dikes." Res. Rep. No. CACR-07-02, Center for Applied Coastal Res., Univ. of Delaware, Newark, Del.
- Kobayashi, N., Farhadzadeh, A., and Melby, J.A. (2007). "Structures of storm surge disaster prevention." Proc. 4th International Workshop on Coastal Disaster Prevention, Yokohama, Japan, 41-49.
- Farhadzadeh, A., Kobayashi, N., and Melby, J.A. (2008). "Wave overtopping and overflow on inclined structures." Proc. 31st Coastal Eng. Conf., World Scientific, 2996-3008.
- Kobayashi, N., Farhadzadeh, A., Melby, J.A., Johnson, B., and Gravens, M. (2010). "Wave overtopping of levees and overwash of dunes." J. Coastal Research, 26(5), 888-900.
- Kobayashi, N., and Farhadzadeh, A. (2009). "Dune erosion and overwash." Proc. Coastal Dynamics 2009, Tokyo, Japan, Paper No. 81.
- Johnson, B., Gravens, M., Wamsley, T., and Kobayashi, N. (2009). "A predictive model for beach profile evolution." Proc. Coastal Dynamics 2009, Tokyo, Japan, Paper No. 64.
- Figlus, J., Kobayashi, N., Gralher, C., and Iranzo, V. (2009). "Experimental and numerical study on transition from minor to major wave overwash of dunes." Res. Rep. No. CACR-09-04, Center for Applied Coastal Res., Univ. of Delaware, Newark, Del.
- Figlus, J., Kobayashi, N., Gralher, C., and Iranzo, V. (2011). "Wave-induced overwash and destruction of sand dunes." 32nd Coastal Eng. Conf., World Scientific, Sediment 34, 1-13.
- Figlus, J., Kobayashi, N., Gralher, C., and Iranzo, V. (2011). "Wave overtopping and overwash of dunes." J. Waterway, Port, Coastal, Ocean Eng., 137(1), 26-33.
- Johnson, B. D., Kobayashi, N., and Gravens, M. B. (2012). "Cross-shore numerical model CSHORE for waves, currents, sediment transport and beach profile evolution." Final Rep. No. ERDC/CHL TR-12-22, U.S. Army Corps of Engineers, Coastal and Hydraulics Laboratory, Vicksburg, MS.
- Farhadzadeh, A., Kobayashi, N., and Melby, J.A. (2009). "Wave overtopping and damage progression on rubble mound structures." Res. Rep. No. CACR-09-05, Center for Applied Coastal Res., Univ. of Delaware, Newark, Del.

- Farhadzadeh, A., Kobayashi, N., and Melby, J.A. (2010). "Evolution of damaged armor layer profile." 32nd Coastal Eng. Conf., World Scientific, Structures 40, 1-13.
- Hicks, B., Kobayashi, N., Puleo, J., and Farhadzadeh, A. (2010). "Cross-shore gravel transport on beaches." 32nd Coastal Eng. Conf., World Scientific, Sediments 43, 1-9.
- Hicks, B.S., Kobayashi, N., Figlus, J., Puleo, J.A., and Farhadzadeh, A. (2010). "Cross-shore transport of coarse grained sediment." Res. Rep. No. CACR-10-01, Center for Applied Coastal Research, Univ. of Delaware, Newark, Del.
- Kobayashi, N., Farhadzadeh, A., and Melby, J.A. (2010). "Wave overtopping and damage progression of stone armor layer." J. Waterway, Port, Coastal, Ocean Eng., 136(5), 257-265.
- Kobayashi, N., Hicks, B.S., and Figlus, J. (2011). "Evolution of gravel beach profile." J. Waterway, Port, Coastal, Ocean Eng., 137(5), 258-262.

In addition, CSHORE is being extended to predict the long-term (seasonal and yearly) cross-shore and longshore sediment transport rates on natural and nourished beaches. The field data required for the calibration and verification for the long-term morphological model CSHORE has been obtained and analyzed in the following publications:

- Figlus, J., and Kobayashi, N. (2007). "Seasonal and yearly profile changes of Delaware beaches." Res. Rep. No. CACR-07-01, Center for Applied Coastal Res., Univ. of Delaware, Newark, Del.
- Figlus, J., and Kobayashi, N. (2008). "Inverse estimation of sand transport rates on nourished Delaware beaches." J. Waterway, Port, Coastal, Ocean Eng., 134(4), 218-225.
- Figlus, J., and Kobayashi, N. (2008). "Two-line model for inverse estimation of cross-shore and longshore transport rates on nourished beaches." 31st Coastal Eng. Conf., World Scientific, 2545-2556.

The cross-shore model CSHORE has been expanded to simulate the onshore migration of an emerged ridge and a ponded runnel where the ponded water has been found to act as a settling basin for sediment contained in the overtopping flow over the ridge.

- Figlus, J., Kobayashi, N., and Gralher, C. (2010). "Ridge and runnel migration – Experimental and numerical investigation." Res. Rep. No. CACR-10-02, Center for Applied Coastal Res., Univ. of Delaware, Newark, Del.
- Figlus, J., Kobayashi, N., and Gralher, C. (2012). "Ridge-runnel migration." Proc. 32nd Coastal Eng. Conf., Sediment 46, 1-15.
- Figlus, J., Kobayashi, N., and Gralher, C. (2012). "Onshore migration of emerged ridge and ponded runnel." J. Waterway, Port, Coastal, Ocean Eng., 138(5), 331-338.

To include the longshore and cross-shore tidal currents in CSHORE, an alongshore pressure gradient term has been added to the longshore momentum equation and the cross-shore water flux associated with the temporal variation of the still water level in the computation domain has been included in the continuity equation. Furthermore, CSHORE has been extended to multiple cross-shore lines in order to include the alongshore gradient of the longshore sediment transport rate in the beach profile computation.

- Farhadzadeh, H., Kobayashi, N., and Gravens, M.B. (2010). "Longshore current and sediment transport due to breaking waves and alongshore pressure gradient." Res. Rep. No. CACR-10-04, Center for Applied Coastal Res., Univ. of Delaware, Newark, Del.
- Farhadzadeh, A., Kobayashi, N., and Gravens, M.B. (2012). "Effect of breaking waves and external current on longshore sediment transport." J. Waterway, Port, Coastal, Ocean Eng., 138(3), 256-260.
- Do, K., Kobayashi, N., and Suh, K.-D. (2012). "Erosion and accretion on curved beach." Proc. 32nd Coastal Eng. Conf., Sediment 11, 1-12.
- Jung, H., and Kobayashi, N. (2011). "Numerical modeling of erosion and recovery of Rehoboth and Dewey Beaches in Delaware." Res. Rep. No. CACR-11-01, Center for Applied Coastal Res., Univ. of Delaware, Newark, Del.
- Kobayashi, N., and Jung, H. (2012). "Beach erosion and recovery." J. Waterway, Port, Coastal, Ocean Eng., 138(6), 473-483.

Coastal flood-risk mapping requires the prediction of wave runup and overtopping of dikes and beaches. CSHORE has been calibrated to predict irregular wave runup and overtopping of impermeable dikes using 137 wave runup tests and 97 wave overtopping tests. CSHORE has also been compared with 120 tests for wave runup on gentle uniform slopes as well as extensive wave runup data on natural beaches. Furthermore, CSHORE has been extended to the landward zone of a low-crested stone structure for the prediction of the temporal variations of the damage and wave transmission during a severe storm.

- Pietropaolo, J., Kobayashi, N., and Melby, J.A. (2011). "Numerical modeling of wave transformation, breaking and runup on dikes and gentle slopes." Res. Rep. No. CACR-11-05, Center for Applied Coastal Res., Univ. of Delaware, Newark, Del.
- Pietropaolo, J., Kobayashi, N., and Melby, J.A. (2012). "Wave runup on dikes and beaches." Proc. 32nd Coastal Eng. Conf., Current 19, 1-13.
- Melby, J.A., Nadal, N., and Kobayashi, N. (2012). "Wave runup prediction for flood mapping." Proc. 32nd Coastal Eng. Conf., Management 79, 1-15.
- Kobayashi, N., Pietropaolo, J.A., and Melby, J.A. (2013). "Wave transformation and runup on dikes and gentle slopes." J. Coastal Research, 29(3), 615-623.
- Kobayashi, N., Pietropaolo, J., and Melby, J.A. (2013). "Deformation of reef breakwaters and wave transmission." J. Waterway, Port, Coastal, Ocean Eng., 139(4), 336-340.

The publications above were based on the documented CSHORE 2013 (Kobayashi 2013) limited to cohesionless sediment (sand, gravel, and stone). The CSHORE 2013 manual may be sufficient for standard coastal engineering problems associated with sand beaches, gravel beaches, and rubble mound structures. Kobayashi (2016) reviewed the extended version of CSHORE up to 2015, which included a drag force model for piles (idealized tree stems) interacting with waves and sand dunes as well as an erosion model for grassed earthen dikes (levees) by wave action.

This manual of CSHORE 2022 includes additional capabilities (options) developed after the CSHORE 2013 manual, as explained concisely in Section 10. Necessary publications are provided to understand

and utilize each of the following options:

- Effect of woody plants and piles on dune erosion and overwash
- Effect of grassed dike and consolidated cohesive sediment
- Wave overtopping of barrier beach and bay flooding
- Sand transport on and inside porous stone structures
- Intertidal mudflat profile evolution under waves and currents

3. Two-Dimensional Wave and Current Models

Cross-shore sediment transport on beaches has been investigated extensively (e.g., Kriebel and Dean 1985; van Rijn et al. 2003) but we still cannot predict beach profile evolution accurately. In order to improve our predictive capabilities, sediment transport models have become more sophisticated but less transparent. For example, Thornton et al. (1996) and Gallagher et al. (1998) used the energetics-based total load model of Bailard (1981) to explain the offshore movement of a bar at Duck, North Carolina, during storms. The onshore bar migration on the same beach was predicted by both Hoefel and Elgar (2003), using the skewed acceleration effect on bedload, and Henderson et al. (2004), using a suspended sediment model. The roles of bedload and suspended load are not clear at present. Kobayashi et al. (2008b) made an attempt to synthesize and simplify existing cross-shore sediment transport models with the aim of developing a simple and robust model that is suited for engineering applications including the berm and dune erosion. This model has been extended to predict the cross-shore and longshore transport rates of bedload and suspended load under the combined wave and current action (Kobayashi et al. 2007a; 2009a). Recent two-dimensional morphological models were discussed in the review paper by Kobayashi (2016). Each model has its capabilities and shortcomings.

Sediment transport on beaches is caused by the combined action of waves and currents. The hydrodynamic input required for a sediment transport model depends on whether the sediment transport model is time-dependent (phase-resolving) or time-averaged over a number of waves. A time-dependent sediment transport model such as that by Kobayashi and Johnson (2001) is physically appealing because it predicts intense but intermittent sand suspension under irregular breaking waves (Kobayashi and Tega 2002) in which Cox and Kobayashi (2000) measured intense, intermittent coherent motions under regular waves shoaling and spilling on a rough impermeable slope. However, the time-dependent model requires considerable computation time and is not necessarily more accurate in predicting slow morphological changes than the corresponding time-averaged model presented in the following. Horizontally two-dimensional wave and current models are presented first before the cross-shore model CSHORE based on the assumption of alongshore uniformity.

Fig. 1 shows obliquely incident irregular waves on an essentially straight shoreline where the cross-shore coordinate x is positive onshore and the longshore coordinate y is positive in the downwave direction. The beach is assumed to be impermeable, and the bottom elevation z_b is positive upward with $z = 0$ at the

datum. The depth-averaged cross-shore and longshore velocities are denoted by U and V, respectively. Incident waves are assumed to be unidirectional with θ = incident angle relative to the shore normal. The height and period of the irregular waves are represented by the root-mean-square wave height H_{rms} and the representative wave period, which may be taken as the spectral peak period T_p or the spectral wave period (van Gent 2001) specified at the seaward boundary located at $x = 0$. In the following, use is made of T_p for the simplicity of its notation. The location of the seaward boundary is normally taken to be outside the surf zone so that wave set-down or setup is very small at $x=0$. The incident wave angle θ at x=0 is assumed to be in the range of $|\theta| < 80°$ to ensure that the incident waves propagate landward and $(\cos\theta) > 0$. The wind speed and direction at the elevation of 10 m above the sea surface are denoted by W_{10} and θ_w, respectively.

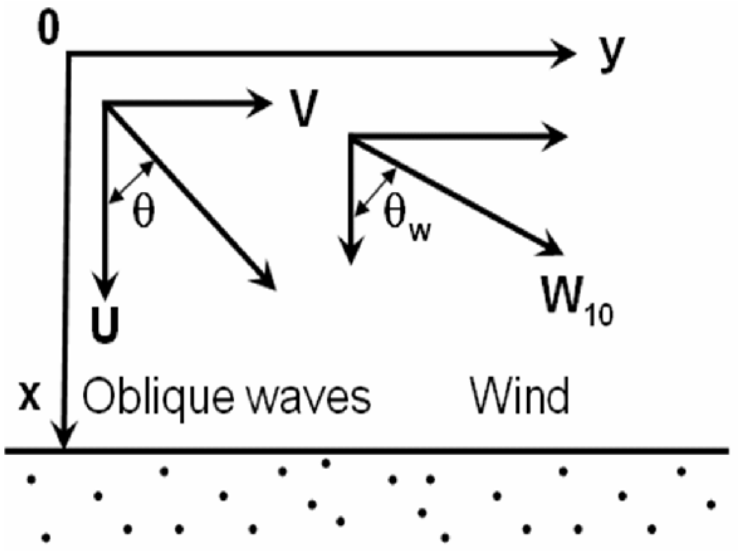

Fig. 1. Definition sketch for incident irregular waves and wind on beach.

The mean water depth $\overline{h}$ is given by

$$\overline{h} = \left(\overline{\eta} + S - z_b\right) \tag{1}$$

where $\overline{\eta}$ = wave setup above the still water level (SWL); and S = storm tide above the datum $z = 0$ which is assumed to be uniform in the computation domain with a cross-shore distance of the order of 1 km and is specified as input at $x=0$. Linear wave and current theory for wave refraction (e.g., Phillips 1977; Mei 1989; Dalrymple 1988) is used to predict the spatial variations of H_{rms} and θ. The dispersion relation for linear waves is expressed as

$$\omega^2 = kg\tanh\left(k\overline{h}\right) \quad ; \quad \omega_p = \omega + k\left(Q_x\cos\theta + Q_y\sin\theta\right)/\overline{h} \tag{2}$$

where ω = intrinsic angular frequency; k = wave number; g = gravitational acceleration; $\overline{h}$ = mean water depth with the overbar indicating time-averaging; ω_p = absolute angular frequency given by $\omega_p = 2\pi/T_p$; Q_x and Q_y = time-averaged volume flux per unit width in the x and y directions, respectively, and θ =

incident wave angle. Eq. (2) can be solved iteratively to obtain *k and* ω for known ω_p, $\bar{h}$, θ, Q_x and Q_y. The phase velocity *C* and the group velocity C_g are given by

$$C = \omega / k \quad ; \quad C_g = nC \quad ; \quad n = \frac{1}{2}\left[1 + \frac{2k\bar{h}}{\sinh\left(2k\bar{h}\right)}\right] \tag{3}$$

The wave angle θ is computed using the irrotationality of the wave number

$$\frac{\partial}{\partial x}\left(k\sin\theta\right) - \frac{\partial}{\partial y}\left(k\cos\theta\right) = 0 \tag{4}$$

The root-mean-square wave height H_{rms} defined as $H_{rms} = \sqrt{8}\,\sigma_\eta$ with σ_η = standard deviation of the free surface elevation η which is computed using the wave action equation

$$\frac{\partial}{\partial x}\left[\frac{E}{\omega}\left(C_g\cos\theta + \frac{Q_x}{\bar{h}}\right)\right] + \frac{\partial}{\partial y}\left[\frac{E}{\omega}\left(C_g\sin\theta + \frac{Q_y}{\bar{h}}\right)\right] = -\frac{D_B + D_f}{\omega} \tag{5}$$

with

$$E = \rho g \sigma_\eta^2 = \frac{1}{8}\rho g H_{rms}^2 \tag{6}$$

where *E* = specific wave energy; ρ = fluid density; and D_B and D_f = wave energy dissipation rate per unit horizontal area due to wave breaking and bottom friction, respectively. The formulas for D_B and D_f are presented later in relation to the cross-shore model CSHORE.

The time-averaged volume fluxes Q_x and Q_y in Eq. (2) are expressed as

$$Q_x = \bar{h}\overline{U} + Q_{wx} \quad ; \quad Q_y = \bar{h}\overline{V} + Q_{wy} \tag{7}$$

with

$$Q_{wx} = \frac{g\sigma_\eta^2\cos\theta}{C} + q_r\cos\theta \quad ; \quad Q_{wy} = \frac{g\sigma_\eta^2\sin\theta}{C} + q_r\sin\theta \tag{8}$$

where $\overline{U}$ and $\overline{V}$ = time-averaged, depth-averaged velocities in the *x* and *y* directions; Q_{wx} and Q_{wy} = wave-induced volume fluxes in the *x* and *y* directions; $\left(g\sigma_\eta^2 / C\right)$ = volume flux due to linear waves propagating in the direction of θ; and q_r = volume flux of a roller on the front of a breaking wave. The roller volume flux q_r is estimated using the roller energy equation as explained by Kobayashi et al. (2005, 2007a)

$$\frac{\partial}{\partial x}\left(\rho C^2 q_r \cos\theta\right)+\frac{\partial}{\partial y}\left(\rho C^2 q_r \sin\theta\right)=D_B-D_r \tag{9}$$

with

$$D_r=\rho g\beta_r q_r \quad ; \quad \beta_r=\left(0.1+S_b\right)\geq 0.1 \tag{10}$$

$$S_b=\frac{\partial z_b}{\partial x}\cos\theta+\frac{\partial z_b}{\partial y}\sin\theta \tag{11}$$

where D_r = roller dissipation rate; β_r = wave-front slope; S_b = bottom slope in the direction of wave propagation; and z_b = bottom elevation relative to the datum $z = 0$ with z = vertical coordinate taken to be positive upward. The wave front slope β_r is assumed to be 0.1 unless it is increased by the positive bottom slope S_b.

The mean water depth $\overline{h}$ and the current velocities $\overline{U}$ and $\overline{V}$ are computed using the time-averaged continuity and momentum equations (Phillips 1977; Svendsen et al. 2002).

$$\frac{\partial}{\partial x}\left(Q_x\right)+\frac{\partial}{\partial y}\left(Q_y\right)=0 \tag{12}$$

$$\frac{\partial}{\partial x}\left(\frac{Q_x^2}{\overline{h}}\right)+\frac{\partial}{\partial y}\left(\frac{Q_x Q_y}{\overline{h}}\right)+g\overline{h}\frac{\partial\overline{\eta}}{\partial x}+\frac{\tau_{bx}}{\rho}=\tau_{wx}+\frac{\tau_{sx}}{\rho} \tag{13}$$

$$\frac{\partial}{\partial x}\left(\frac{Q_x Q_y}{\overline{h}}\right)+\frac{\partial}{\partial y}\left(\frac{Q_y^2}{\overline{h}}\right)+g\overline{h}\frac{\partial\overline{\eta}}{\partial y}+\frac{\tau_{by}}{\rho}=\tau_{wy}+\frac{\tau_{sy}}{\rho} \tag{14}$$

with

$$\tau_{wx}=-\frac{\partial}{\partial x}\left(\frac{S_{xx}}{\rho}-\frac{Q_{wx}^2}{\overline{h}}\right)-\frac{\partial}{\partial y}\left(\frac{S_{xy}}{\rho}-\frac{Q_{wx}Q_{wy}}{\overline{h}}\right) \tag{15}$$

$$\tau_{wy}=-\frac{\partial}{\partial x}\left(\frac{S_{xy}}{\rho}-\frac{Q_{wx}Q_{wy}}{\overline{h}}\right)-\frac{\partial}{\partial y}\left(\frac{S_{yy}}{\rho}-\frac{Q_{wy}^2}{\overline{h}}\right) \tag{16}$$

$$S_{xx}=\left(nE+M_r\right)\cos^2\theta+E\left(n-\frac{1}{2}\right) \quad ; \quad M_r=\rho C q_r \tag{17}$$

$$S_{xy}=\left(nE+M_r\right)\cos\theta\sin\theta \quad ; \quad S_{yy}=\left(nE+M_r\right)\sin^2\theta+E\left(n-\frac{1}{2}\right) \tag{18}$$

where τ_{bx} and τ_{by} = bottom shear stresses in the x and y directions; τ_{sx} and τ_{sy} = wind stresses on the sea surface in the x and y directions; and S_{xx}, S_{xy}, and S_{yy} = radiation stresses including the momentum flux M_r of a roller propagating with the phase speed C. It is noted that the terms Q_{wx}^2, $Q_{wx}Q_{wy}$, and Q_{wy}^2 in Eqs.

(15) and (16) included by Phillips (1977) are of 4-th order in terms of the wave height and normally neglected. The present circulation model based on Eqs. (12) – (18) is a simplified version of SHORECIRC (Svendsen et al. 2002) for irregular waves where SHORECIRC assumes monochromatic waves. The formulas for τ_{bx}, τ_{by}, τ_{sx}, and τ_{sy} are presented later in relation to the cross-shore model CSHORE.

A horizontally two-dimensional model C2SHORE has been developed in the MORPHOS project (Shi et al. 2008). The directional spectral wave model STWAVE (Smith et al. 2001) or SWAN (Booij et al. 1999) is used to predict the wave transformation. The wave-induced fluxes Q_{wx} and Q_{wy} and the radiation stresses S_{xx}, S_{xy} and S_{yy} are computed from the predicted directional wave spectra. The roller effects included in Eqs. (8), (17), and (18) are neglected. The circulation model is based on Eqs. (12) – (16) with the formulas for τ_{bx}, τ_{by}, τ_{sx}, and τ_{sy} used in CSHORE. The wave and circulation models are coupled and run iteratively for several times. The wave field is computed to estimate τ_{wx} and τ_{wy} given by Eqs. (15) and (16) for the circulation model which computes the wave setup and wave-induced currents. An efficient finite difference method is used to solve Eqs. (12) – (14) and reduce the computation time considerably (Shi et al. 2007). The iteration between the wave and circulation models is necessary in the region near and landward of the still water shoreline where wave setup determines the mean water depth $\overline{h}$ for the wave model. The wave and current models in this section are limited to the wet zone below the mean water level. Shi et al. (2008) compared C2SHORE with the morphological change data at the U.S. Army Corps of Engineers Field Research Facility (FRF) during Hurricane Isabel and found the need to include the effects of the FRF piling.

4. Combined Wave and Current Model in Wet Zone of CSHORE

The cross-shore model CSHORE assumes alongshore uniformity but computes the wave and current fields simultaneously in the wet zone where water is present always. The depth-integrated continuity equation of water given by Eq. (12) requires that the cross-shore volume flux Q_x is constant and equal to the wave overtopping rate q_o at the landward end of the computation domain. Eqs. (7) and (8) yield

$$Q_x = \overline{h}\,\overline{U} + \frac{g\sigma_\eta^2}{C}\cos\theta + q_r\cos\theta = q_o \tag{19}$$

$$Q_y = \overline{h}\,\overline{V} + \frac{g\sigma_\eta^2}{C}\sin\theta + q_r\sin\theta \tag{20}$$

where $\overline{h}$ = mean water depth; $\overline{U}$ = mean cross-shore velocity; which is negative and offshore because $\cos\theta > 0$ if $q_o = 0$ (no wave overtopping); g = gravitational acceleration; σ_η = standard deviation of the free surface elevation η; C = linear wave phase velocity in the mean water depth $\overline{h}$ corresponding to the spectral peak period T_p; and q_r = volume flux of a roller on the front of a breaking wave. The longshore volume flux Q_y is independent of y. The cross-shore volume flux associated with the temporal

variation of the still water level S may be added on the right hand side of Eq. (19) to include the cross-shore tidal current if the tidal range is very large and the bottom slope is very gentle (Do et al. 2012, 2014). If the incident wave angle θ is small, Eq. (20) can be approximated by $Q_y \simeq \overline{h}\overline{V}$ for most applications.

For the case of alongshore uniformity, Eq. (4) reduces to Snell's law which is used to obtain the wave direction θ

$$k \sin\theta = \text{constant} \tag{21}$$

The constant value is obtained from the values of θ, $\overline{h}$, and T_p specified at the seaward boundary $x = 0$ located outside the surf zone where ω can be approximated by ω_p in Eq. (2). Reflected waves are neglected in this model partly because it is difficult to estimate the correlation between the incident and reflected waves (Baquerizo et al. 1997).

The cross-shore and longshore momentum equations (13) and (14) are simplified as

$$\frac{d}{dx}\left(S_{xx} + \rho \frac{Q_x^2}{\overline{h}} \right) = -\rho g \overline{h} \frac{d\overline{\eta}}{dx} - \tau_{bx} + \tau_{sx} \tag{22}$$

$$\frac{d}{dx}\left(S_{xy} + \rho \frac{Q_x Q_y}{\overline{h}} \right) = -\tau_{by} + \tau_{sy} \tag{23}$$

where S_{xx} = cross-shore radiation stress; ρ = water density; τ_{bx} = cross-shore bottom stress; τ_{sx} = cross-shore wind stress on the sea surface; S_{xy} = shear component of the radiation stress; τ_{by} = longshore bottom stress; and τ_{sy} = longshore wind stress on the sea surface. The wind shear stresses may not be negligible especially outside surf zones on natural beaches (Lentz et al. 1999). The term associated with the alongshore gradient of $\overline{\eta}$ may be added on the right hand side of Eq. (23) to include the effect of the alongshore tidal current near a tidal inlet (Farhadzadeh et al. 2012). For brevity, this term is omitted in the following. Linear wave theory for progressive waves is used to estimate S_{xx} and S_{xy} as in Eqs. (17) and (18)

$$S_{xx} = \left(nE + M_r \right) \cos^2\theta + E\left(n - \frac{1}{2} \right) \;\; ; \;\; S_{xy} = \left(nE + M_r \right) \cos\theta \sin\theta \tag{24}$$

with

$$n = C_g / C \;\; ; \;\; E = \rho g \sigma_\eta^2 \;\; ; \;\; M_r = \rho C q_r \tag{25}$$

where C_g = linear wave group velocity; E = specific wave energy with the root-mean-square wave height defined as $H_{rms} = \sqrt{8}\,\sigma_\eta$; and M_r = momentum flux of a roller propagating with the phase velocity C (Svendsen et al. 2002). It is noted that the equations used in CSHORE are presented again for clarity.

The time-averaged bottom shear stresses in Eqs. (22) and (23) are written as

$$\tau_{bx} = \frac{1}{2}\rho f_b \overline{UU_a} \quad ; \quad \tau_{by} = \frac{1}{2}\rho f_b \overline{VU_a} \quad ; \quad U_a = \left(U^2 + V^2\right)^{0.5} \tag{26}$$

where U = depth-averaged cross-shore velocity; V = depth-averaged longshore velocity; f_b = bottom friction factor; and the overbar indicates time averaging. Cox et al. (1996) measured the velocities inside the bottom boundary layer for regular waves shoaling and spilling on a rough impermeable 1/35 (vertical/horizontal) slope. The bottom friction factor f_b of the order of 0.01 on sand beaches has been assumed, but it should be calibrated using longshore current data because of the sensitivity of longshore currents to f_b. The equivalency of the time and probabilistic averaging is assumed to express τ_{bx} and τ_{by} in terms of the mean and standard deviation of the depth-averaged velocities U and V expressed as

$$U = \sigma_T F_U \quad ; \quad V = \sigma_T F_V \quad ; \quad U_a = \sigma_T F_a \quad ; \quad F_a = \left(F_U^2 + F_V^2\right)^{0.5} \tag{27}$$

with

$$F_U = U_* + r\cos\theta \quad ; \quad F_V = V_* + r\sin\theta \quad ; \quad U_* = \frac{\overline{U}}{\sigma_T} \quad ; \quad V_* = \frac{\overline{V}}{\sigma_T} \tag{28}$$

where $\overline{U}$ and $\overline{V}$ = depth-averaged cross-shore and longshore currents; σ_T = standard deviation of the oscillatory (assumed Gaussian) depth-averaged velocity U_T with zero mean; and r = Gaussian variable defined as $r = U_T/\sigma_T$ whose probability density function is given by

$$f\left(r\right) = \frac{1}{\sqrt{2\pi}}\exp\left(-\frac{r^2}{2}\right) \tag{29}$$

Linear progressive wave theory is used locally to express U_T in terms of the oscillatory free surface elevation $\left(\eta - \overline{\eta}\right)$

$$U_T = \frac{C}{\overline{h}}\left(\eta - \overline{\eta}\right) \tag{30}$$

which yields the standard deviation σ_T of the oscillatory velocity U_T

$$\sigma_T = C\,\sigma_* \quad ; \quad \sigma_* = \sigma_\eta / \overline{h} \tag{31}$$

It is noted that $U_* = \overline{U}/\sigma_T$ and $V_* = \overline{V}/\sigma_T$ are of the order of unity or less. The standard deviations of U and V are given by

$$\sigma_U = \sigma_T \cos\theta \quad ; \quad \sigma_V = \sigma_T \left|\sin\theta\right| \tag{32}$$

where $\cos\theta > 0$ but $\sin\theta$ can be negative. Substitution of Eq. (27) into Eq. (26) yields

$$\tau_{bx} = \frac{1}{2}\rho f_b \sigma_T^2 G_{bx} \quad ; \quad \tau_{by} = \frac{1}{2}\rho f_b \sigma_T^2 G_{by} \tag{33}$$

with

$$G_{bx} = \int_{-\infty}^{\infty} F_U F_a f(r) dr \quad ; \quad G_{by} = \int_{-\infty}^{\infty} F_V F_a f\left(r\right) dr \tag{34}$$

which can be integrated analytically only for $\theta = 0$ (Kobayashi et al. 2007b).

The wind shear stress in Eqs. (22) and (23) are expressed as

$$\tau_{sx} = \rho_a C_D W_{10}^2 \cos\theta_w \quad ; \quad \tau_{sy} = \rho_a C_D W_{10}^2 \sin\theta_w \tag{35}$$

where ρ_a = air density ($\rho_a \approx 1.225$ kg/m^3); C_D = drag coefficient, W_{10} = 10-m wind speed; and θ_w = wind direction defined in Fig. 1. The formula by Large and Pond (1981) is used to estimate C_D where C_D = 0.0012 for W_{10} < 11 m/s and C_D = (0.00049 + 0.000065 W_{10}) for $W_{10} \geq$ 11 m/s. It is noted that the measured values of C_D during tropical cyclones by Powell et al. (2003) indicated no increase of C_D with the increase of W_{10} above 25 m/s. In short, available data is insufficient to estimate C_D for extreme wind conditions.

The wave action equation (5) for the case of alongshore uniformity becomes

$$\frac{d}{dx}\left[\frac{E}{\omega}\left(C_g \cos\theta + \frac{Q_x}{\bar{h}}\right)\right] = -\frac{D_B + D_f}{\omega} \tag{36}$$

which reduces to the following wave energy equation if ω is constant and $Q_x = 0$.

$$\frac{dF_x}{dx} = -D_B - D_f \quad ; \quad F_x = EC_g \cos\theta \tag{37}$$

where F_x = cross-shore energy flux based on linear progressive wave theory; and D_B and D_f = energy dissipation rates due to wave breaking and bottom friction, respectively.

The energy dissipation rate D_B due to wave breaking in Eq. (36) is estimated using the simple formula by Battjes and Stive (1985), which was modified by Kobayashi et al. (2005) to account for the local bottom slope and to extend the computation to the lower swash zone. The modified formula is expressed as

$$D_B = \frac{\rho g a_s Q H_B^2}{4T} \quad ; \quad \frac{Q-1}{\ell nQ} = \left(\frac{H_{rms}}{H_m}\right)^2 \quad ;$$
$$H_m = \frac{0.88}{k}\tanh\left(\frac{\gamma k\bar{h}}{0.88}\right) \quad ; \quad a_s = \frac{2\pi S_b}{3k\bar{h}} \geq 1 \tag{38}$$

where a_s = slope effect parameter; Q = fraction of breaking waves; H_B = breaker height used to estimate D_B; T = intrinsic wave period given by $T = 2\pi/\omega$ with ω obtained using Eq. (2); $H_{rms} = \sqrt{8}\sigma_\eta$ = local root-mean-square wave height; H_m = local depth-limited wave height; k = wave number; $\overline{h}$ = mean water depth including wave setup; γ = empirical breaker ratio parameter; and S_b = local bottom slope given by Eq. (11) where the alongshore bottom slope is zero. The parameter a_s is the ratio between the wave length ($2\pi/k$) and the horizontal length ($3\overline{h}/S_b$) imposed by the small depth and relatively steep slope where the lower limit of $a_s = 1$ corresponds to the formula by Battjes and Stive (1985) who also assumed $H_B = H_m$. The fraction Q is zero for no wave breaking and unity when all waves break. The requirement of $0 \le Q \le 1$ implies $H_{rms} \le H_m$ but H_{rms} can become larger than H_m in very shallow water. When $H_{rms} > H_m$, use is made of $Q = 1$ and $H_B = H_{rms}$. In addition, the upper limit of $\sigma_* = \sigma_\eta / h$ is imposed as $\sigma_* \le 1$ in very shallow water (Kobayashi et al. 1998). The breaker ratio parameter γ in Eq. (38) is typically in the range of $\gamma = 0.5 - 1.0$ (Kobayashi et al. 2007a) but should be calibrated to obtain a good agreement with the measured cross-shore variation of σ_η if such data is available. If no data is available, the value of γ may be taken as a typical value of 0.7 (0.6 for very gentle slope) or estimated using the empirical formula developed by Apotsos et al. (2008) using field data. Irregular wave breaking is very complex, and Eq. (38) is a crude approximation.

On the other hand, the energy dissipation rate D_f due to bottom friction in Eq. (36) is expressed as

$$D_f = \frac{1}{2}\rho f_b \overline{U_a^3} \tag{39}$$

Substitution of U_a given in Eq. (27) into Eq. (39) yields

$$D_f = \frac{1}{2}\rho f_b \sigma_T^3 G_f \quad ; \quad G_f = \int_{-\infty}^{\infty} F_a^3 f(r)\, dr \tag{40}$$

where $f(r)$ is given by Eq. (29), and G_f can be integrated analytically only for $\theta = 0$ (Kobayashi et al. 2007b).

The energy equation for the roller given by Eq. (9) reduces to that used by Ruessink et al. (2001) for the case of alongshore uniformity

$$\frac{d}{dx}\left(\rho C^2 q_r \cos\theta\right) = D_B - D_r \quad ; \quad D_r = \rho g \beta_r q_r \tag{41}$$

where the roller dissipation rate D_r is assumed to equal the rate of work to maintain the roller on the wave-front slope β_r of the order of 0.1. Use is made of the empirical formula given by Eq. (10) proposed by Kobayashi et al. (2005) who included the local bottom slope effect. If the roller is neglected, $q_r = 0$ and Eq. (41) yields $D_r = D_B$. The roller effect improves the agreement for the longshore current (Ruessink et al. 2001; Kobayashi et al. 2007a).

Eqs. (19) – (41) are the same as those used by Kobayashi et al. (2007a) who assumed $Q_x = q_o = 0$ in Eq. (19) and neglected the wind shear stresses in Eqs. (22) and (23), and used linear shallow-water wave theory with $C = (g\overline{h})^{0.5}$ in Eq. (30). Substitution of Eqs. (31) and (32) into Eq. (19) yields the following equation of the mean cross-shore current:

$$\overline{U} = -\frac{g\overline{h}}{C^2}\sigma_U\sigma_*\left(1+\frac{Cq_r}{g\sigma_\eta^2}\right)+\frac{Q_x}{\overline{h}} \tag{42}$$

which is negative and offshore except for the zone of the very small water depth $\overline{h}$ affected by the onshore flux $Q_x = q_o$ in Eq. (19). A number of models were proposed to predict the vertical distribution of the undertow current (e.g., Cox and Kobayashi 1997, 1998) but none may have been adopted for practical applications.

The landward-marching computation based on Eqs. (22), (23), (36) and (41) starting from $x = 0$ outside the surf zone is based on an improved Euler finite difference method of second-order accuracy (e.g., Chaudhry 1993).

Approximate analytical equations of G_{bx}, G_{by}, and G_f given by Eqs. (34) and (40) are obtained by Kobayashi et al. (2009b) to reduce the computation time and improve the numerical stability. The function F_a given in Eq. (27) with Eq. (28) is rewritten as

$$F_a = \left[\left(r-r_m\right)^2 + F_m^2\right]^{0.5} \tag{43}$$

with

$$r_m = -\left(U_*\cos\theta + V_*\sin\theta\right) \quad ; \quad F_m = V_*\cos\theta - U_*\sin\theta \tag{44}$$

Eq. (43) is approximated as

$$\begin{aligned} F_a &= \left(r-r_m\right)+\left|F_m\right| \quad \text{for} \quad r \ge 0 \\ F_a &= -\left(r-r_m\right)+\left|F_m\right| \quad \text{for} \quad r < 0 \end{aligned} \tag{45}$$

Substituting Eq. (45) into Eqs. (34) and (40) and integrating the resulting equations analytically, we obtain approximate expressions for G_{bx}, G_{by}, and G_f

$$G_{bx} = \sqrt{\frac{2}{\pi}}\left(U_* - r_m\cos\theta\right)+U_*\left|F_m\right| \tag{46}$$

$$G_{by} = \sqrt{\frac{2}{\pi}}\left(V_* - r_m\sin\theta\right)+V_*\left|F_m\right| \tag{47}$$

$$G_f = 2\sqrt{\frac{2}{\pi}} + \left(1 + U_*^2 + V_*^2\right)\left|F_m\right| + \sqrt{\frac{2}{\pi}}\left(U_*^2 + V_*^2 + 2r_m^2\right) \qquad (48)$$

which depends on $\sin\theta$ ($\cos\theta > 0$ assumed), r_m and F_m where Eq. (44) yields $U_* = -(r_m \cos\theta + F_m \sin\theta)$ and $V_* = (F_m \cos\theta - r_m \sin\theta)$.

For the case of normally incident waves with no wind, $\sin\theta = 0$ and $V_* = 0$. Eqs. (46) – (48) yield $G_{bx} = 1.6\, U_*$, $G_{by} = 0$, and $G_f = (1.6 + 2.4\, U_*^2)$. For this case, Eq. (23) requires $\tau_{by} = 0$ for $Q_x = 0$ (no wave overtopping) and Eq. (33) yields $G_{by} = 0$. As a result, Eq. (47) is exact. For $\sin\theta = 0$ and $V_* = 0$, G_{bx} and G_f given by Eqs. (34) and (40) can be integrated analytically as presented by Kobayashi et al. (2007b) who approximated the analytical expressions of G_{bx} and G_f as $G_{bx} = 1.64\, U_*$ and $G_f = (1.6 + 2.6\, U_*^2)$. These approximate equations are very similar to the above equations obtained from Eqs. (46) and (48). For the case of $|\sin\theta| \ll 1$ and $|U_*| \ll |V_*|$, Eq. (47) can be approximated as $G_{by} = V_* (0.8 + |V_*|)$. Using field data and probabilistic analyses, Feddersen et al. (2000) obtained $G_{by} = V_* (1.16^2 + V_*^2)^{0.5}$. The difference between these two approximate equations for G_{by} is less than 20% for $|V_*| < 1.4$, which is typically satisfied.

Kobayashi et al. (2009b) compared the approximate values of G_{bx}, G_{by}, and G_f given by Eqs. (46) – (48) with the exact values of G_{bx}, G_{by}, and G_f obtained by the numerical integration of Eqs. (34) and (40). The percentage error was typically about 10% and always less than 35% for the ranges of $|\sin\theta| < 1$, $|r_m| < 1$ and $|F_m| < 1$. This error is probably less than the uncertainty of the bottom friction factor f_b.

The combined wave and current model has been shown to predict the cross-shore variations of the mean and standard deviation of η, U, and V within errors of about 20% (Kobayashi et al. 2005; 2007a, b; 2009a). However, it may be necessary to calibrate the bottom friction factor f_b in Eq. (26) and the breaker ratio parameter γ in Eq. (38).

5. Cohesionless Sediment Transport Model in Wet Zone

The combined wave and current model in the wet zone predicts the spatial variations of the hydrodynamic variables used in the following cohesionless sediment transport model for a given beach profile, water level and seaward wave conditions at $x = 0$. The bottom sediment is assumed to be uniform and characterized by d_{50} = median diameter; w_f = sediment fall velocity; and s = sediment specific gravity. The sediment particles in the wet zone are always submerged. The wet zone assumption is appropriate if the entire computation domain is submerged always.

First, the spatial variation of the degree of sediment movement is estimated using the critical Shields parameter ψ_c (Madsen and Grant 1976), which is taken as $\psi_c = 0.05$. The instantaneous bottom shear stress τ_b' is assumed to be given by $\tau_b' = 0.5\rho f_b U_a^2$ with U_a given in Eq. (26). The sediment movement

is assumed to occur when τ_b' exceeds the critical shear stress, $\rho g(s-1)d_{50}\psi_c$. The probability P_b of sediment movement can be shown to be the same as the probability of $\left(r-r_m\right)^2 > F_b^2 = \left(R_b^2 - F_m^2\right)$ (Kobayashi et al. 2008b)where $R_b = [2g(s-1)d_{50}\psi_c f_b^{-1}]^{0.5} / \sigma_T$ and r_m and F_m are defined in Eq. (44). For the Gaussian variable r given by Eq. (29), P_b is given by

$$P_b = \frac{1}{2} erfc\left(\frac{F_b - r_m}{\sqrt{2}}\right) + \frac{1}{2} erfc\left(\frac{F_b + r_m}{\sqrt{2}}\right) \quad \text{for} \quad F_b^2 > 0 \tag{49}$$

and $P_b = 1$ for $F_b^2 \le 0$ where erfc is the complementary error function (e.g., Press et al. 1989). The value of P_b computed from $x = 0$ located outside the surf zone increases landward and fluctuates in the surf and swash zones, depending on the presence of a bar or a terrace that increases the local fluid velocity.

Second, the spatial variation of the degree of sediment suspension is estimated using the experimental finding of Kobayashi et al. (2005) who showed that the turbulent velocities measured in the vicinity of the bottom were related mostly to the energy dissipation rate due to bottom friction. Representing the magnitude of the instantaneous turbulent velocity by $(D_f' / \rho)^{1/3}$ with $D_f' = 0.5\rho f_b U_a^3$ in light of Eq. (39), the probability P_s of sediment suspension has been assumed by Kobayashi et al. (2008b) to be the same as the probability of $(D_f' / \rho)^{1/3}$ exceeding the sediment fall velocity w_f. The probability P_s is then equal to the probability of $\left(r-r_m\right)^2 > F_s^2 = \left(R_s^2 - F_m^2\right)$ with $R_s = [(2/f_b)^{1/3} w_f / \sigma_T]$ and is given by

$$P_s = \frac{1}{2} erfc\left(\frac{F_s - r_m}{\sqrt{2}}\right) + \frac{1}{2} erfc\left(\frac{F_s + r_m}{\sqrt{2}}\right) \quad \text{for} \quad F_s^2 > 0 \tag{50}$$

and $P_s = 1$ for $F_s^2 \le 0$. If $P_s > P_b$, use is made of $P_s = P_b$ assuming that sediment suspension occurs only when sediment movement occurs. Fine sands on beaches tend to be suspended once their movement is initiated.

Third, the suspended sediment volume V_s per unit horizontal bottom area is estimated by modifying the sediment suspension model by Kobayashi and Johnson (2001)

$$V_s = P_s \frac{e_B D_r + e_f D_f}{\rho g\left(s-1\right) w_f} \left(1 + S_{bx}^2\right)^{0.5} \left(1 + S_{by}^2\right)^{0.5} \quad ; \quad S_{bx} = \frac{\partial z_b}{\partial x} \; ; \; S_{by} = \frac{\partial z_b}{\partial y} \tag{51}$$

where S_{bx} = cross-shore bottom slope; S_{by} = longshore bottom slope; and e_B and e_f = suspension efficiencies for the energy dissipation rates D_r and D_f due to wave breaking and bottom friction, respectively. Use has been made of $e_B = 0.005$ and $e_f = 0.01$ as typical values in the computation of berm and dune erosion but the value of e_B is uncertain and should be calibrated in the range of $e_B = 0.002 - 0.01$ if V_s is measured (Kobayashi et al. 2007a). In other words, the error of Eq. (51) can be about 100%. The sediment suspension probability P_s is added in Eq. (51) to ensure $V_s = 0$ if $P_s = 0$. The term involving S_{bx} and S_{by} is the actual bottom area per unit horizontal bottom area and essentially unity except for very steep slopes. For the case of alongshore uniformity, $S_{by} = 0$. The cross-shore and longshore suspended sediment transport rates q_{sx} and q_{sy} are expressed as

$$q_{sx} = a_x \overline{U} V_s \quad ; \quad q_{sy} = \overline{V} V_s \quad ; \quad a_x = \left[a + \left(S_{bx} / \tan\phi \right)^{0.5} \right] \geq a \tag{52}$$

where a = empirical suspended load parameter and ϕ = angle of internal friction of the sediment with $\tan\phi$ = 0.63 for sand (Bailard 1981). The parameter a accounts for the onshore suspended sediment transport due to the positive correlation between the time-varying cross-shore velocity and suspended sediment concentration. The value of a increases to unity as the positive correlation decreases to zero. For the three small-scale equilibrium profile tests conducted by Kobayashi et al. (2005), a was of the order of 0.2. The effect of the cross-shore bottom slope on a_x was included by Kobayashi et al. (2009a) to increase berm and dune erosion. For $S_{bx} \leq 0$, a_x = a. The cross-shore suspended sediment transport rate q_{sx} is negative (offshore) because the return (undertow) current $\overline{U}$ is negative (offshore). On the other hand, the longshore suspended sediment transport rate q_{sy} in Eq. (52) neglects the correlation between the time-varying longshore velocity and suspended sediment concentration, which appears to be very small if the longshore current $\overline{V}$ is sufficiently large. Payo et al. (2009) verified Eq. (52) using velocities and sand concentrations measured along 20 transects at the Field Research Facility at Duck, North Carolina, during a storm in 1997.

Fourth, the formulas for the cross-shore and longshore bedload transport rates q_{bx} and q_{by} are devised somewhat intuitively because bedload in the surf zone has never been measured. The time-averaged rates q_{bx} and q_{by} are tentatively expressed as

$$q_{bx} = B_b \overline{\left(U^2 + V^2 \right) U} \quad ; \quad q_{by} = B_b \overline{\left(U^2 + V^2 \right) V} \tag{53}$$

where B_b = empirical parameter. Eq. (53) may be regarded as a quasi-steady application of the formula of Meyer-Peter and Mueller (e.g., Ribberink 1998). Substitution of U and V given in Eq. (27) with Eqs. (28) and (29) into Eq. (53) yields

$$q_{bx} = B_b \sigma_T^3 \left(b_* + U_* V_*^2 + 2 F_m \sin\theta \right) \tag{54}$$

$$q_{by} = B_b \sigma_T^3 \left[V_* \left(1 + U_*^2 + V_*^2 \right) - 2 r_m \sin\theta \right] \tag{55}$$

where $b_* = (3U_* + U_*^3)$ and F_m and r_m are defined in Eq. (44).

Instantaneous bed load transport rates may be expressed as a function of instantaneous velocities (Bailard 1981), but the corresponding time-averaged rates are small (zero for sinusoidal flow) and may not be very accurate (Kobayashi 1982). Eqs. (54) and (55) yield $q_{bx} = b_* B_b \sigma_T^3$ and q_{by} = 0 for normally incident waves with $\sin\theta$ = 0 and V_* = 0. The expressions of B_b and b_* are obtained by requiring that $q_{bx} = b_* B_b \sigma_T^3$ reduces to the onshore bedload formula proposed by Kobayashi et al. (2008b) for normally incident waves, which synthesized existing data and simple formulas. The proposed formulas are written as

$$q_{bx} = \frac{b P_b}{g\left(s - 1 \right)} \sigma_T^3 \left(1 + U_* V_*^2 + 2 F_m \sin\theta \right) G_s \left(S_{bx} \right) \tag{56}$$

$$q_{by} = \frac{bP_b}{g(s-1)}\sigma_T^3\left[V_*\left(1+U_*^2+V_*^2\right)-2r_m\sin\theta\right]G_s\left(S_{by}\right) \tag{57}$$

where b = empirical bedload parameter of the order of 0.002; and G_s = bottom slope function. The sediment movement probability P_b given in Eq. (49) accounts for the initiation of sediment movement. It is noted that b_* = 1 in Eq. (56) to compensate for the limitations of Eq. (53) and the Gaussian distribution of the horizontal velocity used in Eqs. (28) and (29) as discussed by Kobayashi et al. (2008b). They calibrated b = 0.002 using the 20 water tunnel tests of Ribberink and Al-Salem (1994), the 4 large-scale wave flume tests of Dohmen-Janssen and Hanes (2002), and the 24 sheet flow tests by Dohmen-Janssen et al. (2002). Furthermore, this simple bedload formula is consistent with the sheet flow model for onshore bar migration by Trowbridge and Young (1989) and the energetics-based bedload formula for steady flow by Bagnolds (1966) if the steady flow formula is applied in the time-averaged manner. The onshore bedload transport predicted by Eq. (56) for θ = 0 and V_* = 0 is consistent with the field observations of onshore ripple migration by Becker et al. (2007) and Masselink et al. (2007). The offshore suspended sediment transport predicted by Eq. (52) is consistent with the field measurement during a storm by Madsen et al. (1994). The condition of $\left(q_{bx}+q_{sx}\right)=0$ for an equilibrium profile along with additional assumptions can be shown to yield the equilibrium profile popularized by Dean (1991). Kobayashi et al. (2018) extended the equilibrium profile model to include net cross-shore sand transport and estimate the seaward shift of the shoreline on periodically nourished beaches. The parameter b with the uncertainty of a factor of 2 needs to be calibrated using beach accretion data. To reproduce the 221-day recovery of eroded beaches after a severe storm, Kobayashi and Jung (2012) adopted $b = B(0.5+Q)$ with B = 0.002 and Q = fraction of irregular breaking waves computed using Eq. (38), where b = 0.001 outside the surf zone (Q = 0) was increased to b = 0.003 near the shoreline (Q = 1).

The bottom slope function $G_s(S_{bx})$ was introduced by Kobayashi et al. (2008b) to account for the effect of the steep cross-shore slope S_{bx} on the bedload transport rate and is expressed as

$$G_s\left(S_{bx}\right) = \tan\phi/\left(\tan\phi+S_{bx}\right) \quad \text{for} \quad -\tan\phi < S_{bx} < 0 \tag{58}$$

$$G_s\left(S_{bx}\right) = \left(\tan\phi-2S_{bx}\right)/\left(\tan\phi-S_{bx}\right) \quad \text{for} \quad 0<S_{bx}<\tan\phi \tag{59}$$

where G_s = 1 for S_{bx} = 0. Eq. (58) corresponds to the functional form of G_s used by Bagnold (1966) for steady stream flow on a downward slope with $S_{bx} < 0$ where the downward slope increases q_{bx}. Eq. (59) ensures that G_s approaches negative infinity as the upward slope S_{bx} approaches $\tan\phi$. Eqs. (58) and (59) reduce to $G_s = (1 - S_{bx}/\tan\phi)$ for $|S_{bx}| \ll \tan\phi$. Eq. (56) with G_s given by Eqs. (58) and (59) implies that the bedload transport rate q_{bx} is positive (onshore) for $S_{bx} < (\tan\phi)/2$ and negative (offshore) for $S_{bx} > (\tan\phi)/2$. Use is made of $|G_s| < G_m$ = 10 to avoid an infinite value in the computation. The computed profile change is not very sensitive to the assumed value of G_m because the beach profile changes in such a way to reduce a very steep slope except in the region of scarping (e.g., Seymour et al. 2005). The effect of the longshore bottom slope S_{by} is included in Eq. (57) using the same bottom slope function $G_s(S_{by})$ but has never been validated for lack of suitable data.

The landward marching computation of the time-averaged model in the wet zone ends at the cross-shore location $x = x_r$ where the mean water depth $\bar{h}$ at the subsequent landward node becomes less than 0.1 cm. No reliable data exists for suspended sand and bedload transport rates in the zone which is wet and dry intermittently. In the absence of wave overtopping [$q_o = 0$ in Eq. (19)], the following simple procedure was proposed by Kobayashi et al. (2008b) to deal with the zone with the bottom slope $S_{bx} > \tan\phi$. The cross-shore total sediment transport rate $q_x = (q_{sx} + q_{bx})$ at $x = x_r$ is denoted by q_{xr}. If q_{xr} is negative (offshore), q_x is extrapolated linearly to estimate q_x on the scarped face with $S_{bx} > \tan\phi$

$$q_x = q_{xr}\left(x_e - x\right)/\left(x_e - x_r\right) \quad \text{for} \quad x_r < x < x_e \tag{60}$$

where x_e = landward limit of the scarping zone with $S_{bx} > \tan\phi$. The extrapolated q_x is in the range of $q_{xr} \le q_x \le 0$ and the scarping zone is eroded due to the offshore sediment transport. This simple procedure is effective for a high and wide dune, which is typical in the Netherlands (e.g., van Gent et al. 2006), but does not allow onshore sediment transport due to overwash. The model for the wet and dry zone in Section 8 has been developed to predict wave overtopping and overwash of dunes.

Finally, the beach profile change is computed using the continuity equation of bottom sediment

$$\left(1-n_p\right)\frac{\partial z_b}{\partial t} + \frac{\partial q_x}{\partial x} + \frac{\partial q_y}{\partial y} = 0 \tag{61}$$

where n_p = porosity of the bottom sediment which is normally taken as $n_p = 0.4$; t = slow morphological time for the change of the bottom elevation z_b; and $q_y = (q_{sy} + q_{by})$ = longshore total sediment transport rate. For the case of alongshore uniformity, the third term in Eq.(61) is zero. Eq. (61) is solved using an explicit Lax-Wendroff numerical scheme (e.g., Nairn and Southgate 1993) to obtain the bottom elevation at the next time level. This computation procedure is repeated starting from the initial bottom profile until the end of a profile evolution test. The computation time is of the order of 10^{-3} of the test duration.

Kobayashi and Jung (2012) expanded CSHORE to allow the simultaneous computation of the multiple cross-shore lines and included the effect of the alongshore gradient of q_y in Eq. (61) on the temporal variation of z_b along each line in an approximate but computationally efficient manner. The bottom elevation z_b is expressed as $z_b = (z_x + z_y)$ and Eq. (61) is rewritten as

$$\left(1-n_p\right)\frac{\partial z_x}{\partial t} + \frac{\partial q_x}{\partial x} = 0 \tag{62}$$

$$\left(1-n_p\right)\frac{\partial z_y}{\partial t} + \frac{\partial q_y}{\partial y} = 0 \tag{63}$$

Eq. (62) is solved using the numerical method for the case of no alongshore gradient of q_y. Eq. (63) is integrated with respect to time t for the duration Δt of constant water level and wave conditions where $\Delta t = 1h$ for the field data examined by Kobayashi and Jung (2012). The bottom elevation change Δz_y during the interval Δt is expressed as

$$\Delta z_y = \frac{-\left|\Delta z_x\right|}{\left(1-n_p\right)A_x}\frac{\partial V_y}{\partial y} \quad ; \quad A_x = \int_0^{x_m}\left|\Delta z_x\right|dx \quad ; \quad V_y = \int_0^{x_m} dx \int_t^{t+\Delta t} q_y dt \tag{64}$$

where Δz_x = bottom elevation change based on Eq. (62) during time t to $\left(t+\Delta t\right)$; A_x = sum of the absolute value of Δz_x along the cross-shore line; x_m = cross-shore distance of the line starting from the seaward boundary $x = 0$; and V_y = longshore sediment volume across the entire cross-shore line during time t to $\left(t+\Delta t\right)$. Eq. (64) implies that Δz_y is proportional to the magnitude of the bottom elevation change Δz_x due to the cross-shore sediment transport. This eliminates the need to specify the seaward and landward limits of the profile change for one-line models (e.g., Coastal Engineering Manual 2003). The sign (accretion or erosion) of Δz_y in Eq. (64) depends on the alongshore gradient of V_y which is approximated by an upstream differencing method for its numerical stability (Anderson et al. 1984). The value of Δz_y based on Eq. (64) is added to the bottom elevation z_x computed using Eq. (62) to obtain the bottom elevation z_b at time $\left(t+\Delta t\right)$. Eq. (64) may not be rigorous but allows the use of a large alongshore spacing of two adjacent cross-shore lines.

6. Permeable Layer Model in Wet Zone for Gravel and Stone Bottoms

The combined wave and current model in the wet zone has been extended to allow the presence of a permeable layer in the wet zone because the permeability effect is not negligible for gravel beaches and stone structures. Fig. 2 shows an example of irregular wave overtopping of a permeable slope where x = onshore coordinate: z = vertical coordinate, $\overline{\eta}$ = mean free surface elevation above SWL; S = storm tide above $z = 0$; z_b = bottom elevation; $\overline{h}$ = mean water depth; U = instantaneous depth-averaged cross-shore velocity above the bottom; z_p = elevation of the lower boundary of the permeable layer; $h_p = (z_b - z_p)$ = vertical thickness of the permeable layer; and U_p = instantaneous cross-shore discharge velocity inside the permeable layer. The cross-shore profiles of $z_b(x)$ and $z_p(x)$ are specified as input where $h_p = 0$ in the zone of no permeable layer. The lower boundary located at $z = z_p$ is assumed to be impermeable for simplicity. Kobayashi et al. (2007b) developed a permeable layer model in the wet zone for normally incident waves. This model was extended by Kobayashi (2009) to obliquely incident waves and was applied by Garcia and Kobayashi (2015) to predict oblique wave transmission over and through low-crested porous breakwaters (Burcharth et al. 2006).

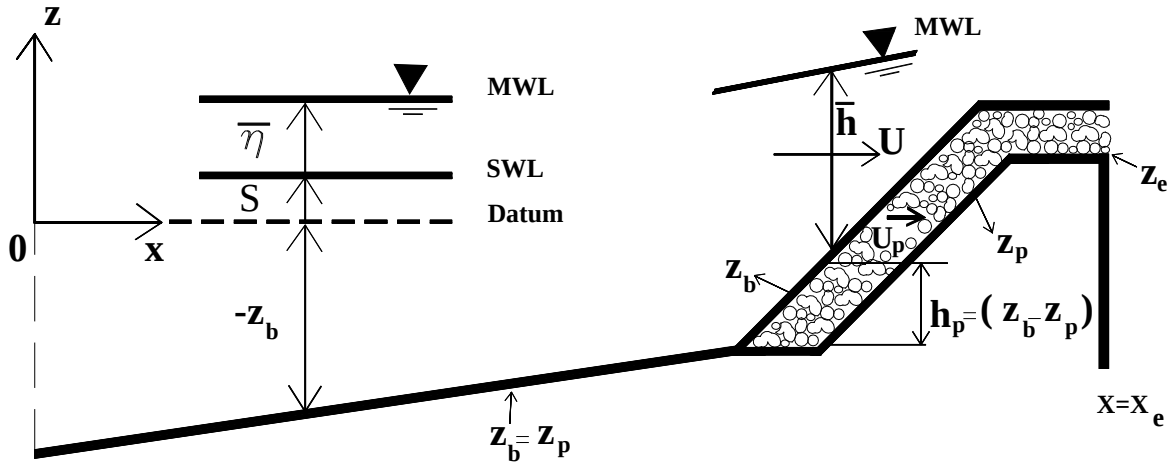

Fig. 2. Definition sketch of permeable layer model.

The time-dependent model for the flow over a permeable layer in shallow water developed by Kobayashi and Wurjanto (1990) and Wurjanto and Kobayashi (1993) is time averaged and simplified to account for the permeable layer in the cross-shore model CSHORE. The vertically integrated continuity equation (19) is modified as

$$Q_x = \overline{h}\,\overline{U} + \frac{g\sigma_\eta^2}{C}\cos\theta + q_r\cos\theta \quad ; \quad Q_x + h_p\overline{U_p} = q_o \tag{65}$$

where $\overline{U_p}$ = time-averaged cross-shore discharge velocity; $\left(h_p\overline{U_p}\right)$ = water flux inside the permeable layer with its vertical thickness h_p; and q_o = combined wave overtopping rate above and through the permeable layer. The cross-shore and longshore momentum equations (22) and (23) are assumed to remain the same, neglecting the momentum fluxes into and out of the permeable layer in the wet zone which is saturated with water. The bottom friction factor f_b for τ_{bx} and τ_{by} given by Eq. (33) includes the effect of the surface roughness of the permeable layer and was calibrated in the range of f_b = 0.01 – 0.05 (Kobayashi et al. 2007b) in which the permeability effect on the flow over the permeable layer is included in Eq. (65) explicitly. For the case of alongshore uniformity and negligible momentum fluxes into and out of the permeable layer in the wet zone, the time-averaged longshore discharge velocity $\overline{V_p}$ is assumed to be zero because of no or negligible driving force to cause the longshore discharge inside the permeable layer. It is noted that the assumption of $\overline{V_p} = 0$ cannot be validated at present for lack of suitable data.

On the other hand, the wave action equation (36) is modified as

$$\frac{d}{dx}\left[\frac{E}{\omega}\left(C_g\cos\theta + \frac{Q_x}{\overline{h}}\right)\right] = -\frac{D_B + D_f + D_p}{\omega} \tag{66}$$

where D_p = energy dissipation rate due to flow resistance in the permeable layer, assuming that the

energy influx into the permeable layer equals the dissipation rate D_p per unit horizontal area. The dissipation rate D_p is expressed as (Wurjanto and Kobayashi 1993)

$$D_p = \rho h_p \left[\alpha_p \left(\overline{U_p^2 + V_p^2} \right) + \beta_p \left(\overline{U_p^2 + V_p^2} \right)^{1.5} \right] \tag{67}$$

where α_p and β_p = laminar and turbulent flow resistance coefficients, respectively; and V_p = instantaneous longshore discharge velocity. Kobayashi et al. (2007b) modified the formulas for α_p and β_p proposed by van Gent (1995) as follows:

$$\alpha_p = \alpha_0 \frac{\left(1-n_p\right)^2}{n_p^2} \frac{\nu}{D_{n50}^2} \quad ; \quad \beta_p = \beta_1 + \frac{\beta_2}{\sigma_p} \tag{68}$$

with

$$\beta_1 = \frac{\beta_0 \left(1-n_p\right)}{n_p^3 D_{n50}} \quad ; \quad \beta_2 = \frac{7.5 \beta_0 \left(1-n_p\right)}{\sqrt{2}\, n_p^2 T} \tag{69}$$

where α_0 and β_0 = empirical parameters calibrated as α_0 = 1,000 and β_0 = 5; n_p = porosity of the permeable layer consisting of gravel or stone; ν = kinematic viscosity of the fluid; D_{n50} = nominal stone diameter defined as $D_{n50} = \left(M_{50} / \rho_s\right)^{1/3}$ with M_{50} = median stone mass and ρ_s = stone density; σ_p = standard deviation of the instantaneous discharge velocity; and T = intrinsic wave period used in Eq. (38).

The discharge velocities U_p and V_p in Eq. (67) are assumed to be expressed as

$$U_p = \overline{U_p} + r \sigma_p \cos\theta \quad ; \quad V_p = r \sigma_p \sin\theta \tag{70}$$

where r = Gaussian variable whose probability density function is given by Eq. (29); and θ = incident wave angle for the oscillatory velocity direction above and inside the permeable layer. The assumptions of the Gaussian velocity distribution and $\overline{V_p} = 0$ allow one to represent the discharge velocities by the mean cross-shore discharge velocity $\overline{U_p}$ and the standard deviation σ_p. Substitution of Eq. (70) into Eq. (67) yields

$$D_p = \rho h_p \left\{ \alpha_p \left(\overline{U_p}^2 + \sigma_p^2 \right) + \sqrt{\frac{2}{\pi}} \left(\beta_2 + \beta_1 \sigma_p \right) \left[2\sigma_p^2 + \overline{U_p}^2 \left(1 + 2\cos^2\theta \right) \right] \right\} \tag{71}$$

where use is made of the approximate expression of G_f given by Eq. (48) and the assumption of $\left| \overline{U_p} \sin\theta \right| \ll \sigma_p$ to simplify Eq. (71). Approximate equations for $\overline{U_p}$ and σ_p are derived in the following.

Neglecting the inertia terms in the cross-shore momentum equation for the flow inside the permeable layer (Kobayashi and Wurjanto 1990), the local force balance between the cross-shore hydrostatic pressure gradient and flow resistance is assumed

$$g\frac{\partial \eta}{\partial x}+\alpha_p U_p+\beta_p U_p\left(U_p^2+V_p^2\right)^{0.5}=0 \tag{72}$$

Eq. (72) is averaged probabilistically using Eq. (70). For the case of alongshore uniformity, the averaged force balance equation is expressed as

$$g\frac{\partial \overline{\eta}}{\partial x}+\overline{U_p}\left[\alpha_p+\sqrt{\frac{2}{\pi}}\left(\beta_2+\beta_1\sigma_p\right)\left(1+\cos^2\theta\right)\right]=0 \tag{73}$$

where use is made of the approximate expression of G_{bx} given by Eq. (46) and the assumption of $\left|\overline{U_p}\sin\theta\right| \ll \sigma_p$ to simplify Eq. (73). It is noted that the local force balance between the longshore hydrostatic pressure gradient and flow resistance yields $\overline{V_p}=0$ for the case of alongshore uniformity where $\overline{\eta}$ is independent of the longshore coordinate y. To derive an equation σ_p, the approximate analytical method used by Kobayashi et al. (2007b) is adopted. Eq. (72) is linearized as

$$g\frac{\partial \eta}{\partial x}+\left(\alpha_p+1.9\,\beta_p\sigma_p\right)U_p=0 \tag{74}$$

which is used to obtain

$$\left[\alpha_p+1.9\left(\beta_2+\beta_1\sigma_p\right)\right]\sigma_p=gk\overline{h}\sigma_* \quad ; \quad \sigma_*=\sigma_\eta/\overline{h} \tag{75}$$

where the wave number k is computed using Eq. (2). Eq. (75) can be solved analytically to obtain σ_p for known $\left(k\overline{h}\sigma_*\right)$. After σ_p is obtained, Eq. (73) is used to calculate $\overline{U_p}$ for known $\partial\overline{\eta}/\partial x$. The energy dissipation rate D_p is computed using Eq. (71). Eq. (65) for assumed q_o is used to obtain Q_x and $\overline{U}$ where $\overline{U}$ is expressed by Eq. (42).

This simple permeable layer model is coupled with the combined wave and current model above the permeable layer to predict irregular wave breaking and transmission over a submerged porous breakwater. The coupled model was compared with wave-flume experiments with no water flux (q_o = 0) in Eq. (65) by Kobayashi et al. (2007b) and Garcia and Kobayashi (2015). The degree of agreement (within errors of about 20%) is similar for impermeable beaches and permeable structures.

7. Irregular Wave Runup above Still Water Level

Wave run-up on beaches and coastal structures determines the landward extent of wave action. A number of empirical formulas and numerical models were developed to predict wave run-up on permeable and impermeable slopes (Kobayashi 1999). Irregular wave run-up depends on methods used to obtain and analyze run-up data.

The time-averaged model CSHORE in the wet zone does not predict the shoreline oscillations on beaches

and coastal structures unlike time-dependent models (e.g., Wurjanto and Kobayashi 1993). Kobayashi et al. (2008a) proposed a probabilistic model for irregular wave runup as illustrated in Fig. 3. The shoreline oscillation is assumed to be measured by a runup wire (RW) placed parallel to the bottom elevation z_b at a vertical height of δ_r. The runup wire measures the instantaneous elevation η_r above SWL of the intersection between the wire and the free surface elevation. The mean $\overline{\eta}_r$ and standard deviation σ_r of η_r are estimated using the computed cross-shore variations of $\overline{\eta}(x)$ and $\sigma_\eta(x)$ of the free surface elevation η above SWL. The point (x_r, z_r) corresponds to the landward limit of the wet zone computation. The probabilities of η_r exceeding $(\overline{\eta}_r + \sigma_r)$, $\overline{\eta}_r$, and $(\overline{\eta}_r - \sigma_r)$ are assumed to be the same as the probabilities of η exceeding $(\overline{\eta} + \sigma_\eta)$, $\overline{\eta}$, and $(\overline{\eta} - \sigma_\eta)$, respectively. The elevations of Z_1, Z_2, and Z_3 of the intersections located at x_1, x_2 and x_3 of $(\overline{\eta} + \sigma_\eta)$, $\overline{\eta}$, and $(\overline{\eta} - \sigma_\eta)$ with the runup wire are obtained for the given wire elevation ($z_b + \delta_r$). The obtained elevations are assumed to correspond to $Z_1 = (\overline{\eta}_r + \sigma_r)$, $Z_2 = \overline{\eta}_r$, and $Z_3 = (\overline{\eta}_r - \sigma_r)$. The mean and standard deviation of η_r are estimated as

$$\overline{\eta}_r = (Z_1 + Z_2 + Z_3)/3 \quad ; \quad \sigma_r = (Z_1 - Z_3)/2 \quad ; \quad S_r = (Z_1 - Z_3)/(x_1 - x_3) \qquad (76)$$

where S_r = representative slope in the zone of the runup measurement introduced by Kobayashi et al. (2013b) for arbitrary slopes and $S_r = \tan\theta$ for uniform seaward slopes. Kobayashi et al. (2010b) extended CSHORE to the wet and dry zone and replaced $\overline{\eta}$ and σ_η by $(P_w \overline{h} + z_b)$ and $P_w \sigma_\eta$ for the computation of Z_1, Z_2, and Z_3 to account for the transition from the wet zone $(P_w = 1)$ to the wet and dry zone $(P_w < 1)$ where P_w is the wet probability of water presence as explained in Section 8. It is noted that the vertical coordinate z in Fig. 3 is above SWL, corresponding to S=0 in Fig. 2, because wave run-up is measured above SWL. The mean depth $\overline{h}$ and standard deviation σ_η in the wet and dry zone are computed only for the wet duration at given cross-shore location x above SWL. CSHORE does not predict individual wave runup events.

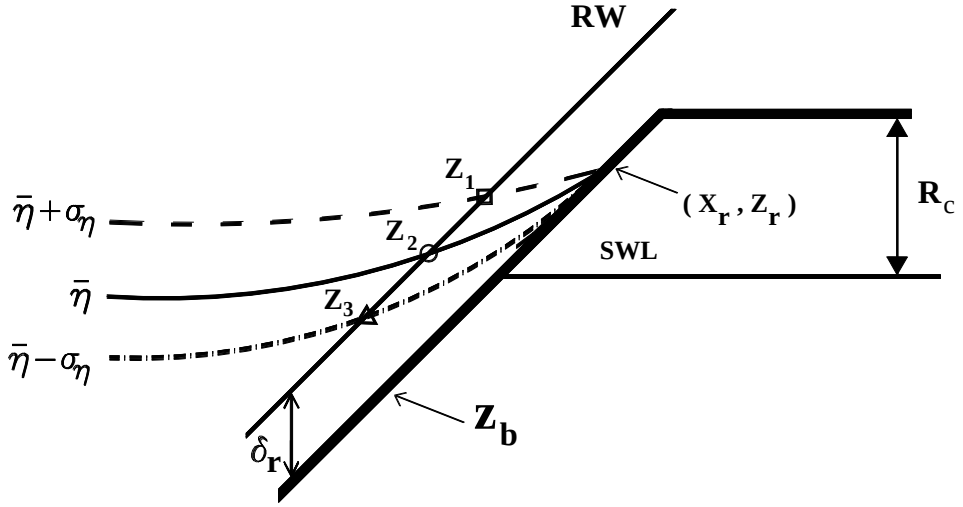

Fig. 3. Definition sketch for probabilistic model for irregular wave runup.

The runup height R is defined as the crest height above SWL of the temporal variation of η_r. The probability distribution of linear wave crests above the mean water level (MWL) is normally given by the Rayleigh distribution. For the case of no wave overtopping, the runup height $\left(R-\overline{\eta}_r\right)$ above the mean elevation $\overline{\eta}_r$ is assumed to be given by the Rayleigh distribution (Kobayashi et al. 2008a)

$$P\left(R\right)=\exp\left[-2\left(\frac{R-\overline{\eta}_r}{R_{1/3}-\overline{\eta}_r}\right)^2\right] \tag{77}$$

where *P(R)* = exceedance probability of the runup height R above SWL; and $R_{1/3}$ = significant runup height defined as the average of 1/3 highest values of R. The mean $\overline{\eta}_r$ related to wave setup is normally neglected in Eq. (77) for the prediction of irregular wave runup on steep coastal structures. For the 1/5 and 1/2 permeable slope experiments conducted by Kobayashi et al. (2008a), $R_{1/3}$ was estimated as

$$R_{1/3}=\overline{\eta}_r+\left(2+S_r\right)\sigma_r \tag{78}$$

where the representative slope S_r equals the uniform slopes $\tan\theta$ = 1/5 and 1/2 in the experiments. It is cautioned that Eq. (78) has been calibrated only for permeable slopes with $\tan\theta$ = 0.2 – 0.5 in the absence of wave overtopping.

Wave overtopping occurs when the individual runup height R above SWL exceeds the structure crest height R_c above SWL as depicted in Fig. 3. Wave overtopping reduces R exceeding R_c because of overtopping flow on the crest. Kobayashi and de los Santos (2007) adopted the following Weibull distribution:

$$P\left(R\right)=\exp\left[-2\left(\frac{R-\overline{\eta}_r}{R_{1/3}-\overline{\eta}_r}\right)^{\kappa}\right] \tag{79}$$

with

$$\kappa=2+0.5R_*^{-3}\qquad;\qquad R_*=\left(R_c-\overline{\eta}_r\right)/\left(R_{1/3}-\overline{\eta}_r\right) \tag{80}$$

where κ = shape parameter with κ = 2 for the Rayleigh distribution given by Eq.(77); and R_* = normalized crest height. It should be noted that the empirical formula for κ given by Eq. (79) has been calibrated using only 22 permeable slope tests. The formula for $R_{1/3}$ given by Eq. (78) has been found to be applicable to these 22 tests. The runup height $R_{2\%}$ ($R_{1\%}$) for the 2% (1%) exceedance probability obtained using Eq. (79) is given by

$$R_{2\%}=\overline{\eta}_r+\left(1.40\right)^{2/\kappa}\left(R_{1/3}-\overline{\eta}_r\right)\quad\text{for}\quad P=0.02 \tag{81}$$

$$R_{1\%}=\overline{\eta}_r+\left(1.52\right)^{2/\kappa}\left(R_{1/3}-\overline{\eta}_r\right)\quad\text{for}\quad P=0.01 \tag{82}$$

where the shape parameter κ given by Eq. (80) accounts for the decrease of $R_{2\%}$ and $R_{1\%}$ due to wave

overtopping.

The wave overtopping rate q_o in Eq. (19) for an impermeable slope and in Eq. (65) for a permeable slope needs to be estimated if wave overtopping occurs at the landward end of the computation domain located at $x = x_e$ in Fig. 2. The overtopping rate q_o is estimated later using the computed hydrodynamic variables at the crest (highest elevation) of the bottom elevation z_b. If the landward marching computation starting from $x = 0$ does not reach the crest, $q_o = 0$ for the impermeable bottom but water can flow through the permeable layer.

For the experimental setup shown in Fig. 2, Kobayashi and de los Santos (2007) estimated the seepage rate q_p for normally incident waves

$$q_p = 0.2\left(z_r - z_e\right)^{1.5}\left[\frac{g}{\left(x_e - x_r\right)\beta_1}\right]^{0.5} \quad \text{for} \quad z_r > z_e \tag{83}$$

where z_e = elevation of the landward end of the impermeable surface z_p at $x = x_e$ as shown in Fig. 2; and β_1 = turbulent flow resistance coefficient defined in Eq. (69). To derive Eq. (83), the seepage flow was assumed to be driven by the horizontal pressure gradient from the most landward point $\left(x_r, z_r\right)$ of the wet zone computation in Fig. 3 to the point $\left(x_e, z_e\right)$. Consequently, $q_p = 0$ if $z_r < z_e$. If $x_r = x_e$, the permeable layer is wet always and $q_p = h_p\overline{U}_p$ at $x = x_e$ where the water flux $h_p\overline{U}_p$ in the permeable layer is included in the continuity equation (65). To predict wave transmission through a permeable breakwater, Kobayashi et al. (2013c) adopted Eq. (83) with the point $\left(x_e, z_e\right)$ taken at the still water shoreline on the landward slope of the breakwater.

Kobayashi et al. (2013b) compared CSHORE with 137 tests for wave runup on impermeable dikes (van Gent 2001) and 120 tests for wave run-up on impermeable uniform slopes (Mase 1989). For the impermeable slopes, Eq. (78) is modified as

$$R_{1/3} = \left(1 + 4S_r\right)\left(\overline{\eta}_r + 2\sigma_r\right) \quad \text{with} \quad S_r \le 0.5 \tag{84}$$

where the slope correction term $\left(4S_r\right)$ is limited by the maximum value of 2. These dike tests were conducted for the conditions of no or little wave overtopping. As a result, use was made of the Rayleigh distribution given by Eq. (77) and Eqs. (81) and (82) were simplified as

$$R_{2\%} = \overline{\eta}_r + 1.40\left(R_{1/3} - \overline{\eta}_r\right) \quad \text{for} \quad P = 0.02 \tag{85}$$

with

$$R_{1\%} = \overline{\eta}_r + 1.52\left(R_{1/3} - \overline{\eta}_r\right) \quad \text{for} \quad P = 0.01 \tag{86}$$

The measured 2% and 1% exceedance runup heights for the 257 tests were predicted within errors of about 20% for the spectral period (van Gent 2001) at $x = 0$ specified as input to CSHORE. Melby et al.

(2012) compared CSHORE with extensive wave runup data on natural beaches to assess the capability and limitation of CSHORE for the use of flood mapping by the Federal Emergency Management Agency (FEMA). Wave run-up on dissipative beaches may not be predicted well by CSHORE when infragravity waves dominate shoreline oscillations.

8. Model for Impermeable Wet and Dry Zone of Sand Berm and Dune

Time-dependent numerical models, such as the nonlinear shallow-water wave model by Kobayashi et al. (1989), can predict the water depth and horizontal velocity in the intermittently wet and dry (swash) zone on beaches and inclined structures. However, the time-dependent hydrodynamic computation requires considerable computation time and may not lead to an accurate prediction of beach profile evolution in view of the earlier attempt by Tega and Kobayashi (1996). A time-averaged probabilistic model is developed here to predict the cross-shore variations of the wet probability and the mean and standard deviation of the water depth and cross-shore velocity in the swash zone. The developed model is very efficient computationally and can be calibrated using a large number of data sets. A sediment transport model in the swash zone is formulated by modifying the sediment transport model in the wet zone. The wet and dry zone is normally included in the computation domain of a sand beach with a shoreline.

8.1 Water depth and velocity of overtopping flow

Van Gent (2002a) and Schüttrumpf and Oumeraci (2005) analyzed the water depth and velocity of waves overtopping of dikes. Kobayashi et al. (2010b) expanded their analyses for the prediction of wave overtopping and overwash as presented in the following.

For normally incident waves on impermeable beaches and inclined structures of alongshore uniformity, the time-averaged cross-shore continuity and momentum equations derived from the nonlinear shallow-water wave equations are expressed as

$$\overline{hU} = q_o \tag{87}$$

$$\frac{d}{dx}\left(\overline{hU^2} + \frac{g}{2}\overline{h^2}\right) = -gS_{bx}\overline{h} - \frac{1}{2}f_b\overline{|U|U} \quad ; \quad S_{bx} = \frac{dz_b}{dx} \tag{88}$$

where h and U = instantaneous water depth and cross-shore velocity, respectively; q_o = wave overtopping rate; g = gravitational acceleration; S_{bx} = cross-shore bottom slope; and f_b = bottom friction factor, which is allowed to vary spatially. The wave energy equation corresponding to Eqs. (87) and (88) was given by Kobayashi and Wurjanto (1992) who used it to estimate the rate of wave energy dissipation due to wave breaking. The wave energy equation is not used in CSHORE because no formula is available to estimate the time-averaged energy dissipation rate associated with the interaction of wave uprush and downrush in the swash zone.

The instantaneous water depth h depends on the cross-shore coordinate x and the swash hydrodynamic time t. The water depth h at given x is described probabilistically rather than in the time domain. Kobayashi et al. (1998) analyzed the probability distributions of the free surface elevations measured in the shoaling, surf, and swash zones. The measured probability distributions were shown to be in agreement with the exponential gamma distribution, which reduces to the Gaussian distribution and the exponential distribution when the skewness approaches zero offshore and two in the swash zone, respectively. The assumption for the Gaussian distribution assumed in Eq. (29) has simplified the cross-shore model CSHORE in the wet zone significantly. The assumption of the exponential distribution is made here to simplify the cross-shore model in the wet and dry zone. The probability density function $f(h)$ is expressed as

$$f(h) = \frac{P_w^2}{\overline{h}} \exp\left(-P_w \frac{h}{\overline{h}}\right) \quad \text{for} \quad h > 0 \tag{89}$$

with

$$P_w = \int_0^\infty f(h)\, dh \quad ; \quad \overline{h} = \int_0^\infty h f(h)\, dh \tag{90}$$

where P_w = wet probability for the water depth $h > 0$; and $\overline{h}$ = mean water depth for the wet duration. The dry probability of $h = 0$ is equal to $(1 - P_w)$. The mean water depth for the entire duration is equal to $P_w \overline{h}$. The overbar in Eqs. (87) and (88) indicates averaging for the wet duration only. The free surface elevation $(\eta - \overline{\eta})$ above MWL is equal to $(h - \overline{h})$. The standard deviations of η and h are the same and given by

$$\frac{\sigma_\eta}{\overline{h}} = \left(\frac{2}{P_w} - 2 + P_w\right)^{0.5} \tag{91}$$

which yields $\sigma_\eta = \overline{h}$ for $P_w = 1$. This equality was supported by the depth measurements in the lower swash zone by Kobayashi et al. (1998) who assumed $P_w = 1$ in Eq. (89).

The cross-shore velocity U depends on x and t and is related to the depth h in the swash zone. The following relationship between U and h may be assumed to express U as a function of h

$$U = \alpha \sqrt{gh} + U_s \tag{92}$$

where α = positive constant exceeding unity for supercritical flow; and U_s = steady velocity which is allowed to vary with x. The steady velocity U_s is intended to account for offshore return flow on the seaward slope and the downward velocity increase on the landward slope. Holland et al. (1991) measured the bore speed and flow depth on a barrier island using video techniques and obtained $\alpha = 2$ where the celerity and fluid velocity of the bore are assumed to be approximately the same. Tega and Kobayashi (1996) computed wave overtopping of dunes using the nonlinear shallow-water wave equations and

showed $\alpha = 2$ for the computed U and h. As a result, use was made of $\alpha = 2$ as a first approximation. The calibrated value by Figlus et al. (2012) for wave overtopping of sand dunes was $\alpha = 1.6$. Eq. (92) implies that the cross-shore velocity U increases monotonically with the increase of h at given x. Eq. (92) yields $U = U_s$ when $h = 0$, which may be acceptable in view of the very small depth in the wet and dry zone. Using Eqs. (89) and (92), the mean $\overline{U}$ and standard deviation σ_U of the cross-shore velocity U can be expressed as

$$\overline{U} = \frac{\sqrt{\pi}}{2}\alpha\left(P_w g\overline{h}\right)^{0.5} + P_w U_s \tag{93}$$

$$\sigma_U^2 = \alpha^2 g\overline{h} - 2\left(\overline{U} - U_s\right)\left(\overline{U} - P_w U_s\right) + P_w\left(\overline{U} - U_s\right)^2 \tag{94}$$

Eq. (92) is substituted into Eqs. (87) and (88) which are averaged for the wet duration using Eq. (89). The continuity equation (87) yields

$$\frac{3\sqrt{\pi}\alpha}{4}\overline{h}\left(\frac{g\overline{h}}{P_w}\right)^{0.5} + U_s\overline{h} = q_o \tag{95}$$

After lengthy algebra, the cross-shore momentum equation (88) is expressed as

$$\frac{d}{dx}\left(B\frac{g\overline{h}^2}{P_w} + \frac{q_o^2}{\overline{h}}\right) = -gS_{bx}\overline{h} - \frac{f_b}{2}\alpha^2 g\overline{h}G_b\left(r_s\right) \tag{96}$$

with

$$B = \left(2 - \frac{9\pi}{16}\right)\alpha^2 + 1 \quad ; \quad r_s = \frac{3\sqrt{\pi}}{4}\frac{U_s\overline{h}}{q_o - U_s\overline{h}} \tag{97}$$

The function $G_b\left(r_s\right)$ in Eq. (95) with $r = r_s$ for simplicity is given by

$$G_b(r) = 1 + \sqrt{\pi}\, r + r^2 \qquad \text{for } r \geq 0 \tag{98}$$

$$G_b\left(r\right) = 2\exp\left(-r^2\right) - r^2 - 1 + \sqrt{\pi}\, r\left[2\,erf\left(r\right) + 1\right] \quad \text{for } r < 0 \tag{99}$$

where *erf* is the error function. The function G_b increases monotonically with the increase of r and $G_b = 0$ and 1 for $r = -0.94$ and 0.0, respectively, as shown in Fig. 4. For $r < -1.5$, $G_b = -\left(1 + \sqrt{\pi}r + r^2\right)$.

.

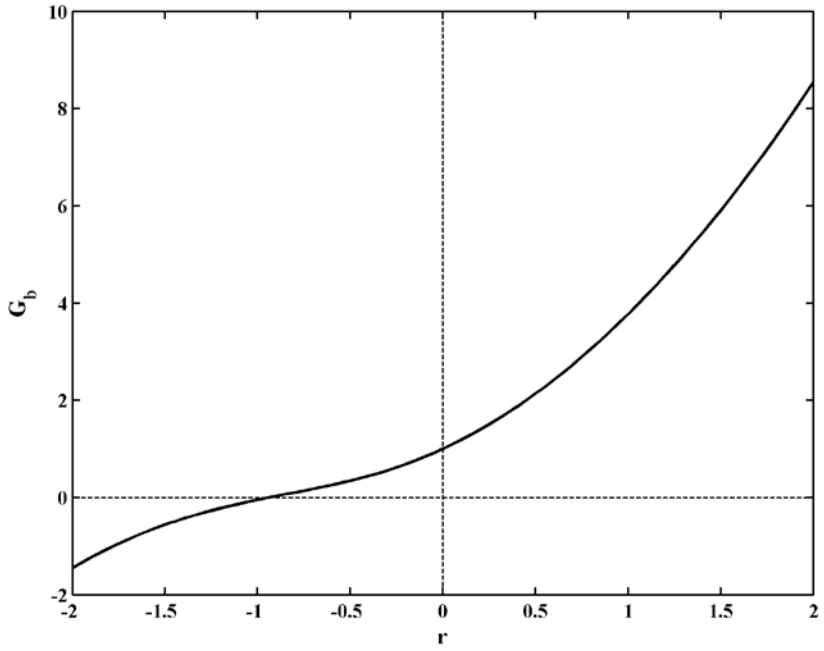

Fig. 4. Function $G_b(r)$ for wet and dry zone.

Eqs. (95) and (96) are used to predict the cross-shore variation of $\overline{h}$ and U_s for assumed q_o where σ_η, $\overline{U}$, and σ_U are computed using Eqs. (91), (93), and (94), respectively. It is necessary to estimate the wet probability P_w empirically. To simplify the integration of the momentum equation (96), the following formula is adopted:

$$P_w = \left[\left(1 + A_o\right) \left(\frac{\overline{h}_1}{\overline{h}} \right)^n - A_o \left(\frac{\overline{h}_1}{\overline{h}} \right)^3 \right]^{-1} \quad ; \quad A_o = \frac{q_o^2}{Bg\overline{h}_1^3} \quad \text{for} \quad x \le x_c \qquad (100)$$

where $\overline{h}_1$ = mean water depth at the location of $P_w = 1$; n = empirical parameter for P_w; A_o = parameter related to the wave overtopping rate q_o normalized by the depth $\overline{h}_1$ where water is always present. The transition from the wet ($P_w = 1$ always) zone to the wet and dry ($P_w < 1$) zone may be taken at $x = x_{SWL}$ where x_{SWL} is the cross-shore location of the still water shoreline of an emerged slope (see Fig. 5). Eq. (100) is assumed to be valid on the seaward slope and crest in the region of $x \le x_c$ where x_c = most landward location of the crest (maximum z_b) in Fig. 5. Eq. (100) produces the decrease of P_w with the decrease of $\overline{h}$ in the swash zone and allows the analytical integration of Eq. (96) to reduce numerical difficulties in the zone of very small water depth. However, Eq. (100) is purely empirical and may be improved in the future.

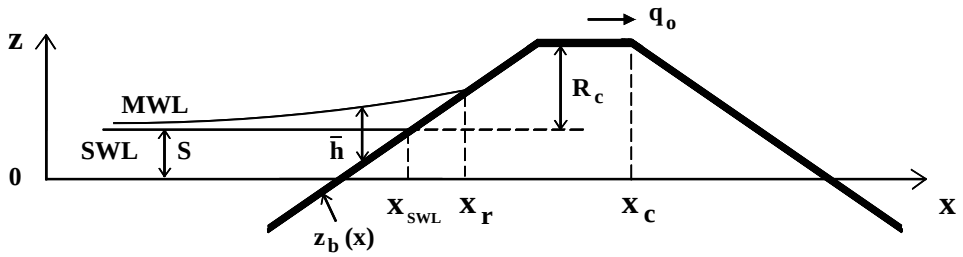

Fig. 5. Transition from wet model $\left(x < x_r\right)$ ***to wet and dry model*** $\left(x > x_{SWL}\right)$ ***for emerged impermeable structure*** $\left(R_c > 0\right)$**.**

Integration of Eq. (96) for P_w given by Eq. (100) with $\bar{h} = \bar{h}_1$ at $x = x_1$ yields $\bar{h}(x)$ for $x_1 \le x \le x_c$

$$B_n\left(1+A_o\right)\bar{h}_1\left[\left(\frac{\bar{h}_1}{\bar{h}}\right)^{n-1} - 1\right] = z_b\left(x\right) - z_b\left(x_1\right) + \frac{\alpha^2}{2}\int_{x_1}^{x} f_b G_b dx \qquad (101)$$

where $B_n = B\left(2-n\right)/\left(n-1\right)$; and $z_b\left(x\right)$ = bottom elevation at the cross-shore location x. The mean water depth $\bar{h}$ at given x is computed by solving Eq. (101) iteratively, where the bottom friction factor f_b is allowed to vary with x and the function G_b given by Eqs. (98) and (99) depends on r_s defined in Eq. (97). The empirical parameter n is taken to be in the range of $1 < n < 2$ so that $B_n > 0$. The formula for n calibrated using the 107 tests of wave overtopping and overflow on a dike by Kobayashi et al. (2010b) was expressed as $n = 1.01 + 0.98\left[\tanh\left(A_o\right)\right]^{0.3}$ where $1.01 \le n \le 1.99$.

The wave overtopping and overflow rate q_o is predicted by imposing $U_s = 0$ in Eq. (95) at the crest location x_c

$$q_o = \frac{3\sqrt{\pi}\alpha}{4}\bar{h}_c\left(\frac{g\bar{h}_c}{P_c}\right)^{0.5} \quad \text{at} \quad x = x_c \qquad (102)$$

where $\bar{h}_c$ and P_c are the computed mean depth $\bar{h}$ and wet probability P_w at x_c. The wave overtopping probability P_o may be related to the wet probability P_c at $x = x_c$ where both P_o and P_c are in the range of 0.0 – 1.0. The empirical relation of $P_o = \left[\tanh(5P_c)\right]^{0.8}$ was fitted for the 107 tests by Kobayashi et al. (2010b). If the landward marching computation does not reach the crest location, $q_o = 0$ and $P_o = 0$.

On the slope landward of the crest, the wet probability P_w is assumed to be constant and equal to P_c

$$P_w = P_c \qquad \text{for} \quad x \ge x_c \qquad (103)$$

Substituting Eq. (103) into Eq. (96) and integrating the resulting equation from x_c to x, the mean depth $\bar{h}(x)$ on the landward slope in the region of $x > x_c$ is expressed as

$$\frac{\overline{h}}{\overline{h}_c}-1+\frac{9\pi\alpha^2}{64B}\left[\left(\frac{\overline{h}_c}{\overline{h}}\right)^2-1\right]=\frac{P_c}{2B\overline{h}_c}\left[z_b\left(x_c\right)-z_b\left(x\right)-\frac{\alpha^2}{2}\int_{x_c}^{x}f_bG_b dx\right] \tag{104}$$

where the bottom elevation $z_b\left(x\right)$ decreases with the landward increase of x in the region of $x>x_c$. Eq. (104) is solved iteratively to compute $\overline{h}$ at given x.

For assumed q_o, the landward marching computation of $\overline{h}$, σ_η, $\overline{U}$, and σ_U is initiated using the wet model in Section 4 from the seaward boundary $x=0$ to the landward limit located at $x=x_r$, which corresponds to the location where the computed $\overline{h}$ or σ_η becomes negative or $\overline{h}$ becomes less than 0.1 cm for an emerged crest, as shown in Fig. 5. For a submerged crest, the landward limit of x_r is the landward end of the computation domain with no wet and dry zone. The landward marching computation is continued using the wet and dry model in this section from the location of $x=x_{SWL}$, where $\overline{h}=\overline{h}_1$ in Eq. (101) to the landward end of the computation domain or until the mean depth $\overline{h}$ becomes less than 0.001 cm. Then, the rate q_o is computed using Eq. (102). This landward computation starting from $q_o=0$ is repeated until the difference between the computed and assumed values of q_o is less than 1%. This convergency is normally obtained after several iterations. The computed values of $\overline{h}$, σ_η, $\overline{U}$ and σ_U by the two different models in the overlapping zone of $x_{SWL}<x<x_r$ (see Fig. 5) are averaged to smooth the transition from the wet zone to the wet and dry zone.

Kobayashi et al. (2010b) compared this hydrodynamic model for the impermeable wet and dry zone with their 107 tests of wave overtopping and overflow on an impermeable smooth levee and the 100 tests conducted by van Gent (2002b) who measured the water depth and velocity on the crest and landward (inner) slopes of six different dikes. The agreement was mostly within a factor of two for the wave overtopping rates and probabilities as well as the water depth, velocity, and discharge on the crest and landward slope exceeded by 2% of the incident 1000 waves. Kobayashi et al. (2010b) modified Eqs. (101) and (104) to allow the integration of Eq. (96) starting from an arbitrary location landward of the still water shoreline. This modification has been made to allow a dip above SWL such as the dip between a downward sloping berm and a dune. The wet probability P_w on the downward berm slope in front of the dune is assumed to be the same as that at the seaward end of this downward slope in the same way as in Eq. (103) for the downward dune slope. On the other hand, Farhadzadeh et al. (2012) extended CSHORE to allow oblique waves in the swash zone for the small incident wave angle. The mean $\overline{V}$ and standard deviation σ_V of the longshore velocity V in the wet and dry zone are expressed as

$$\overline{V}=\frac{\sqrt{\pi}}{2}\alpha\left(P_w g\overline{h}\right)^{0.5}\sin\theta_1 \tag{105}$$

$$\sigma_V=\alpha\left(g\overline{h}\right)^{0.5}\left[1-\frac{\pi}{4}P_w(2-P_w)\right]^{0.5}\left|\sin\theta_1\right| \tag{106}$$

using $\overline{h}$, P_w, and θ_1 where the wave angle θ_1 at $x=x_{SWL}$ is assumed to satisfy $\left(\sin\theta_1\right)^2\ll 1$ and the equations for $\overline{h}$ and P_w remain the same as those for $\sin\theta_1=0$.

8.2 Sand transport in swash zone

The sediment transport model for the wet zone in Section 5 is adjusted for the wet and dry zone. Normally incident waves and alongshore uniformity are assumed as has been assumed by Kobayashi et al. (2010b). The Gaussian velocity distribution has been assumed in Section 5, whereas U in the wet and dry zone is expressed as Eq. (92) along with the exponential distribution of h given by Eq. (89)

First, the movement of sediment particles is assumed to occur when the instantaneous bottom shear stress given by $0.5\rho f_b U^2$ exceeds the critical shear stress $\rho g(s-1)d_{50}\psi_c$, as has been assumed for Eq.(49). The probability P_b of sediment movement is then the same as the probability of $|U| > U_{cb}$, where $U_{cb} = \left[2g(s-1)d_{50}\psi_c f_b^{-1}\right]^{0.5}$. Using Eqs. (89) and (92), P_b can be shown to be given by

$$P_b = P_w \qquad \text{for} \quad U_s > U_{cb} \tag{107}$$

$$P_b = P_w \exp\left[-\frac{P_w(U_{cb}-U_s)^2}{\alpha^2 g\bar{h}}\right] \qquad \text{for} \quad |U_s| \le U_{cb} \tag{108}$$

$$P_b = P_w\left\{1-\exp\left[-\frac{P_w(U_{cb}+U_s)^2}{\alpha^2 g\bar{h}}\right]+\exp\left[-\frac{P_w(U_{cb}-U_s)^2}{\alpha^2 g\bar{h}}\right]\right\} \qquad \text{for} \quad -U_s > U_{cb} \tag{109}$$

where the upper limit of P_b is the wet probability P_w because no sediment movement occurs during the dry duration.

Second, sediment suspension is assumed to occur when the instantaneous turbulent velocity estimated as $(f_b/2)^{1/3}|U|$ exceeds the sediment fall velocity w_f, as has been assumed for Eq. (50). The probability P_s of sediment suspension is then the same as the probability of $|U| > U_{cs}$, where $U_{cs} = w_f(2/f_b)^{1/3}$. The probability P_s is then given by

$$P_s = P_w \qquad \text{for} \quad U_s > U_{cs} \tag{110}$$

$$P_s = P_w \exp\left[-\frac{P_w(U_{cs}-U_s)^2}{\alpha^2 g\bar{h}}\right] \qquad \text{for} \quad |U_s| \le U_{cs} \tag{111}$$

$$P_s = P_w\left\{1-\exp\left[-\frac{P_w(U_{cs}+U_s)^2}{\alpha^2 g\bar{h}}\right]+\exp\left[-\frac{P_w(U_{cs}-U_s)^2}{\alpha^2 g\bar{h}}\right]\right\} \qquad \text{for} \quad -U_s > U_{cs} \tag{112}$$

which reduces to Eqs. (107) – (109) if U_{cs} is replaced by U_{cb}. If $P_s > P_b$, use is made of $P_s = P_b$ because sediment suspension occurs only when sediment movement occurs.

Third, the suspended sediment volume V_s per unit horizontal bottom area in the wet zone is estimated using Eq. (51) where $S_{by} = 0$ for alongshore uniformity. In the wet and dry zone, V_s is assumed to be

given by

$$V_s = P_s V_{Bf} \left(1 + S_{bx}^2\right)^{0.5} \tag{113}$$

where V_{Bf} = potential suspended sediment volume on a horizontal bottom when $P_s = 1$. The value of V_{Bf} is assumed to be constant and chosen so that the suspended sediment volume V_s is continuous at $x = x_{SWL}$ at the seaward end of the wet and dry zone. The assumption of constant V_{Bf} may be reasonable because suspended sediment in the swash zone tends to remain suspended. It is noted that P_s given by Eqs. (110) – (112) decreases landward with the decrease of P_w.

Kobayashi et al. (2010b) estimated the cross-shore suspended sediment transport rate q_{sx} using Eq. (52).

$$q_{sx} = a_x \overline{U} V_s \quad ; \quad a_x = \left[a + \left(S_{bx} / \tan\phi \right)^{0.5} \right] \geq a \tag{114}$$

where $\overline{U}$ is given by Eq. (93). The parameter a_x had to be taken as unity in the zone of $\overline{U} > 0$ over the dune crest to predict minor wave overwash. However, Eq. (114) was found to underpredict major wave overwash in the three small-scale tests conducted by Figlus et al. (2011) to investigate the transition from minor to major wave overwash of dunes constructed of fine sand. For these tests, suspended load was computed to be dominant. To include the effect of the wave overtopping rate q_o on the cross-shore suspended sediment transport rate q_{sx}, Eq. (114) is modified as

$$q_{sx} = \left(a_x \overline{U} + a_o U_o \right) V_s \quad ; \quad U_o = q_o / \overline{h} \tag{115}$$

where a_o = empirical parameter with $a_o = 0$ in Eq. (114); and U_o = onshore current due to q_o, which is significant only in the zone of the very small depth $\overline{h}$. The parameter a_x is the same as in Eq. (114) without any adjustment in the zone of $\overline{U} > 0$. The calibrated value for the three laboratory tests by Figlus et al. (2011) was in the range of a_o = 1.3 – 1.8. However, the range of a_o = 0.1 – 0.5 was necessary for the field data with minor overwash used by Kobayashi et al. (2010b) to calibrate Eqs. (113) and (114). Figlus et al. (2012) recalibrated a_o along with α in Eq. (92) using additional data and obtained $\alpha = 1.6$ and $a_o = 3.3$ for their laboratory overwash data. The accurate prediction of wave overtopping and overwash is very difficult because of the small water depth and large velocity in the zone which is wet intermittently. In short, Eq. (113) is uncertain and the parameter a_o may need to be calibrated in the range of a_o = 0.1–3.3.

Fourth, the cross-shore bedload transport rate q_{bx} is estimated using Eq. (56) for the case of normally incident waves $\left(\sin\theta = 0\right)$ and no longshore current $\left(\overline{V} = 0\right)$ where $\sigma_T = \sigma_U$ for $\sin\theta = 0$ in Eq. (32). For this case, q_{bx} is given by

$$q_{bx} = \frac{b P_b \sigma_U^3}{g\left(s-1\right)} G_s\left(S_{bx}\right) \tag{116}$$

where the bottom slope function $G_s\left(S_{bx}\right)$ is given by Eqs. (58) and (59), and the standard deviation σ_U

is given by Eq. (94) for the wet and dry zone. The parameter b in the wet and dry zone is chosen so that the value of q_{bx} is continuous at $x = x_{\mathrm{SWL}}$ because q_{bx} in the wet zone is regarded to be more reliable.

The cross-shore sediment transport rates q_{sx} and q_{bx}, computed for the wet zone and the wet and dry zone, are averaged in the overlapping zone of $x_{SWL} < x < x_r$ for the smooth transition between the two zones in the same way as the smooth transition of $\overline{h}$, σ_η, $\overline{U}$, and σ_U as explained at the end of Section 8.1. The linear extrapolation for the case of no overwash given by Eq. (60) for scarping is applied only when the landward marching computation stops at the landward limit x_r of the wet zone computation. The continuity equation of bottom sediment given by Eq. (61) with $q_y = 0$ is solved numerically to obtain the bottom elevation at the next time level.

Figlus et al. (2012) conducted a laboratory experiment on onshore migration of an emerged ridge and a ponded runnel because the onshore migration of the ridge and runnel can have a significant influence on the sediment budget and beach recovery after a storm. The experiment was focused on the effect of water ponding and runnel drainage on the onshore ridge migration. The test scenario with a drained runnel showed a ridge migration speed five times larger than the other scenario in which water and sediment could only exit the runnel as offshore return flow over the ridge. CSHORE was modified to predict the ponded water level in the runnel and estimate the reduced bedload and suspended sediment transport rates in the ponded water zone. This modification enabled CSHORE to reproduce the observed sand transport asymmetry between onshore transport into the runnel and offshore transport out of the runnel where this asymmetry resulted in the deposition at the seaward end of the runnel. Measured hydrodynamics, wave overtopping and sediment overwash rates were predicted reasonably well in light of the strong interaction between the hydrodynamics and morphological evolution. The ponded water effect for these two tests will need to be confirmed using field data. The equations used in CSHORE for the ridge and runnel modification are omitted here for brevity.

For small incident wave angles with $(\sin\theta)^2 \ll 1$ in the swash zone, the cross-shore sediment transport rates q_{sx} and q_{bx} are estimated using Eqs. (115) and (116), respectively. The longshore suspended sediment transport rate q_{sy} is predicted using $q_{sy} = \overline{V} V_s$ in Eq. (52). The longshore bedload transport rate q_{by} is estimated using Eq. (57) with $\sigma_T = \sigma_U$ with the assumption of $(\sin\theta)^2 \ll 1$ where the mean $\overline{V}$ and standard deviation σ_V of the longshore velocity V given by Eqs. (105) and (106) are of the order of $\sin\theta$ (Farhadzadeh et al. 2012).

On the other hand, infiltration of water into the sand might not be negligible in the zone of infrequent wetting. Do et al. (2012, 2014) included the terms of water volume and momentum infiltration into the sand landward of the dune crest in the time-averaged continuity and momentum equations expressed as Eqs. (87) and (88) for the case of no infiltration. The infiltration effect was evaluated using field data of sand beaches with the median diameter of 0.31 mm. The computed beach and dune profile changes without and with the infiltration effect were practically the same. The infiltration effect is expected to increase with the increase of the sediment diameter and permeability.

The effects of seawalls on sand beaches were investigated by a number of researchers. Saitoh and Kobayashi (2012) conducted an experiment to examine cross-shore sand transport on a sloping beach in front of a vertical wall located well above the SWL. An initial semiequilibrium beach accreted slightly above SWL in which approximately 5% of incident waves reached the vertical wall. The cross-shore variations of the suspended sand and bed load transport rates predicted by CSHORE were examined to explain the net onshore sand transport, but CSHORE could not reproduce the slight accretion adequately.

Finally, Johnson et al. (2012) evaluated the 2009 version of CSHORE (Kobayashi 2009) using severe beach erosion data at seven sites on the mid-Atlantic east coast and two sites on the southern California coast. The degree of agreement for the seven mid-Atlantic sites was similar to the other comparisons discussed in this paper. The transition from no or minor overwash to major overwash of a dune is difficult to predict consistently because of the large uncertainty of the overwash parameter a_o in Eq. (115). For the two California sites with gentler beach slopes and smaller storm surge, fairly good agreement was obtained by increasing the computed offshore suspended sediment transport rate in which the suspension efficiency e_B in Eq. (51) was increased from 0.005 to 0.01 and the suspended load parameter a in Eq. (52) was increased from 0.2 to 0.5. In short, the degree of adjustment of the sediment transport parameters in CSHORE was similar to the other comparisons discussed earlier.

9. Model for Permeable Wet and Dry Zone of Gravel Beach and Rubble Mound

The model in Section 8 is extended to a permeable wet and dry zone. The extended model is calibrated and verified using laboratory data for stone structures and gravel beaches built on fixed impermeable bottoms. However, bathymetric changes of sandy bottoms can be considerable (e.g., Burcharth et al. 2006).

A number of time-dependent hydrodynamic models for rubble mound structures have already been developed as reviewed by Losada et al. (2008). These numerical models try to predict the temporal and spatial variations of wave dynamics as accurately as possible. The computation time normally increases with the increase of the resolution and accuracy. The computationally advanced models are used to predict hydrodynamic variables for relatively short durations. To reduce computation time considerably, Kobayashi et al. (2007b) proposed the probabilistic model CSHORE. The time-varying wave variables are expressed using a probability distribution. The spatial variations of the mean and standard deviation are computed using the time-averaged governing equations. The probabilistic time-averaged model requires additional assumptions, but its computational efficiency allows the calibration of the model parameters using a large number of tests. This probabilistic model for the wet zone on the permeable armor layer was extended by Kobayashi et al. (2010a, 2011) to the wet and dry zone in order to predict the wave motion above the still water level (SWL). The extended model provides the hydrodynamic input to a damage or erosion progression model that predicts the slow evolution of the stone or gravel

layer profile.

The movement of individual stone units on the armor layer may be computed using the equation of motion for each armor unit (Kobayashi and Otta 1987). The profile evolution of the armor layer may then be predicted by computing the displacements of all the armor units (Norton and Holmes 1992). However, this approach has never been adopted for practical applications probably because of its computation time and the uncertainty of initial individual stone locations. The sediment transport model in Section 8.2 is modified in this section to predict the profile evolution of the stone or gravel layer in the same manner as the prediction of the sand beach profile evolution. This simple approach neglects the discrete nature of armor stone units but is very convenient for the prediction of the armor layer profile evolution averaged alongshore where the alongshore averaging reduces the discrete nature.

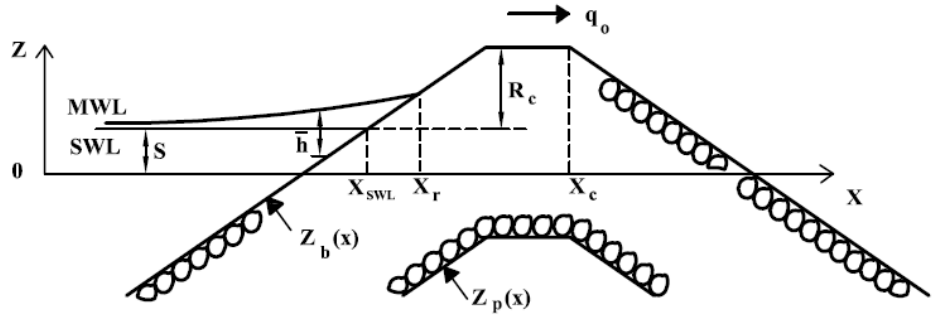

Fig. 6. Transition from wet model $\left(x < x_r\right)$ ***to wet and dry model*** $\left(x > x_{\mathrm{SWL}}\right)$ ***on permeable stone layer***

9.1 Water depth and velocity including water seepage

Fig. 6 depicts the permeable stone layer analyzed by Kobayashi et al. (2010a). Alongshore uniformity and normally incident waves are assumed. The cross-shore coordinate x is positive onshore with $x=0$ at the offshore location of the wave measurement. The vertical coordinate z is positive upward with $z=0$ at the datum. The still water level (SWL) above the datum is allowed to vary in time during a storm or an experiment. The upper and lower boundaries of the permeable stone layer are located at $z = z_b(x)$ and $z_p(x)$, respectively, where the lower boundary is assumed to be fixed and impermeable to simplify the analysis. The crest height R_c is taken conventionally as the structure height above SWL. The crest location x_c is defined here as the highest and most landward location. The wave overtopping rate is denoted as q_o. The SWL shoreline on the seaward slope is located at x_{SWL}. The mean water level (MWL) is located at $z = \left(S + \overline{\eta}\right)$ where $\overline{\eta}$ is the wave setup above SWL. The mean water depth $\overline{h}$ above $z = z_b$ is given by $\overline{h} = \left(S + \overline{\eta} - z_b\right)$. The cross-shore location x_r is the landward limit of the time-averaged model in the wet zone.

The time-averaged model for the permeable slope in the wet zone developed by Kobayashi et al. (2007b) has been modified using linear wave and current theory where wave overtopping induces onshore current. The time-averaged continuity, momentum, and wave energy or action equations are used to predict the cross-shore variations of the mean $\overline{U}$ of the depth-averaged cross-shore velocity U, the mean $\overline{\eta}$ of the

free surface elevation η above SWL, and the free surface standard deviation σ_η. The overbar denotes time averaging. The root-mean-square (RMS) wave height is defined as $H_{\rm rms} = \sqrt{8}\,\sigma_\eta$. Linear progressive wave theory is used locally to express the velocity standard deviation σ_U in terms of σ_η. The probability distributions of η and U are assumed to be Gaussian. The equivalency of the time averaging and probabilistic averaging is assumed to express the time-averaged terms in the governing equations in terms of $\overline{\eta}$, σ_η, $\overline{U}$, and σ_U. The permeability effects are included in Section 6.

The landward-marching computation using this model for the wet zone is continued as long as the computed $\overline{h}$ and σ_η are larger than 0.1 cm. The end location of the computation is denoted as x_r in Fig. 6. The time-average model for the wet zone cannot predict wave overtopping. A separate model for the wet and dry zone is developed and connected with the model for the wet zone (Kobayashi et al. 2010a). This procedure is the same as that used in Section 8.1. The time-averaged cross-shore continuity and momentum equations derived from the nonlinear shallow-water wave equations on the permeable slope (Wurjanto and Kobayashi 1993) are expressed as

$$\frac{d}{dx}\left(\overline{hU}\right) = -\overline{w_p} \tag{117}$$

$$\frac{d}{dx}\left(\overline{hU^2} + \frac{g}{2}\overline{h^2}\right) = -g\overline{h}\frac{dz_b}{dx} - \frac{1}{2}f_b\overline{|U|U} - \overline{u_b w_p} \tag{118}$$

where h and U = instantaneous water depth and cross-shore velocity, respectively; w_p = vertical seepage velocity, which is taken to be positive downward; g = gravitational acceleration; z_b = bottom elevation above the datum $z=0$; f_b = bottom friction factor which is allowed to vary spatially; and u_b = horizontal fluid velocity at $z = z_b$. The last term on the right hand side of Eq. (118) represents the time-averaged flux of the horizontal momentum into the permeable layer. The overbar in Eqs. (117) and (118) for the wet and dry zone indicates averaging for the wet duration only because no water exists during the dry duration. The continuity and approximate momentum equations for the flow inside the permeable layer are expressed as

$$\frac{dq_p}{dx} = \overline{w_p} \tag{119}$$

$$\left(\alpha_p + \beta_1\left|\overline{U_p}\right|\right)\overline{U_p} = -g\frac{d\overline{\eta}}{dx} \tag{120}$$

with

$$\alpha_p = 1000\left(\frac{1-n_p}{n_p}\right)^2\frac{\nu}{D_{n50}^2} \quad ; \quad \beta_1 = \frac{5\left(1-n_p\right)}{D_{n50}n_p^3} \tag{121}$$

where q_p = time-averaged horizontal volume flux in the permeable layer; $\overline{U_p}$ = time-averaged horizontal discharge velocity; α_p and β_1 = coefficients associated with the laminar and turbulent flow resistance in Eq. (68), respectively; n_p = porosity of the permeable layer; D_{n50} = nominal stone diameter; and ν =

kinetic viscosity of the fluid. Eq. (121) is based on the formula developed by van Gent (1995) and calibrated by Kobayashi et al. (2007b). The resistance component β_2 given in Eq. (69) associated with the oscillatory flow is simply neglected in Eq. (120), which is solved analytically to obtain the discharge velocity $\overline{U_p}$ driven by the horizontal pressure gradient due to $\overline{\eta} = \left(\overline{h} + z_b - S\right)$ where $\overline{h}$ and z_b vary with x. It is noted that Eq. (120) retains only the leading terms in the horizontal momentum equation given by Wurjanto and Kobayashi (1993).

Adding Eqs. (117) and (119) and integrating the resulting equation with respect to *x*, the vertically integrated continuity equation is obtained

$$\overline{hU} + q_p = q_o \tag{122}$$

where the wave overtopping rate q_o is defined as the sum of the volume fluxes above and inside the permeable layer in the same way as in Eq. (65). The volume flux q_p is estimated as

$$q_p = P_w \overline{U_p} \left(\overline{\eta_p} - z_p\right) \tag{123}$$

where P_w = wet probability defined as the ratio between the wet and entire durations; $\overline{\eta_p}$ = average water level inside the permeable layer; and z_p = elevation of the impermeable lower boundary. The elevation $\overline{\eta_p}$ and z_p are relative to the datum $z = 0$ in Fig. 6 and $\left(\overline{\eta_p} - z_p\right)$ is the thickness of water inside the permeable layer. The elevation $\overline{\eta_p}$ is estimated as

$$\overline{\eta_p} = P_w z_b + \left(1 - P_w\right) z_p \quad \text{for} \quad z_p \geq S \tag{124}$$

$$\overline{\eta_p} = P_w z_b + \left(1 - P_w\right) S \quad \text{for} \quad z_p < S \tag{125}$$

The upper bound of $\overline{\eta_p}$ for $P_w = 1$ is the upper boundary of the permeable layer located at $z = z_b$. The lower bound of $\overline{\eta_p}$ for $P_w = 0$ is the higher elevation of the lower boundary z_p of the permeable layer and the still water level *S*. The wet probability P_w in Eq. (123) ensures that $q_p = 0$ if $P_w = 0$. Eqs. (123) – (125) based on physical reasoning may be crude but are used along with Eqs. (120) and (121) to estimate q_p for the known $\overline{h}$ and P_w.

The momentum flux in Eq. (118) is expressed as

$$\overline{u_b w_p} = \alpha_m P_w \left(g\overline{h}\right)^{0.5} w_m \tag{126}$$

with

$$\left(\alpha_p + \beta_1 w_m\right) w_m = g \tag{127}$$

where α_m =empirical parameter; and w_m = maximum downward seepage velocity due to the gravity force, obtained by solving Eq. (127) analytically. The seepage velocity w_p is assumed to be of the order of w_m or less. The horizontal velocity u_b at $z = z_b$ is assumed to be of the order of $\left(g\overline{h}\right)^{0.5}$. Eq. (126) assumes that the downward flux of the horizontal momentum during the wet duration is much larger than the upward

momentum flux from the permeable layer.

The cross-shore variation of the mean water depth $\overline{h}$ is obtained by solving the momentum equation (118) together with the continuity equation (122). The probability density function *f(h)* in the wet and dry zone is assumed to be exponential and given by

$$f\left(h\right)=\frac{P_w^2}{\overline{h}}\exp\left(-P_w\frac{h}{\overline{h}}\right)\quad\text{for}\quad h>0 \tag{128}$$

with

$$P_w=\int_0^\infty f\left(h\right)dh\quad;\quad\overline{h}=\int_0^\infty hf\left(h\right)dh \tag{129}$$

Eqs. (128) and (129) are the same as Eqs. (89) and (90) but presented again for clarity. The wet probability P_w equals the probability of the instantaneous water depth $h > 0$. The dry probability of $h = 0$ is equal to $(1 - P_w)$. The mean water depth for the wet duration is $\overline{h}$ but the mean depth for the entire duration is equal to $P_w\overline{h}$. The free surface elevation η above SWL is given by $\eta=\left(h+z_b-S\right)$ where z_b and S are assumed to be invariant during the averaging. The standard deviations of η and h are the same and given by

$$\frac{\sigma_\eta}{\overline{h}}=\left(\frac{2}{P_w}-2+P_w\right)^{0.5} \tag{130}$$

which is the same as Eq. (91).

The cross-shore velocity U may be related to the depth h in the wet and dry zone in the same way as in Eq. (92)

$$U=\alpha\sqrt{gh}+U_s \tag{131}$$

where α = positive constant taken as $\alpha=2$ for permeable steep slopes; and U_s = steady velocity which is allowed to vary with x. The steady velocity U_s is included to account for offshore return flow on the seaward slope and crest and the downward velocity increase on the landward slope. Using Eqs. (128) and (131), the mean $\overline{U}$ and standard deviation σ_U of the cross-shore velocity U can be expressed as

$$\overline{U}=\frac{\sqrt{\pi}}{2}\alpha\left(P_wg\overline{h}\right)^{0.5}+P_wU_s \tag{132}$$

$$\sigma_U^2=\alpha^2g\overline{h}-2\left(\overline{U}-U_s\right)\left(\overline{U}-P_wU_s\right)+P_w\left(\overline{U}-U_s\right)^2 \tag{133}$$

Eqs. (130), (132) and (133) express σ_η, $\overline{U}$, and σ_U in terms of $\overline{h}$, P_w, and U_s which vary with x. The mean $\overline{V}$ and standard deviations σ_V of the longshore velocity V are given by Eqs. (105) and (106).

Eq. (131) is substituted into Eqs. (118) and (122), which are averaged for the wet duration using Eq. (128).

The continuity equation (122) yields

$$\frac{3\sqrt{\pi}\alpha}{4}\overline{h}\left(\frac{g\overline{h}}{P_w}\right)^{0.5}+U_s\overline{h}=q \quad ; \quad q=q_o-q_p \tag{134}$$

where q = volume flux above the permeable layer. After lengthy algebra, the momentum equation (118) is expressed as

$$\frac{d}{dx}\left(B\frac{g\overline{h}^2}{P_w}+\frac{q^2}{\overline{h}}\right)=-g\overline{h}\frac{dz_b}{dx}-\frac{f_b}{2}\alpha^2 g\overline{h}G_b\left(r_s\right)-\alpha_m P_w\left(g\overline{h}\right)^{0.5}w_m \tag{135}$$

with

$$B=\left(2-\frac{9\pi}{16}\right)\alpha^2+1 \quad ; \quad r_s=\frac{3\sqrt{\pi}}{4}\frac{U_s\overline{h}}{q-U_s\overline{h}} \tag{136}$$

where the parameter B and variable r_s are defined in Eq. (97) with q_o replaced by q for the permeable layer. The parameter B is related to the momentum flux term on the left hand side of Eq. (118). The function $G_b\left(r_s\right)$ in Eq. (135) is given by Eqs. (98) and (99).

Eqs. (134) and (135) are used to predict the cross-shore variation of $\overline{h}$ and U_s for assumed q_o. It is necessary to estimate the wet probability P_w empirically. To simplify the integration of Eq. (135), the following formula is adopted:

$$P_w=\left[\left(1+A_1\right)\left(\frac{\overline{h}_1}{\overline{h}}\right)^n-A\left(\frac{\overline{h}_1}{\overline{h}}\right)^3\right]^{-1} \quad ; \quad A=\frac{q^2}{Bg\overline{h}_1^3} \; ; \; A_1=\frac{q_1^2}{Bg\overline{h}_1^3} \tag{137}$$

where $\overline{h}$ and q_1 = mean water depth and volume flux, respectively, at the location of $x = x_1$ where $P_w = 1$; n = empirical parameter for P_w ; and A and A_1 = dimensionless variables related to q and q_1, respectively. The transition from the wet ($P_w = 1$ always) zone to the wet and dry ($P_w < 1$) zone may be taken at $x_1 = x_{SWL}$ where x_{SWL} is the cross-shore location of the still water shoreline of an emerged crest, as shown in Fig. 6. Eq. (137) is assumed to be valid on the upward slope and horizontal crest in the region of $x_1 \le x \le x_c$ where x_c is the highest and most landward location of the structure.

Integration of Eq. (135) for P_w given by Eq. (137) starting from $\overline{h}=\overline{h}_1$ at $x=x_1$ yields $\overline{h}\left(x\right)$

$$B_n\left(1+A_1\right)\overline{h}_1\left[\left(\frac{\overline{h}_1}{\overline{h}}\right)^{n-1}-1\right]=z_b\left(x\right)-z_b\left(x_1\right)+\int_{x_1}^{x}\left[\frac{f_b}{2}\alpha^2 G_b+\alpha_m\frac{P_w w_m}{\left(g\overline{h}\right)^{0.5}}\right]dx \tag{138}$$

where $B_n = B(2-n)/(n-1)$; and $z_b(x)$ = bottom elevation at the cross-shore location x. The mean water

depth $\overline{h}$ at given x is computed by solving Eq. (138) iteratively. The empirical parameter n is taken to be in the range of $1 < n < 2$ so that $B_n > 0$. The formula for n for the impermeable wet and dry zone in Section 8.1 is adopted and expressed as $n = 1.01 + 0.98\left[\tanh\left(A_o\right)\right]^{0.3}$ where $1.01 \le n \le 1.99$ and $A_o = q_o^2 / (bg\overline{h}_1^3)$.

On the downward slope in the region of $x > x_c$, the wet probability P_w is assumed to be given by

$$P_w^{-1} = P_c^{-1} + \frac{q_c^2 - q^2}{Bg\overline{h}^3} \tag{139}$$

where P_c and q_c are the computed wet probability P_w and volume flux q at $x = x_c$. Substituting Eq. (139) into Eq . (135) and integrating the resulting equation from x_c to x, the mean depth $\overline{h}(x)$ is expressed as

$$\frac{\overline{h}}{\overline{h}_c} - 1 + \frac{P_c q_c^2}{4gB\overline{h}_c^3}\left[\left(\frac{\overline{h}_c}{\overline{h}}\right)^2 - 1\right] = \frac{P_c}{2B\overline{h}_c}\left\{z_b\left(x_c\right) - z_b\left(x\right) - \int_{x_c}^{x}\left[\frac{f_b}{2}\alpha^2 G_b + \alpha_m \frac{P_w w_m}{\left(g\overline{h}\right)^{0.5}}\right]dx\right\} \tag{140}$$

where $\overline{h}_c$ is the computed mean depth at $x = x_c$.

The wave overtopping rate q_o is predicted by imposing $U_s = 0$ in Eq. (134) at the crest location x_c

$$q_o = \frac{3\sqrt{\pi}\alpha}{4}\overline{h}_c\left(\frac{g\overline{h}_c}{P_c}\right)^{0.5} + q_p \qquad \text{at} \quad x = x_c \tag{141}$$

The wave overtopping probability P_o may be related to the wet probability P_c at $x = x_c$ where both P_o and P_c are in the range of 0.0 – 1.0. The empirical relation of $P_o = \left[\tanh\left(5P_c\right)\right]^{0.8}$ for the impermeable wet and dry zone in Section 8.1 is adopted to estimate P_o.

For assumed q_o, the landward marching computation of $\overline{h}$, σ_η, $\overline{U}$, and σ_U is initiated using the wet model in Section 6 from the seaward boundary $x = 0$ to the landward limit located at $x = x_r$. The landward marching computation is continued using the wet and dry model in this section from the location of $x = x_{SWL}$ where $\overline{h} = \overline{h}_1$ to the landward end of the computation domain or until the mean depth $\overline{h}$ becomes less than 0.001 cm. The rate q_o is computed using Eq. (141) together with the overtopping probability P_o. This landward computation starting from $q_o = 0$ is repeated until the difference between the computed and assumed values of q_o is less than 1%. This convergency is normally obtained after several iterations. The computed values of $\overline{h}$, σ_η, $\overline{U}$, and σ_U by the two different models in the overlapping zone of $x_{SWL} < x < x_r$ (see Fig. 6) are averaged to smooth the transition from the wet zone to the wet and dry zone.

Kobayashi et al. (2010a) compared CSHORE with S, OS, and O test series explained by Kobayashi and de los Santos (2007) and D' test series by van Gent (2002b). The number of tests for the four test series

was 52. The seaward slope was in the range of 1/5 to 1/2. The nominal stone diameter D_{n50} varied from 0.49 to 4.23 cm. The maximum vertical thickness t_a of the armor layer was in the range of 0.49 to 14.0 cm where t_a corresponds to the maximum value of $[z_b(x) - z_p(x)]$ in Fig. 6. The measured porosity of the stone was n_p = 0.5 for S and OS test series. The same value of n_p was used for O and D' test series. The maximum downward seepage velocity w_m estimated using Eq. (127) along with Eq. (121) and ν = 0.01 cm^2/s was in the range of 4.4 to 14.3 cm/s. The still water level S, root-mean-square wave height $H_{\rm rms}$, and spectral peak period T_p measured at the offshore boundary $x = 0$ for each test were specified as input to the numerical model.

Initially, the downward momentum flux was neglected in Eq. (118), corresponding to $\alpha_m = 0$ in Eq. (126). The computed wave overtopping rates for $\alpha_m = 0$ were too large by one order of magnitude, probably because the permeable layer above SWL may not be saturated, and accept larger fluxes of water volume and momentum. The empirical formula developed using the 52 tests was expressed as

$$\alpha_m = \alpha \left(\frac{z_b - z_p}{D_{n50}} \right)^{0.3} \tag{142}$$

where the constant α is the same as α = 2 in Eq. (131) and $\left(z_b - z_p\right) / D_{n50}$ is the local thickness of the permeable layer normalized by the nominal stone diameter. This thickness correction reduces the computed q_o for S and OS test series with $t_a / D_{n50} = 4.1$. For O and D' test series, $\sigma_m \simeq \alpha$ on the thin permeable layer. Eq. (142) ensures $\alpha_m = 0$ in the zone of $z_b = z_p$ and no permeable layer. The measured and computed wave overtopping rates q_o were compared for O, S, OS, and D' test series. The wave overtopping probability P_o was measured for O and D' test series. The agreement for q_o and P_o was mostly within the factor of about 2.

For D' test series, van Gent (2002b) measured the water depth and velocity at five points for each test. Points P1 and P2 were located at the seaward and landward ends of the crest, respectively. Points P3, P4, and P5 were located on the landward slope at elevations of 10, 25, and 40 cm, respectively, below the crest. The measured water depth and velocity at each point were analyzed on the basis of individual wave overtopping events. The values tabulated in his report were the water depth $h_{2\%}$, velocity $U_{2\%}$, and discharge $q_{2\%}$ corresponding to the values exceeded by 2% of the incident 1,000 waves.

For the probability density function $f(h)$ given by Eq. (128), the water depth h_e corresponding to the exceedance probability e is given by

$$h_e = \frac{\bar{h}}{P_w} \ln\left(\frac{P_w}{e} \right) \quad \text{for} \quad P_w > e \tag{143}$$

Using Eq. (131), the water velocity U_e and discharge q_e corresponding to the exceedance probability e are expressed as

$$U_e = \alpha\sqrt{gh_e} + U_s \quad ; \quad q_e = h_e U_e \tag{144}$$

The probability e of $h > h_e$ at given x is not directly related to the probability based on individual overtopping events. The probability 2% used by van Gent (2002b) is assumed to correspond to the range of e = 0.01 – 0.02 where Eq. (143) is not very sensitive to e = 0.01 – 0.02 as long as the wet probability P_w is larger than about 0.1. The computed values of h_e, U_e and q_e based on e = 0.01 where use is made of $e = P_w / 1.1$ if $P_w < 0.011$ so that $\left(P_w / e\right) \geq 1.1$ in Eq. (143), were compared the measured values of $h_{2\%}$, $U_{2\%}$, and $q_{2\%}$ at the five points P1 to P5 for D' test series. The agreement was mostly within the factor of 2, but the hydrodynamic variables in the wet and dry zone are difficult to predict accurately due to the small water depth and larger velocity during intermittent wave overtopping.

9.2 Gravel or stone movement

The sediment transport model for the impermeable sand beach in Sections 5 and 8.2 is modified to predict the deformation of gravel or stone structures on fixed bottom. The probability P_b of gravel or stone movement under the Gaussian velocity U on the permeable bottom is estimated by assuming that the stone movement occurs when the absolute value of the instantaneous velocity U exceeds the critical velocity U_{cb} estimated as

$$U_{cb} = \left[N_c g \left(s-1\right) D_{n50} \right]^{0.5} \tag{145}$$

where s and D_{n50} = specific gravity and nominal diameter of the gravel or stone; and N_c = empirical parameter. If the wave height H_c corresponding to U_{bc} is given by $H_c = U_{bc}^2 / g$, Eq. (145) yields $N_c = H_c / \left[\left(s-1\right) D_{n50}\right]$ and N_c may be regarded as the critical stability number for the stone which is of the order of unity (Kobayashi et al. 2003). Eqs. (49) and (107) - (109) are based on the critical Shields parameter $\Psi_c = 0.05$ for the initiation of sand movement. The two parameters are related by $N_c = 2\Psi_c / f_b$, and these equations for the probability P_b are applicable using $\Psi_c = 0.5\, f_b N_c$. The value of N_c is calibrated as N_c = 0.7 using the damage progression tests of a stone structure with s = 2.66 and D_{n50} = 3.64 cm conducted by Melby and Kobayashi (1998). The probability of stone suspension is estimated using Eqs. (50) and (110) - (112), where the stone fall velocity w_f is estimated using $w_f = 1.8\left[g \left(s-1\right) D_{n50} \right]^{0.5}$ for a sphere (e.g., Jiménez and Madsen 2003). For the stone with s = 2.66 and D_{n50} = 3.64 cm, w_f = 1.4 m/s and the computed probability of suspension of this stone is essentially zero. The stone armor units are assumed to move like bedload particles. For the computation for arbitrary stone or gavel, suspended load is included to allow the comparison of bed load and suspended load. The formulas for bed load and suspended load are assumed to be the same for sand, gravel, and stone in which the permeability and roughness differences are accounted for in the hydrodynamic models for the impermeable and permeable bottoms. CSHORE cannot predict the movement of sand and stone (or gravel) simultaneously.

The time-averaged volumetric rate q_b of stone transport in the wet zone is estimated using the formula

for bedload given by Eq. (116) which is modified as

$$q_{bx} = bP_b G_s B_r \sigma_U^3 / \left[g(s-1) \right] \quad ; \quad B_r = \left(\frac{z_b - z_p}{D_{n50}} \right)^m \le 1 \tag{146}$$

where b = bedload parameter specified as b = 0.002 as discussed below Eq. (57); G_s = function of the bottom slope given by Eqs. (58) and (59); B_r = reduction factor due to limited stone availability; m = empirical parameter; and σ_U = velocity standard deviation representing the wave action on the stone. The rate q_{bx} becomes negative (offshore) on the steep slope with $G_s < 0$. The reduction factor B_r was added by Kobayashi et al. (2010a) to account for the thickness $(z_b - z_p)$ of the stone layer, where $B_r = 1$ if $(z_b - z_p) > D_{n50}$ and $B_r = 0$ in the zone of $z_b = z_p$ and no stone. The computed profile changes were found to be insensitive to the parameter m in the range of 0.5 to 2.0. The value of m = 1.0 was adopted. The rate q_{bx} of stone transport in the wet and dry zone is also estimated using Eq. (146) where the parameter b is chosen so that the values of q_{bx} computed for the two different zones are the same at the still water shoreline located at $x = x_{\mathrm{SWL}}$. The computed cross-shore variations of q_{bx} in the two zones are averaged in the overlapping zone of $x_{\mathrm{SWL}} \le x \le x_r$ for the smooth transition between the two zones. The temporal change of the bottom elevation z_b is computed using the conservation equation of gravel or stone volume in the same way as in Section 8.2. A fixed impermeable bottom can be located below sediment including stone at the elevation $z_p(x)$. To limit sediment suspension for the case of limited sediment supply, the suspended sediment volume V_s given by Eq. (51) and (113) is multiplied by B_r as well. The suspended sediment transport rates q_{sx} and q_{sy} given in Eqs. (52) and (115) are proportional to V_s.

Comparison was made of the three damage progression tests by Melby and Kobayashi (1998). The armor stone was placed in a traditional two-layer thickness with the seaward slope of 1/2. The armor stone was characterized by D_{n50} = 3.64 cm, s = 2.66, and n_p = 0.4 where the maximum seepage velocity was w_m = 8.7 cm/s using Eq. (127). The thickness of the armor layer was 7.3 cm. The test duration was in the range of 8.5 to 28.5 h. The numerical model overpredicted the deposited area below SWL at the end of the test mostly because it does not account for discrete stone units dislodged and deposited at a distance seaward of the toe of the damaged armor layer. The eroded area above SWL was predicted better. The temporal variation of the eroded area A_e was compared using damage S_e defined as $S_e = A_e / D_{n50}^2$. The numerical model predicted the damage progression well partly because the critical stability number N_c introduced in Eq. (145) was calibrated to be N_c = 0.7 for the three damage progression tests. The temporal variations of S_e computed for N_c = 0.7 and 0.6 were fairly sensitive to N_c.

Kobayashi et al. (2011) compared CSHORE with four gravel beach evolution tests conducted in the wave flume. The median gravel diameter was 2.0 mm and the fall velocity was 25 cm/s. The profile changes of two erosion tests on a steep slope of 1/2 were predicted well by CSHORE with N_c = 0.7. The accretional change on a mild slope of 1/5 and the onshore bar migration and formation of an equilibrium gravel beach profile were reproduced sufficiently after the bedload parameter b in Eq. (146) was increased to b = 0.002 (1 + 8Q) where Q is the fraction of breaking waves given by Eq. (38) in the wet

zone and $Q = 1$ in the wet and dry zone. The bed load formula for onshore gravel and stone transport is still uncertain and will need to be improved using additional laboratory and field data.

The numerical model shown in Fig. 6 is limited to the seaward wet zone and the wet and dry zone above SWL. Kobayashi et al. (2013c) extended the model to the landward wet zone to predict the temporal variations of the damage and wave transmission of a reef breakwater during a storm. Intermittent plunging water produces complex hydrodynamics in the landward wet zone. The mean $\overline{\eta}$ and standard deviation σ_η for the free surface elevation η in the landward wet zone are simply assumed to be constant and the same as those computed at the landward end of the wet and dry zone. The mean $\overline{U}$ and standard deviation σ_U of the cross-shore velocity U are computed using the continuity Eq. (65) and the linear wave relation between η and U given by Eqs. (31) and (32). The mean $\overline{V}$ and standard deviation σ_V of the longshore velocity V are assumed to be negligible. The cross-shore and longshore stone transport rates in the landward wet zone are computed using the formulas used in the seaward wet zone. The extended model was compared with the 148 tests of Ahrens (1989) for a reef breakwater with a narrow crest at or above SWL in which the narrow crest was lowered by wave action. The numerical model simulates the transition from an emerged crest to a submerged crest. The model was also compared with the experiment of Ota et al. (2006) on a wide-crested submerged breakwater in which the crest height increased during 20-h wave action. The damage, crest height, and wave transmission coefficient were predicted reasonably well, but the damaged profile was not predicted accurately. The rudimentary model for the landward wet zone will need to be improved with the aid of detailed measurements in the zone of plunging water above the landward slope.

Garcia and Kobayashi (2015) applied the numerical model extended to the landward wet zone to examine the spatial variation of damage on different sections of the trunk and head of a low crested stone structure under normally and obliquely incident irregular waves. The computed wave transmission coefficient and damage on the front slope, back slope, and total section of the trunk were compared with the 188 tests of Vidal and Mansard (1995) and Kramer and Burcharth (2003). Similarity of trunk and head damage for the low-crested breakwater was proposed to predict damage on the front head and back head using the numerical model for the trunk. The agreement was mostly within a factor of 2 after the calibrations of N_c = 0.6 in Eq. (145) and $\tan\phi = 0.54$ in Eqs. (58) and (59). The numerical model may not be very accurate but provides an additional tool for the design of low-crested stone structures based on laboratory experiments (Burcharth et al. 2006). A numerical wire mesh was created to mimic the wire mesh used by Vidal and Mansard (1995) who examined the stability of different stone sizes on the front slope, crest, and back slope of a low crested rubble mound structure. This numerical wire mesh will need to be tested for practical applications.

10. CSHORE Extensions during 2014 – 2022

The components of CSHORE 2013 in Sections 4 – 9 were developed for common coastal engineering applications in the U.S., such as dune erosion and overwash; beach erosion and recovery; wave runup, overtopping, and transmission over coastal structures; damage to rubble mound breakwaters. The CSHORE extensions during 2014 – 2022 were aimed at other specific applications of practical importance but limited knowledge. The extensions are separated into the following five themes: (1) woody plants and piles; (2) dike and clay erosion; (3) barrier beach overtopping and bay flooding; (4) sand and stone interactions; and (5) intertidal mudflat. The CSHORE extension for the given theme is explained in such a way that coastal engineers and scientists may be able to judge the applicability of each CSHORE extension to their specific problems. The details of each CSHORE extension are available in the journal publications cited in the following. Conference papers are omitted because some conferences do not require printed papers nowadays. Research reports authored by graduate students and visiting researchers are included because the research reports published by the Center for Applied Coastal Research (CACR), University of Delaware, are posted on the CACR webpage (www.coastal.udel.edu).

10.1 Effects of woody plants and piles on dune erosion and overwash

Vegetation may be present on natural beaches, and buildings may exist on urban beaches. A cluster of discrete objects modify waves and currents and affect beach profile changes during storms. Interactions of waves and aquatic vegetation (e.g., kelp) were investigated earlier (e.g., Kobayashi et al. 1993). Kobayashi et al. (2013a) conducted five tests in a wave flume to examine the effects of wooden dowels (idealized tree stems) on erosion and overwash of high and low sand dunes. A wide vegetation covering the high dune reduced scarping, prevented wave overtopping initially, and reduced sand overwash after initiation of wave overtopping. A wide vegetation zone covering an entire low dune reduced dune erosion by retarding wave uprush and reducing wave overtopping and overwash. Ayat and Kobayashi (2015) conducted additional four tests to examine the placement density and toppling effects of the dowels. The effectiveness of the dowels in reducing dune erosion and overwash decreased significantly with the density decrease and dowel toppling. Ayat and Kobayashi (2015) extended CSHORE to include the drag force acting on the dowel. The drag coefficient was calibrated within the range of 1 – 2 on the basis of available wave force data for a single plie (Tørum 1989). The cross-shore variations of the mean and standard deviation of the free surface elevation and cross-shore velocity were predicted within errors of about 20%. The profile evolutions of the dunes with and without dowels were predicted within a factor of about 2. The effectiveness of the wide dowel zone covering the high and low dunes in reducing the wave overtopping and sand overwash rates were also reproduced, but these small rates are difficult to predict accurately. The details of these two studies were published in the following CACR reports:

- Gralher, C., Kobayashi, N., and Do, K. (2012). "Experiments on wave overtopping and overwash of bare and vegetated dunes." Res. Rep. No. CACR-12-05, Center for Applied Coastal Res., Univ. of Delaware, Newark, Del. (Master's thesis by Christine Grahler).
- Ayat, B., and Kobayashi, N. (2013). "Expansion of numerical model CSHORE to predict erosion and overwash of wooded dunes." Res. Rep. No. CACR-13-07, Center for Applied Coastal Res., Univ. of

Delaware, Newark, Del. (Berna Ayat was visiting researcher).

Quan and Kobayashi (2015) examined the utility of a pile fence in reducing dune erosion and overwash during a storm. Six tests were conducted to compare the effectiveness of six different pile fences. The experiment suggested that the pile fence with a porosity of about 0.5 should be placed near the toe of the dune foreslope with a sufficient burial depth to avoid toppling. The fence porosity is defined as the fraction of alongshore opening encountered by uprush and downrush. The measured time series were used to propose the exceedance probability distributions of the free surface elevation and onshore velocity. The measured extreme values (5%, 1%, and 0.013% exceedance probabilities) were predicted by CSHORE with about 20% errors. The measured dune crest lowering in the presence of pile fence was predicted fairly, but the steep scarped foreslope was underpredicted. The detail of this study was published in the following CACR report:

- Quan, R., and Kobayashi, N. (2014). "Numerical modeling of wave overtopping and overwash of dune fronted with pile fence." Res. Rep. No. CACR-14-09, Center for Applied Coastal Res., Univ. of Delaware, Newark, Del. (Master's thesis by Rebecca Quan).

Shore protection projects require the prediction of coastal storm damage and economic loss. Cárdenas and Kobayashi (2017) conducted 11 tests on a sand beach to examine the movement of 10 wooden blocks (floatable objects) placed on the foreshore and berm as well as short and long pilings. The initial block elevation above the sand surface had little effect on the hydrodynamics, sediment transport, and profile evolution in this experiment with widely-spaced blocks. The block floating (by buoyancy force) and sliding (by wave drag force) on the sand surface and the block falling from the pilings depended on the swash hydrodynamics and block clearance above the foreshore and berm whose profile varied during each test. A simple probabilistic model was developed to estimate the immersion, sliding, and floating probabilities for the blocks in the swash zone. The predicted probabilities are compared with the observed cross-shore variation of the block response on or above the accretional and erosional beach profiles which influenced the block response noticeably. The detail of this study was published in the following CACR report:

- Cárdenas, C.X., and Kobayashi, N. (2015). "Experiment on sliding and floating of wooden blocks in swash zone on sand beach." Res. Rep. No. CACR-15-08, Center for Applied Coastal Res., Univ. of Delaware, Newark, Del. (Xavier Chávez Cárdenas was visiting Ph.D. student).

10.2 Erosion of grassed dike and consolidated cohesive sediment

Large-scale laboratory experimental and field studies were performed to understand the erosion processes of grassed earthen dikes (levees) mostly in the Netherlands (Steendam et al. 2010, 2012). Kobayashi and Weitzner (2015) developed a dike erosion model to predict the evolution of the eroded dike profile during a storm. The developed model was calibrated and verified using available data (Smith et al. 1994; Wolters et al. 2008). The resistance force of the turf per unit horizontal area is denoted as (ρR) where ρ = fluid density and R = resistance force divided by ρ so that its unit is $(\text{m/s})^2$. The value of $\sqrt{R}$ is the

velocity scale for the resistance force. The rate of erosion work is expressed as the product of the resistance force and the rate of the vertical erosion depth increase. The rate of erosion work is assumed to be provided by the wave energy dissipation rates per unit horizontal area due to wave breaking and bottom friction. This assumption is analogous to Eq. (51) based on the rate of work required to keep falling sediment particles in suspension. For the dike turf, the resistance parameter R is assumed to decrease linearly from the turf surface to the underneath clay and remain constant in the clay layer. The turf thickness is typically about 0.1 m. The calibrated values of R based on full-scale testing were 1,000 and 200 $(m/s)^2$ for good (dense roots) and poor grass covers, respectively, and 10 $(m/s)^2$ for boulder clay with a network of cracks formed under long-term weathering (Kobayashi and Weitzner 2014). The detail of this study was published in the following CACR report:

- Weitzner, H., and Kobayashi, N. (2014). "Modeling of grassed levee erosion by wave action." Res. Rep. No. CACR-14-01, Center for Applied Coastal Res., Univ. of Delaware, Newark, Del. (Master's thesis by Heather Weitzner).

Kobayashi and Zhu (2020) formulated the erosion processes of consolidated cohesive sediment (glacial till) under irregular breaking waves to predict the profile evolution of a cohesive sediment beach with a layer of sand. The dike erosion model with no turf above the clay layer is used to predict the erosion of consolidated cohesive sediment containing cohesionless sediment (sand). Sand released from the eroded sediment is transported onshore or offshore by wave action. The cohesive sediment erosion is increased by the abrasive effect of a thin mobile sand layer and decreased by the protective effect of a thick sand layer. The sand layer evolution on the impermeable cohesive sediment is predicted using the sand transport model in Sections 5 and 8 including the limited sand availability represented by the reduction factor B_r in Eq. (146). This extended CSHORE was compared with the flume experiment data by Skafel (1995) who used till blocks excavated from a site on the north shore of Lake Erie. The measured till erosion rates were on the order of 0.05 cm/h. The calibrated R for the glacial till was 30 $(m/s)^2$ in comparison to 10 $(m/s)^2$ for the boulder clay with a network of cracks. The detail including applications was published in the following CACR report:

- Zhu, T., and Kobayashi, N. (2019). "Erosion of consolidated cohesive bottom containing cohesionless sediment by wave action on beaches." Res. Rep. No. CACR-19-01, Center for Applied Coastal Res., Univ. of Delaware, Newark, Del. (Part of Ph.D. dissertation by Tingting Zhu).

  Appendix B includes examples of the input and output of CSHORE computations in this report.

Zhu and Kobayashi (2021a) investigated soft cliff (bluff) erosion using the wave basin data by Damgaard and Dong (2004) and the cross-shore model CSHORE for dune erosion (Kobayashi et al. 2009a, 2010b). The measured cliff recession rates under oblique breaking waves for cliffs built of wet sand (no clay) in 15 tests could be reproduced by CSHORE with a single cross-shore line and a new option that accounts for sand loss associated with the alongshore gradient of longshore sand transport in Eq. (61) using an equivalent alongshore distance (dimensional calibration parameter). The effect of sediment cohesion on cliff erosion was examined using CSHORE extended to cohesive sediment containing sand (Kobayashi and Zhu 2019). Damgaard and Dong (2004) included one test with a sand/clay mixture (9.2% clay). The

calibrated R for this mixture 1 $(m/s)^2$ and the computed cliff recession rate for $R<1$ $(m/s)^2$ was limited by the removed rate of sand deposited at the toe of the eroding bluff. The detail of this study was published in the following CACR report:

- Zhu, T., and Kobayashi, N. (2019). "Numerical study on erosion of soft cliff by oblique breaking waves on cohesionless and cohesive beach." Res. Rep. No. CACR-19-05, Center for Applied Coastal Res., Univ. of Delaware, Newark, Del. (Part of Ph.D. dissertation by Tingting Zhu).
  Appendix C includes examples of the input and output of CSHORE computations in this report.

10.3 Wave overtopping of barrier beach and bay flooding

Low-laying barrier beaches and islands are common along the U.S. East Coast and the Gulf of Mexico. Wave overtopping of a low-laying sand barrier may increase the water level in an enclosed bay or lagoon. CSHORE was used to predict wave overtopping and overwash of dunes (Figlus et al. 2011, Johnson et al. 2012) but the destination of overtopped water was not computed. Kobayashi et al. (2013c) extended CSHORE to the landward wet zone and computed wave transmission over and through a porous breakwater. For an emerged sand barrier, the still water levels in the ocean and bay may be different and wave overtopping can increase the bay water level. Kobayashi and Zhu (2017) computed wave overtopping and overwash over the barrier beach between the Atlantic Ocean and the Rehoboth Bay in Delaware during Hurricane Sandy in 2012 where the measured still water level in the bay was specified as the landward boundary condition. The barrier beach was eroded but remained above the ocean and bay still water levels. The computed wave overtopping rate per unit width on the order of 0.1 m^2/s (100 l/s/m) may have increased the peak bay water level by 0.1 – 0.2 m (10% – 20%). The detail of this study including an analytical model for the peak bay water level was published in the following CACR report:

- Zhu, T., and Kobayashi, N. (2017). "Flooding of Indian River Bay and Rehoboth Bay through Indian River Inlet and by wave overtopping of barrier beach." Res. Rep. No. CACR-17-01, Center for Applied Coastal Res., Univ. of Delaware, Newark, Del. (Master's thesis by Tingting Zhu).
  Appendix A includes examples of the input and output of CSHORE computations in this report.

10.4 Sand transport on and inside porous stone structures

Low rock structures have been constructed on some beaches to reduce storm-induced damage to backshore areas, but no design guideline is available to design such structures. Kobayashi and Kim (2017) conducted four tests in a wave flume with a sand beach and a berm to compare the effectiveness of a narrow dune and a rock (stone) seawall placed on the foreshore in reducing wave overtopping and sand overwash. The dune was effective in eliminating or reducing wave overtopping compared with the corresponding berm with no dune, but the narrow dune was destroyed easily as the water level was increased. The stone seawall was effective in reducing wave overtopping and overwash even after it was deformed by stone settlement. A stone seawall buried inside a dune functioned like the dune initially and like the seawall after the sand on and inside the porous seawall was eroded by overtopping waves. CSHORE was extended to predict sand transport on and inside the porous structure. The fabric filter

under the rock seawall was assumed to be fixed because sand transport processes under the filter were unknown. The simple extension of CSHORE was based on the conservation of sand volume in the pores of the stone structure as well as an empirical reduction factor for sand mobility in the pores. The extended CSHORE predicted little sand deposition inside the exposed seawall and extensive sand removal from the buried seawall. However, the agreement with the profile data in the vicinity of the seawall was marginal partly because of the assumption of no settlement of the seawall. The detail of this study was published in the following CACR report:

- Kim, H.D., Kobayashi, N., and Cárdenas, C.X. (2017). "Experimental and numerical study on rock seawall in swash zone to reduce wave overtopping and overwash of sand beach." Res. Rep. No. CACR-17-02, Center for Applied Coastal Res., Univ. of Delaware, Newark, Del. (Master's thesis by Hyun Dong Kim).

Yuksel and Kobayashi (2020) conducted three tests in a wave flume to compare sand beach profile evolution and wave overtopping of a sand berm for the cases of no structure, a stone revetment protecting the steep sand berm, and a stone sill reducing wave action on the berm. The same stones were used to construct the revetment and sill. The revetment reduced onshore sand transport on the sand beach in front of the revetment and was effective in protecting the sand berm and reducing wave overtopping. The settlement of the revetment placed on a filter occurred, and the revetment crest was damaged during major wave overtopping. The sill reduced the beach profile change but was not very effective in reducing wave overtopping and berm erosion when the sill crest was submerged sufficiently. Piled stones on the narrow sill crest were displaced. The lowered and wider crest became stable. The settlement of the sill placed on the filter did not occur, perhaps because the sill was placed on the stable section of the beach in the test of no structure. CSHORE was upgraded for its application to the sill test where the emerged sill crest became submerged during the test. The reduced beach profile changes in the presence of the revetment and sill were reproduced, but CSHORE could not produce sufficient onshore sand transport near the shoreline. The upgraded CSHORE included an option of no filter to predict the settlement of the stone structure caused by sand erosion below the structure and estimate the settlement reduction provided by the filter. The filter in the revetment test may have reduced the revetment settlement by about 0.1 m. For the sill test of no filter settlement, the settlement reduction provided by the filter was computed to be small. The upgraded CSHORE may be used to estimate the degree of the stone structure settlement for the case of no filter and the beach profile change in the vicinity of the stone structure placed on the filter. The detail of this study was published in the following CACR report:

- Yuksel, Z.T., and Kobayashi, N. (2019). "Experiment and numerical modeling for revetment and sill in reducing shore erosion and wave overtopping." Res. Rep. No. CACR-19-04, Center for Applied Coastal Res., Univ. of Delaware, Newark, Del. (Z. Tugce Yuksel was visiting postdoctoral researcher).

Zhu and Kobayashi (2021b) investigated irregular wave overwash and landward migration of a narrow sand barrier in a wave flume. The emerged crest of a sand barrier was lowered rapidly to the still water level (SWL) and migrated landward slowly with its crest slightly below the SWL. A rock mound consisting of three layers of stable stones was constructed on the submerged sand barrier without any

filter. The rock mound settled but its crest remained above the SWL. The landward migration of the sand barrier was reduced only partially because of onshore sand transport over and through the porous structure. The sand barrier was rebuilt with a rock cover on the crest of the initial sand barrier. The rock cover consisting of a single layer of stable stone reduced the sand barrier deformation only slightly because the stone settlement and spreading exposed underlying sand to direct wave action. CSHORE was compared with the three tests (no rock, rock mound, and rock cover). The mean and standard deviation of the free surface elevation and cross-shore velocity were predicted within errors of 20% as in previous comparisons except that small transmitted waves were difficult to predict accurately. The barrier profile evolution was predicted marginally because of the difficulty in predicting the cross-shore variation of the sand transport rate over the barrier crest and through the porous structure. The detail of this study was published in the following CACR report:

- Zhu, T., and Kobayashi, N. (2021). "Experiment and numerical modeling of rock mound to reduce wave overwash and crest lowering of a sand barrier." Res. Rep. No. CACR-21-01, Center for Applied Coastal Res., Univ. of Delaware, Newark, Del. (Part of Ph.D. dissertation by Tingting Zhu).

  Appendix D includes examples of the input and output of CSHORE computations in this report.

10.5 Intertidal mudflat profile evolution under waves and currents

For typical prototype CSHORE computations, tide effects are included in the input time series of the still water level at the seaward boundary located in water depth of about 10 m. For a macrotidal beach with a gentle bottom slope, the large temporal change of water volume in the computation domain produces measurable cross-shore tidal currents. Do et al. (2016) analyzed 17-day field data in Korea to investigate the cross-shore wave transformation, currents, and sand suspension in the intertidal zone, and beach profile changes of a macrotidal beach with a gentle slope of 0.02 and tidal ranges of 4 – 7 m. The measured beach profile changes were less than 0.5 m despite the occurrence of two consecutive storms with significant wave heights exceeding 2 m. CSHORE including cross-shore tidal current in Eq. (19) was shown to reproduce the gradual wave height decay in the migratory surf zone, the cross-shore current of the order of 0.1 m/s affected by flood and ebb tides, the suspended sand volume varying with the tidal cycle, and the small beach profile changes. CSHORE can predict the morphology of the macrotidal sand beach.

Mudflat morphology is poorly understood due to complex cohesive sediment dynamics. The mudflat is normally composed of a mixture of sand and mud. Miranda and Kobayashi (2022) extended CSHORE to the sand and mud mixture and predicted the erosional and accretional mudflat profile changes measured almost monthly by Yamada and Kobayashi (2004) from 03 July 2001 to 08 August 2002. The field site was located on the coast of Ariake Bay in Japan. The cross-shore survey line was marked by 30 wooden stakes driven into the mudflat at an interval of 50 m. The mudflat elevation could always be measured for the survey points located between 100 and 1,050 m from the seawall near the mouth of Shirakawa River. The average significant wave height and period were 0.2 m and 3 s, respectively, because of the limited fetch lengths in this closed shallow bay. The tide is semidiurnal and the average tidal range was 2.88 m.

The moving averaged water level revealed the yearly oscillation of 0.4 m in height where this water level was higher in summer and lower in winter. The sediment characteristics within 2 m below the mudflat surface were fairly uniform perhaps because of bioturbation. The sand mass, mud mass including organic matters, and water mass per unit volume of the mixed sediment were approximately 400 kg/m^3, 400 kg/m^3, and 500 kg/m^3, respectively. The sediment characteristics are assumed to remain constant during the computation interval. The sand and mud interactions are neglected. The sediment transport model in Section 5 is used to predict the cross-shore and longshore sand transport rates. Mud is assumed to be transported as suspended load. The mud transport rate is estimated by modifying the formula for suspended sand transport in CSHORE.

For the comparison of extended CSHORE with the intertidal mudflat data, the semidiurnal migration of the still water shoreline and surf zone is resolved numerically to predict the net cross-shore and longshore sediment transport rates influenced by the small cross-shore (undertow) and longshore currents induced by breaking waves of about 0.2 m height. Alongshore sediment loss or gain is included by approximating the alongshore sediment transport gradient using an equivalent alongshore length in Eq. (63). The calibrated CSHORE reproduces the measured erosional (accretional) profile change of about 0.1 m (0.1 m) over the cross-shore distance of 950 m during the erosional (accretional) interval of 206 (195) days. The mudflat profile changes are equally affected by mud characteristics, the semidiurnal tide amplitude, and the wave height, period, and direction. In addition, the alongshore water level gradient in Eq. (23) and wind stress in Eqs. (22) and (23) influence longshore current and sediment transport. This study shows the importance of sediment transport in the surf zone which may have been excluded in previous numerical modeling of intertidal mudflat profile evolution. The details of the CSHORE extension, computation, and comparison were published in the following CACR report:

- Miranda, P.S., and Kobayashi, N. (2022). "Numerical modeling of intertidal mudflat profile evolution under waves and currents." Res. Rep. No. CACR-22-01, Center for Applied Coastal Res., Univ. of Delaware, Newark, Del. (Master's thesis by Paterno S. Miranda).

11. Computer Program CSHORE2022

The computer program CSHORE was documented by Kobayashi (2009, 2013). The theories and formulas in CSHORE were explained in the review paper by Kobayashi (2016). This report includes all the options added in CSHORE up to 2022.

The computer program CSHORE2022 is explained sufficiently so that users will be able to use it effectively and modify it if necessary. CSHORE2022 provides various options but only certain combinations of the options have been applied and verified in the publications in Sections 2 and 10. Enough explanations are provided in the computer program so that users will be able to follow the computer program with additional explanations provided in the following. It is noted that the symbols used in this section are based on those used in the computer program rather than those used in the previous sections.

11.1 Main program

The wave action equations (36) and (66), the momentum equations (22) and (23), and the roller energy equation (41) and the equations (101), (104), (138), and (140) for the mean water depth $\bar{h}$ in the wet and dry zone are solved using the finite-difference method with constant nodal spacing Δx of a sufficient resolution in very small water depth. The use of constant small Δx may be justified because CSHORE is very efficient computationally and the use of constant Δx reduces the input preparation time. It is noted that the governing equations (22), (23), (36), (41) and (66) divided by (ρg) are solved in the main program so that the fluid density ρ does not appear in the resulting equations.

The differential equations solved numerically can be expressed in the form

$$\frac{dy}{dx} = f(x, y)$$

where x = cross-shore coordinate, positive onshore; y = unknown variable that needs to be computed; and f = known function of x and y. The computation marches landward from the given x to the next nodal location at $(x + \Delta x)$. An improved Euler method of second-order accuracy (e.g., Chaudhry 1993) is used to approximate the above equation as follows:

$$\text{Predictor: } y^*_{j+1} = y_j + f(x_j, y_j)\Delta x$$

$$\text{Corrector: } y_{j+1} = y_j + \frac{1}{2}\left[f(x_j, y_j) + f(x_{j+1}, y^*_{j+1}) \right]\Delta x$$

where the subscripts j and $(j+1)$ indicate the nodes located at x_j and $x_{j+1} = (x_j + \Delta x)$ and the superscript star denotes a temporary value of y_{j+1} at node $(j+1)$. The wave action equation (36) or (66) for the free surface standard deviation σ_η, the cross-shore momentum equation (22) for the wave setup $\bar{\eta}$, and the roller equation (41) for the roller volume flux q_r are solved using this Euler method.

On the other hand, the longshore momentum equation (23) is approximated by an implicit finite-difference method, which is more stable numerically, to obtain the longshore bottom shear stress τ_{by} at node $(j+1)$ and the corresponding longshore current $\overline{V}$ at node $(j+1)$.

In reality, the four unknown values of σ_η, $\overline{\eta}$, $\overline{V}$, and q_r at node $(j+1)$ involved in the four differential equations are computed in sequence and iteratively. The mean water depth $\overline{h}$ given by Eq. (1) is uniquely related to the wave setup $\overline{\eta}$ for the given storm tide S and bottom elevation z_b. The convergence of the iteration is based on the difference between the computed and guessed values where the metric units are used in the computer program and the gravitational acceleration g = 9.81 m/s^2. The difference for σ_η (m), $\overline{h}$ (m), and $\overline{V}$ (m/s) must be less than EPS1, whereas the difference for q_r (m^2/s) must be less than EPS2. The maximum number of the iteration is MAXITE. The DATA statement in the main program specifies EPS1=10^{-3}, EPS2=10^{-6}, and MAXITE=20 where double precision is used in the entire program. It is noted that q_r involves the product of the length and velocity.

The only input in the main program is as follows:

```
                WRITE(*,*) 'Name of Primary Input-Data-File?'
C               READ(*,5000) FINMIN
                FINMIN = 'infile'
      5000      FORMAT(A12)
```

where FINMIN corresponds to the name of the input file which will be read later before the computation. In order to eliminate this input, the name of the input file is specified as ***infile*** in CSHORE.

11.2 Subroutines

Subroutines are arranged in numerical order after the main program in order to indicate the location of each subroutine in the computer program. The numerical order approximately corresponds to the chronology of the CSHORE development summarized in Sections 2 and 10.

Subroutine 1 **OPENER** opens all input and output files. The input file with its name = FINMIN is assigned to unit=11 for the READ statement. The names of the output files start with the letter O. The output file ODOC (unit=20 for the WRITE statement) is used to store the input (to check the accuracy of the input file) and the summary of the computed results (to check the overall appropriateness of the computed results and to compare with measurements such as wave runup and overtopping rates). The output file OMESSG (unit=40) stores warning and error messages generated during the computation. These messages must be examined carefully if the computed results appear questionable. The other output files are explained in Section 11.4.

Subroutine 2 **INPUT** reads the contents of the input file FINMIN as explained in detail in section 11.3. The gravitational acceleration g is specified as GRAV=9.81 m/s^2 in the DATA statement.

Subroutine 3 **BOTTOM** calculated the bottom elevation $z_b(x_j)$ with $x_j = (j-1)\Delta x$ at node j using the input bottom elevations specified at a number of cross-shore locations. The nodal spacing Δx is read from the input file. Use is made of linear interpolation and smoothing to reduce sharp corners that tend to cause numerical irregularity. This subroutine also computes the integer JMAX which is the number of total nodes along the bottom in the computation domain as well as the cross-shore bottom slope S_{bx} of the smoothed z_b. If the bottom is permeable or the sediment layer thickness is thin, the lower impermeable boundary elevation z_p of the permeable or thin sediment layer (see Figs. 2 and 6) is calculated in the same way as z_b. The thickness h_p of the layer is obtained using $h_p = (z_b - z_p) \geq 0$. For the permeable layer, h_p is the thickness of porous flow. For the thin sediment layer, h_p is the available deposited sediment volume per unit horizontal area and $h_p = 0$ implies no sediment above z_p.

Subroutine 4 **PARAM** computes constant parameters before the landward marching computation. Eqs. (68) and (69) are used to compute the values of α_p, β_1, and β_2 using the default values of ν = 10^{-6} m^2/s, α_0 = 1000 and β_0 = 5. The default value of $\alpha = 2$ (α = 1.6 to compute the profile evolution of an impermeable sand dune) in Eqs. (92) and (131) for the wet and dry zone is specified and the value of B defined in Eq. (97) and other constant parameters are calculated. The exceedance probability *e* = EWD introduced in Eq. (143) specified as 0.015 for an impermeable bottom and 0.01 for a permeable bottom on the basis of the comparison with the data of Van Gent (2002b).

Subroutine 5 **LWAVE** solves the dispersion relation for linear waves given by Eq. (2) which is rewritten in terms of $x = k\bar{h}$

$$x - D\left(1 - \frac{T_p Q}{2\pi \bar{h}^2} x\right)^2 \coth(x) = 0$$

with

$$D = k_o \bar{h} \quad ; \quad Q = Q_x \cos\theta + Q_y \sin\theta$$

where T_p = representative wave period at $x = 0$ specified as input; $\bar{h}$ = mean water depth at given node; k_o = deep water wave number given by $k_o = (2\pi)^2 / (g T_p^2)$ calculated in subroutine 4 PARAM or at the end of the main program if additional wave conditions are specified as input at the seaward boundary $x = 0$. The above equation is solved using the Newton-Raphson method (e.g., Press et al. 1989). After the wave number $k = x / \bar{h}$ is obtained, the linear wave quantities such as those defined in Eq. (3) are computed and the wave angle θ for obliquely incident waves is calculated using Eq. (21). CSHORE provides the option of IWCINT=0 or 1. IWCINT=0 corresponds to the case of no wave and current interaction, which was assumed in the earlier version of CSHORE developed for the condition of no or little wave overtopping. IWCINT=1 corresponds to the present version of CSHORE which allows considerable wave overtopping and overflow. If IWCINT=0, the terms involving Q_x and Q_y in Eqs. (2), (22), (23), (36) and (66) are neglected and $Q = 0$ in the above equation for $x = k\bar{h}$.

Subroutine 6 **GBXAGF** computes G_{bx} and G_f using the approximate equations (46) and (48) for obliquely incident waves and the exact equations given by Kobayashi et al. (2007b) for normally incident waves. The complementary error function *erfc* involved in the exact equations is computed using Function **ERFCC** given by Press et al. (1989). Subroutine 6 **VSTGBY** computes $V_* = \overline{V} / \sigma_T$ for known G_{by} using Eq. (47). The longshore momentum equation (23) is solved numerically to obtain τ_{by} and the corresponding G_{by} is calculated using Eq. (33).

Subroutine 7 **DBREAK** computes the energy dissipation rate D_B due to wave breaking using Eq. (38) and specifies the upper limit of unity for $\sigma_* = \sigma_\eta / \overline{h}$ in the wet zone of very shallow water. The other limit of σ_* introduced for irregular wave transmission over submerged porous breakwaters by Kobayashi et al. (2007b) has been found to be unnecessary for the other applications of CSHORE discussed in Section 2. An option is provided for estimating the breaker ratio parameter γ in Eq. (38) using the empirical formula proposed by Apotsos et al. (2008). This option has been inactivated because the calibration of γ for each experiment or field site is preferable.

Subroutine 8 **OUTPUT** stores most of the computed results in the output files as explained in detail in Section 11.4.

Subroutine 9 **POFLOW** computes the standard deviation σ_p of the discharged velocity in a permeable layer using Eq. (75), the mean cross-shore discharge velocity $\overline{U}_p$ using Eq. (73), and the energy dissipation rate D_p due to flow resistance in the permeable layer using Eq. (71). CSHORE provides the option of IPERM = 0 or 1. IPERM=0 implies an impermeable bottom and this subroutine is not called from the main program. IPERM=1 implies that a permeable layer exists in the computation domain where the permeable layer thickness $h_p = 0$ for impermeable segments next to the permeable segment.

Subroutine 10 **QORATE** is called from the main program after the landward marching computation in the wet zone if the option of IOVER=1 is specified as input to allow wave overtopping and overwash in the computation domain. No wave overtopping is allowed if IOVER=0 and the wave overtopping rate $q_o = 0$ in Eqs. (19) and (65). The wave overtopping rate q_o is obtained by calling subroutine 16 WETDRY. After the convergence of repeated landward computations to obtain q_o, the quantities related to wave runup are computed using the equations in Section 7. Eqs. (143) and (144) are used to compute h_e, U_e, and q_e corresponding to the specified exceedance probability *e*.

Subroutine 11 **SEDTRA** computes the sediment transport quantities in the wet zone using the equations in Section 5 after the landward marching computation of the hydrodynamic quantities is completed. This subroutine is called from the main program only for the option of IPROFL=1, corresponding to a movable bottom. For a fixed bottom, IPROFL=0 must be specified as input. The computation is performed separately for normally incident waves (integer IANGLE=0) and for obliquely incident waves (IANGLE=1) partly because of the CSHORE development history discussed in Section 2 and partly because of no longshore sediment transport for IANGLE=0. The sediment transport quantities in the wet

and dry zone are computed using the equations in Sections 8.2 and 9.2 for IANGLE=0 and 1.

Subroutine 12 **CHANGE** computes the bottom elevation change from the present time level to the next time level using Eq. (61) with $\partial q_y / \partial y = 0$. The finite difference equations for the profile change computation given by Tega and Kobayashi (1999) are of second-order accuracy. The time step Δt for the profile change computation is computed using the numerical stability criterion of the adopted explicit finite difference method. The profile change is computed if IPROFL=1. For the simultaneous computation of multiple cross-shore lines, the bottom profile change due to the alongshore gradient of the longshore sediment transport rate is computed using Eq. (64) when the end of constant water level and wave conditions is reached in Main Program.

Subroutine 13 **INTGRL** integrates a function numerically using a modified Simpson's rule (e.g., Press et al. 1989). This subroutine is used in Subroutine CHANGE to ensure that the computed profile change satisfies the conservation of the sediment volume in the entire computation domain.

Subroutine 14 **SMOOTH** smoothes the cross-shore variation of a variable that depends on x. Simple moving averaging is performed using NPT nodes landward and seaward of a specified node. NPT=0 corresponds to no smoothing. The smoothing of certain variables reduces sudden changes and improves numerical stability. Some variables are smoothed before their storage and plotting. The value of NPT is calculated in Subroutine 03 BOTTOM before the computation and at the end of Main Program during the computation. The calculated value of NPT increases with the ratio between the input wave height and the nodal spacing Δx so that the smoothing distance is more related to the input root-mean-square wave height.

Subroutine 15 **EXTRAPO** called from Subroutine SEDTRA is used to extrapolate a finite sediment transport rate at the landward end node of the computation to zero transport rate on the landward dry zone after the introduction of the scarping algorithm given by Eq. (60). The number of nodes for the extrapolation is specified by NPE. The value of NPE is calculated in a manner similar to the calculation of NPT. If wave overwash is allowed by choosing the option IOVER=1, this subroutine is used only when the landward marching computation stops at the landward limit of the wet zone computation.

Subroutine 16 **WETDRY** computes the hydrodynamic quantities including the wave overtopping rate q_o in the wet and dry zone using the equations in Sections 8.1 and 9.1. Function GBWD following this subroutine computes the value of $G_b(r)$ for given r using Eqs. (98) and (99).

Subroutine 17 **TRANWD** called from the main program and subroutine SEDTRA connects the computed values by the wet model and the wet and dry model in the overlapping zone (see Figs. 5 and 6) because the transition between the two different models is somewhat artificial. The overlapping zone and transition algorithm are discussed at the end of Sections 8.1 and 9.1.

Subroutine 18 **PROBWD** computes the probabilities of sediment movement and suspension using Eqs. (107), (108) and (109) as well as Eqs. (110), (111) and (112) where only the critical fluid velocities U_{cb} and U_{cs} are different in these equations.

Subroutine 19 **TSINTP** interpolates time series specified at given time levels, obtains interpolated time series at different time levels, and converts interpolated time series into time series with stepped temporal changes. This subroutine is created in relation to the option of ILAB=0 or 1 in Subroutine 02 INPUT. For ILAB=0 corresponding to typical field data, the time series of the input wave parameters and water levels can have different time intervals and are read separately as explained in Section 10.3.

Subroutine 20 **PONDED** has been created in response to the laboratory experiment by Figlus et al. (2012) who investigated onshore migration of an emerged ridge and a ponded runnel. If the option of IPOND=1 is specified as input, CSHORE computes the onshore ridge and runnel migration. This subroutine computes the water level in the runnel located landward of the emerged ridge. The computed water level is used to determine whether the water in the runnel is ponded (NOPOND=0) or not ponded (NOPOND=1). For the case of NOPOND=0, the water level in the runnel cannot exceed the emerged ridge crest elevation. The case of no ponding (NOPOND=1) occurs if the ridge becomes submerged below the still water level and the runnel is located seaward of the still water shoreline. For the case of the ponded runnel landward of the still water shoreline, the bedload and suspended sediment transport rates are reduced in the ponded water zone where these sediment transport rates in the wet and dry zone are computed in Subroutine 11 SEDTRA.

Subroutine 21 **WTRANS** computes the mean and standard deviation of the free surface elevation η and depth-averaged horizontal velocity U in the landward wet zone landward of a low-crested, emerged porous structure if the option of IWTRAN=1 is specified as input. This option has been created to predict transmitted waves over and through the porous structure as explained by Kobayashi et al. (2013). This option is also applicable to an impermeable structure and a narrow barrier island (Zhu and Kobayashi 2021b).

Subroutine 22 **EROSON** computes erosion of grassed dike at time level ITIME and along cross-shore line L if IPOROF=2 and ICLAY=0. For ICLAY=1 and IPROFL=1, exposed clay erosion is computed. For IULSTE=1, underlayer stone erosion is computed. The option of IULSTE=1 is still under development.

Subroutine 23 **TRACIN** traces movement of discrete objects (DO) during time step Δt if ITRACE=1. The option of ITRACE=1 is still under development.

11.3 Input

A user of CSHORE must read Subroutine 2 **INPUT** and learn how to prepare the primary input data file. Input parameters and variables were read using the FORMAT statements at the end of Subroutine INPUT in the previous version of CSHORE. A user had to follow the FORMAT requirements so that a correct input value could be assigned to the specific input parameter or variable. This requirement was not convenient, but the resulting input file was orderly and could be checked easily. The free format has been adopted in the present version of CSHORE. In the following, the input parameters and variables are explained in the sequence described in Subroutine INPUT. The examples of the input file and the corresponding output results are presented in Appendices.

- NLINES is the number of comment lines used to identify a specific input file because a number of input files can become large when CSHORE is compared with a number of data sets with different bottom profiles.

- (COMMEN(J), J=1, 14) read for NLINES lines which contain the description of the input file. The comments in these lines do not affect the computed results at all.

Input Computation Options:

- ILINE is the number of cross-shore lines used for the specified computation for given time series of the storm tide and wave height and period at the offshore boundary $x = 0$. The previous version of CSHORE was limited to ILINE=1. ILINE must not exceed the integer NL in the PARAMETER statement where NL=100 is specified and should be sufficient for the alongshore distance of 10 km or less.

- IQYDY = 0 or 1 to neglect or include the alongshore gradient of the longshore sediment transport rate in the beach profile computation using Eq. (64). IQYDY must be specified even for ILINE=1. For the option of IQYDY=1 and ILINE=1, the equivalent alongshore distance y_e (YEADIS) needs to be specified as bottom geometry input. For IPROFL=0 or 2, IQYDY=0 is imposed.

- IPROFL = 0, 1, or 2 for a fixed or movable bottom where the profile evolution is computed for IPROFL=1. Dike erosion is computed only for IPROFL=2. IPROFL must be specified.

- ISEDAV = 0, 1, or 2 (only for IPROFL=1) for unlimited bottom sediment, limited sediment availability by hard bottom, or limited stone availability by wire mesh. ISEDAV=0 is already specified if IPROFL=0 or 2. If IPROFL=1, ISEDAV must be specified. The option of ISEDAV=1 for limited sediment availability has been used for a fixed impermeable bottom including a vertical wall (approximated as a very steep slope). ISEDAV=2 is specifically for wire mesh used to prevent stone erosion

- IPERM = 0 or 1 for an impermeable or permeable bottom where the parameters for the permeable layer must be specified later if IPERM=1. IPERM must be specified. If ISEDAV=2, IPERM=1 is required to specify stone layer characteristics.

- IOVER = 0 or 1 for no wave overtopping or wave overtopping at the landward end of the computation domain where wave overwash and dune profile evolution are computed if IOVER=1 and IPROFL=1. IOVER must be specified. For the computation of dike erosion (IPROFL=2), IOVER=1 predicts erosion of landward dike slope.

- IWTRAN = 0 or 1 for no standing water landward of an emerged crest or wave transmission in the landward wet zone. IWTRAN=0 is already specified if IOVER=0. If IOVER=1, IWTRAN=0 or 1 must be specified. The option of IWTRAN=1 has been created to predict transmitted waves landward of an emerged coastal structure or a barrier island. If the crest is below seaward SWL, the option of IWTRAN=1 and ISWLSL=2 (no water landward of a dike) can be used to predict wave overtopping and overflow on the dike crest (IOFLOW=1) which causes flooding landward of the dike.

- IPOND = 0 or 1 for no or yes for an emerged ridge and a ponded runnel only for IOVER=1 and IWTRAN=0. IPOND=0 is already specified. IPOND=0 or 1 must be specified if IOVER=1 and IWTRAN=0. The option of IPOND=1 has been created to predict the onshore migration of the emerged ridge and ponded runnel.

- INFILT = 0 or 1 for no or yes for water infiltration landward of the crest of a sand dune only for IOVER=1, IPERM=0, and IPROFL=1. INFILT=0 is already specified. INFILT=0 or 1 must be specified if IOVER=1, IPERM=0, and IPROFL=1. The option of INFILT=1 has been created to quantify the infiltration effect on sand dune erosion and overwash. The infiltration effect has been found to be negligible for fine sands but may not be negligible for coarse sands. The permeability effects of gravel beaches and stone structures can be included using the option of IPERM=1.

- IWCINT = 0 or 1 for no or yes for wave and current interactions where the terms involving Q_x and Q_y in Eqs. (2), (22), (23), (36) and (66) for the wet zone are neglected if IWCINT=0. IWCINT must be specified. Wave and current interactions are not negligible if the current velocity becomes as large as the wave phase velocity C. The effect of wave overtopping on the hydrodynamics in the wet and dry zone is included in the models in Sections 8.1 and 9.1.

- IROLL = 0 or 1 for no or yes for roller effects in the wet zone where the roller volume flux $q_r = 0$ and $D_r = D_B$ in Eq. (41) for IROLL=0. IROLL must be specified. The option IROLL=1 improves the prediction of longshore current on a beach, but the roller effects have been found to be negligible for coastal structures with steeper slopes, perhaps because of the limited horizontal distance for roller development. The roller effect in the wet and dry zone may have been included implicitly because of the use of Eq. (92).

- IWIND = 0 or 1 for no or yes for wind effects where the wind stresses τ_{sx} and τ_{sy} on the sea surface are neglected in Eqs. (22) and (23) if IWIND=0. IWIND must be specified. The wind effect is normally small unless the computation domain becomes large and incident waves are small.

- ITIDE = 0 or 1 for no or yes for tidal effects. ITIDE must be specified. If ITIDE=1, the cross-shore volume flux associated with the temporal variation of the still water level is included in Eq. (19) and the term associated with the alongshore gradient of the mean water level is added in Eq. (23) to simulate the longshore tidal current.

- IMUD = 0 or 1 for no mud or mixed mud and sand in bottom sediment. IMUD=0 is already specified if ITIDE=0. If ITIDE=1, IMUD=0 or 1 must be specified. The option of IMUD=1 is created to predict intertidal mudflat profile evolution.

- IVEG = 0, 1, or 2 for no or yes for vegetation effects. IVEG must be specified. IVEG=0 represents no vegetation effect (or vegetation is included in the increased bottom friction factor FBINP). For the option of IVEG=1, the density, width, height, and root depth of vegetation need to be specified to predict vegetation uprooting when sediment erosion reaches the root depth. For the option of IVEG=2 of no uprooting, the density, width, and height of vegetation are constant and specified as input.

- IHOUSE = 0, 1, or 2 for the absence or presence of houses on a beach. IHOUSE must be specified. IHOUSE=0 represents no house on beach. IHOUSE=1 computes floating and sliding probabilities of houses on beach with constant house clearance. IHOUSE=2 is for cross-shore varying house clearance.

- ISTSAN = 0, 1, or 2 for the absence or presence of the stone structure on deforming sand bottom only for IPROFL=1, IPERM=1, and ISEDAV=0. ISTSAN=0 is already specified for the case of no structure or fixed bottom. ISTSAN=0, 1, or 2 must be specified if IPROFL=1, IPERM=1, and ISEDAV=0. The option of ISTSAN=0 includes the fixed bottom and deforming rubble mound if IPROFL=1 and IPERM=1. ISTSAN=1 or 2 represents the fixed stone structure on deforming sand bottom where initially no sand (ISTSAN=1) or full sand (ISTSAN=2) exists inside the porous structure. The option of ISTSAN=1 or 2 is created to include sand transport inside the porous structure.

- IFILTR = 0 or 1 for no or yes for the filter between stone and sand bottom only for IPROFL=1, IPERM=1, and ISEDAV=0. IFILTR=0 is already specified. IFILTR=0 or 1 must be specified if IPROFL=1, IPERM=1, and ISEDAV=0. For the option of IFILTR=1, the filter can prevent sand erosion below stone and the empirical parameter for sand transport reduction on and inside a porous stone structure is specified as 0.01 after calibration using laboratory experiment data (Kobayashi and Kim 2017).

- IULSTE = 0 or 1 for no or yes for erosion of the underlayer below the armor layer only for IPROFL=1, IPERM=1, and ISEDAV=1. IULSTE=0 is already specified. IULSTE=0 or 1 must be specified if IPROFL=1, IPERM=1, and ISEDAV=1 or 2. The option of IULSTE is created to predict armor layer damage and underlayer erosion.

- ICLAY = 0 or 1 for the absence or presence of clay. ICLAY=0 is already specified. ICLAY=0 or 1 must be specified if ISEDAV=1, IPERM=0, and IVEG=0. ICLAY=1 is used to compute sand transport above erodible clay bottom with no vegetation.

- ITRACE = 0 and 1 for no or yes for tracing specified discrete objects (DO) on beaches. ITRACE must be specified. The option of ITRACE=1 is created to predict the destination of placed sand on a beach and improve beach fill design.

Computational Input Parameters

- DX = constant nodal spacing Δx (m). The value of $x_s / \Delta x$ with x_s = cross-shore distance between the seaward boundary $x = 0$ and the shoreline located at the bottom elevation $z_b = 0$ was of the order of 1,000 for the previous computations. The values of Δx were of the order of 0.02 m and 2.0 m for laboratory and field data, respectively. The integer NN in the PARAMETER statement specifies the maximum number of nodes allowed in the computation domain. The default value of NN = 5,000 should be sufficient for the cross-shore distance of 10 km or less.

- GAMMA = empirical breaker ratio parameter γ in Eq. (38) where the range of γ = 0.5 – 1.0 has been used to adjust the computed cross-shore variation of the wave height in comparison with the measured wave height variation. If no wave height data is available, use may be made of γ = 0.7 as a typical value. Alternatively, the empirical formula proposed by Apotsos et al. (2008) may be used for natural beaches but this formula has not been verified for steeper slopes such as gravel beaches and stone structures.

- D50, WF, and SG = median sediment diameter d_{50} (mm) which is immediately converted to d_{50} (m), sediment fall velocity w_f (m/s), and sediment specific gravity s if IPROFL=1. The default values for the sediment in Subroutine INPUT are the sediment porosity SPORO = n_p = 0.4 in Eq. (61) and the critical Shields parameter ψ_c = 0.05 for Eq. (49). The parameter BEDLM = m = 1.0 in Eq. (146) is specified for bedload reduction and suspended sediment volume reduction due to limited sediment availability for the case of ISEDAV=1. CSEDIA is used to distinguish sand transport from gravel or stone movement. CSEDIA = $\left(2\,d_{50}\right) > d_{50}$ for sand transport.

- EFFB, EFFF, SLP, and SLPOT = suspension efficiency e_B due to wave breaking in Eq.(51), suspension efficiency e_f due to bottom friction in Eq. (51), suspended load parameter a in Eq. (52), and suspended load parameter a_o associated with the wave overtopping rate q_o in Eq. (115). These input parameters are required only if IPROFL=1. The input of SLPOT = a_o is required only if

IOVER=1. The calibrated ranges of these parameters are e_B = 0.002 – 0.01 (typically 0.005), e_f = 0.01 (fixed in the previous calibrations), a = 0.1 – 0.4 (typically 0.2), and a_o = 0.1 – 3.6 (typically 0.5 but should be calibrated for each experiment or field site). It is required that $e_B < e_f$ because the turbulence generated by wave breaking decays downward before it suspends bottom sediment.

- TANPHI and BLP = sediment limiting (maximum) slope $\tan\phi$ in Eqs. (52), (58) and (59), and bedload parameter b in Eqs. (56) and (57) if IPROFL=1. These parameters related to bedload have been calibrated in the range of $\tan\phi$ = 0.63 (0.54 for low-crested stone breakwaters) and b = 0.001 – 0.004 (typically 0.002).

- DUM, FMUD, and WMUD = porosity (water) of mixed sediment exceeding 0.4, mud portion of solid volume, and equivalent mud fall velocity (m/s). These parameters need to be specified only if IMUD=1. The sand portion FSAND is given by (1.0-FMUD).

- RWH = runup wire height δ_r (m) above the bottom elevation z_b shown in Fig. 3 only if IOVER=1. If no runup wire is deployed to measure irregular wave runup, use may be made of δ_r = 0.02 m for small-scale experiments and δ_r = 0.1 m for prototype beaches and structures. The range of δ_r = 0.01 – 0.1 m is realistic for a runup wire placed above a slope.

- SNP, SDP, and CSTABN = porosity n_p (SNP) and nominal diameter D_{n50} (m) (SDP) of stone used in Eqs. (68), (69), and (121) as well as the critical stability number N_c (CSTABN) only if IPERM=1 and a permeable layer is constructed of stone or gravel. The maximum seepage velocity WPM = w_m is computed using Eq. (127). The calibrated range of the critical stability number CSTABN is N_c = 0.6 – 1.1 (typically 0.7). If IPROFL=1 and IPERM=1, the default value of SPORO = 0.4 is changed to be equal to the input value of SNP. For stone or gravel movement, CSEDIA = $\left(0.5\ d_{50}\right) < d_{50}$ and input sediment d_{50} = D50 (m) must be the same as SDP (m) because stone movement is predicted on a fixed bottom.

- DEEB and DEEF = empirical efficiency e_B due to wave breaking and empirical efficiency e_f due to bottom friction for the dike erosion model. These parameters need to be specified when IPROFL=2 or ICLAY=1 or IULSTE=1. The calibrated values are $e_B = 0.0002$ and $e_f = 0.01$ for dike erosion and consolidated cohesive bottom erosion.

- C0HOUS, HFHOUS, ABHOUS, and FRHOUS = constant or typical clearance above ground (m) at time=0, water depth to cause floating of a house on ground (m), house bottom area divided by house frontal width (m), and house friction coefficient. These parameters need to be specified only if IHOUSE = 1 or 2. The house drag coefficient CDHOUS is specified as 1.9.

- D50DO, WFDO, SGDO, and CSTNDO = nominal discrete object (DO) diameter (m), DO fall velocity (m/s), DO specific gravity, and DO critical stability number. These parameters need to be specified only if ITRACE=1.

- IDO = the number of discrete objects (DO) only for ITRACE=1.

- XDO, YDO, and BDO = initial cross-shore location (m), alongshore location (m), and burial depth (m) of I-th DO with I = 1, 2, …, IDO. These parameters need to be specified only if ITRACE=1. Initial burial depth BDO is zero or positive. The temporal changes of XDO, YDO, and BDO are computed in Subroutine 23 TRACIN.

Input Wave and Water Level

- ILAB = 0 or 1 for reading the input wave and water level data separately or together where ILAB=1 for laboratory experiments in which offshore waves and water level are normally measured simultaneously.

- NWAVE = number of waves at the seaward boundary $x = 0$. If IPROFL=0 and the bottom is fixed, NWAVE is the number of different waves at $x = 0$ examined for this specific fixed bottom. If IPROFL=1 and the bottom profile evolves from the specified initial profile, NWAVE is the number of sequential waves at $x = 0$ (at an interval of 1 to 3 h for field data) during the profile evolution starting from the morphological time $t = 0$. It is noted that NWAVE must not exceed the integer NB in the PARAMETER statement where NB=30,000 is specified and should be sufficient for the field data duration of 30,000 h (1250 days) or less. The 1-hour interval may be increased for longer duration computations.

- NSURG = number of water levels at the seaward boundary $x = 0$. NSURG must be equal to NWAVE if ILAB=1. The water level for field data corresponds to storm tide (sum of storm surge and tidal water level).

- TIMEBC(I+1), TPBC(I), HRMSBC(I), WSETBC(I), SWLBC(I), and WANGBC(I) for I = 1, 2, …, NTIME only if ILAB=1 where NTIME = NWAVE = NSURG

  TIMEBC(I+1) = morphological time in seconds at the end of the I-th wave and water level during the profile evolution starting from TIMEBC(1) = 0.0. The wave conditions and water level during TIMEBC(I) to TIMEBC(I+1) are assumed to be constant and NTIME is the number of constant wave conditions and water level. For IPROFL=0, TIMEBC(I+1) = 1.0, 2.0, …, NTIME may be used to identify the sequence of the waves and water levels at $x = 0$ used for the computation.

  TPBC(I) = spectral peak period T_p (s) used to represent the I-th irregular wave period at $x = 0$ but any representative wave period such as the spectral wave period (van Gent 2011) can be specified.

  HRMSBC(I) = root-mean-square wave height $H_{rms} = \sqrt{8}\,\sigma_\eta(m)$ used to represent the I-th irregular wave height at $x = 0$. If the spectral significant wave height H_{mo} is known, the

corresponding H_{rms} may be obtained using $H_{rms} = H_{mo} / \sqrt{2}$.

WSETBC(I) = wave setup (positive) or set-down (negative) $\overline{\eta}$ (m) at $x = 0$ relative to the still water level (SWL). If $\overline{\eta}$ is not measured, use may be made of $\overline{\eta}$ = 0.0 at $x = 0$ as long as the seaward boundary $x = 0$ is located outside the surf zone.

SWLBC(I) = still water level S (m) above the datum $z = 0$ as shown in Fig. 2. This value of S corresponds to storm tide (sum of storm surge and tide) during the I-th wave conditions.

WANGBC(I) = incident wave angle θ in degrees at $x = 0$ for the I-th wave conditions (see Fig. 1 for the definition of θ). The angle is limited to the range of θ = – 80° to 80° because the formula for D_B given by Eq. (38) was originally developed for normally incident waves and may not be valid for large incident wave angles. IANGLE=0 or 1 is used to indicate normally or obliquely incident waves in the computer program. For ILINE ≥ 2, the incident wave angle WANGBD(I) measured from the specified reference direction such as the true north is used as input because the ILINE cross-shore lines may have different orientations. For ILINE=1, the reference direction is the orientation of the cross-shore line.

If ILAB=0, NWAVE and NSURG can be different and NTIME is taken as the larger value of NWAVE and NSURG. For ILAB=0 corresponding to field data, offshore wave conditions and water level at $x = 0$ are assumed to change continuously unlike laboratory wave conditions and water level that are normally varied in steps. After the offshore wave data and the water level data are read separately as shown below, Subroutine 19 TSINTP is called to create the stepped time series of TPBC(I), HRMSBC(I), WSETBC(I), SWLBC(I), and WANGBC(I) corresponding to ILAB=1.

- TWAVE(I), TPIN(I), HRMSIN(I), and WANGIN(I) for I = 1, 2, …, (NWAVE+1) only for ILAB=0 where

  TWAVE(I) = time (s) of the I-th wave data where TWAVE(1) = 0.0.

  TPIN(I) = spectral peak period T_p (s) at time = TWAVE(I).

  HRMSIN(I) = root-mean-square wave height $H_{\rm rms}$ (m) at time = TWAVE(I).

  WANGIN(I) = incident wave angle θ in degrees from the reference direction at time = TWAVE(I).

  The wave setup or set-down $\overline{\eta}$ at $x = 0$ is assumed to be zero for field data.

- TSURG(I) and SWLIN(I) for I = 1, 2, …, (NSURG+1) only for ILAB=0 where

  TSURGE(I) = time (s) for the I-th water level where TSURG(1) = 0.0.

  SWLIN(I) = water level S (m) above $z = 0$ at time = TSURG(I).

  It is required that TWAVE (NWAVE+1) = TSURG (NSURG+1) because the durations of the wave data and water level data must be the same.

Bottom Geometry (always) and Porous Layer Bottom if IPERM=1

The bottom profile along the cross-shore line L is specified in the following sequence for L = 1, 2, …, ILINE:

- YEADIS = equivalent alongshore distance (m) for ILINE=1 and IQYDY=1. The value of YEADIS may be calibrated to approximate the alongshore gradient of the longshore sediment transport rate q_y in Eq. (63) along the single cross-shore line.

- YLINE(L) and AGLINE(L) = alongshore distance (m) and orientation angle in degrees from the reference direction for the cross-shore line L. The longshore coordinate y is defined in Fig. 1 and the alongshore distance YLINE(L) increases with the increase of the integer L. The incident wave angle θ at $x = 0$ for the line L is given by θ = [WANGBC(I) – AGLINE(L)] which is adjusted to be in the range of $\theta = -80°$ to $80°$ in Subroutine 5 LWAVE. If ILINE=1, YLINE(1) = 0.0 and AGLINE(1)= 0.0 are already specified and this input line is skipped.

- NBINP(L) = number of points used to describe the input bottom geometry $z_b(x)$ for the cross-shore line L which is the initial profile if IPROFL=1. The bottom geometry is divided into linear segments of different inclination and roughness starting from the seaward boundary $x = 0$. It is noted that NBINP must not exceed NN = 5,000 in the PARAMETER statement. The cross-shore distance to available offshore wave data in given water depth may be reduced by using a steeper bottom slope in the offshore zone but the sensitivity to the assumed slope must be checked.

- NPINP(L) = number of points used to describe the input impermeable fixed boundary $z_p(x)$ in the same way as $z_b(x)$. This input is required only if IPERM=1 or ISEDAV=1.

- XBINP(1,L) and ZBINP(1,L) = values (m) of x and z of the bottom point at the seaward boundary of the line L in the coordinate system (x, z) shown in Fig. 2 where XBINP(1,L) = 0.0 at the seaward boundary and the water depth below the datum $z = 0$ is given by – ZBINP(1,L). If IPERM=1 or ISEDAV=1, XPINP(1,L) = 0.0 and ZPINP(1,L) = ZBINP(1,L) for $z_p(x = 0)$ are specified in the program because the thickness of a permeable layer or sediment layer is assumed to be zero at the seaward boundary where $z_b(x)$ at $x = 0$ is fixed for the profile evolution computation for IPROFL=1.

- XBINP(J,L), ZBINP(J,L), FBINP(J-1,L), CHOUSI(J,L) [input only for IHOUSE=2], and WMINP (J-1,L) [input only for ISEDAV=2] for J = 2, 3, …, NBINP. Input three columns unless IHOUSE=2 or ISEDAV=2
  - XBINP(J,L) = horizontal (landward) distance (m) of the input bottom point J from the seaward boundary $x = 0$ with the distance XBINP(J,L) increasing with the increase of the integer J.
  - ZBINP(J,L) = bottom elevation z_b (m) of the point J. If the point J is below the datum $z = 0$, ZBINP(J,L) is negative and – ZBINP(J,L) is the water depth below the datum. If the point J is above the datum, ZBINP(J,L) is positive and corresponds to the bottom elevation of the point J above the datum.
  - FBINP(J-1,L) = bottom friction factor f_b of the linear segment between the bottom points (J–1) and J. The bottom friction factor can be varied to account for the cross-shore variation of bottom roughness as shown in Fig. 2. The value of f_b must be positive for obliquely incident

waves.

Add the fourth column only if IHOUSE=2

CHOUSI (J,L) = initial house clearance at time=0 only if specified for IHOUSE=2 where CHOUSI(1,L) = 0.0 at $x = 0$.

Add the fourth column only if ISEDAV=2

WMINP(J-1,L) = 1.0 for wire mesh segment between points (J-1) and (J) along cross-shore line L for ISEDAV=2 where WMINP(J-1,L) = 0.0 (no wire mesh) or 1.0 (with wire mesh) between nodes (J-1) and (J).

- XPINP(J,L), ZPINP(J,L), ZBSINP(J,L), RCINP(J,L), and FCINP(J,L) for J = 2, 3, …, NPINP only for IPERM=1 or ISEDAV=1 or 2. Input two columns if ICLAY=0, IULSTE=0, and ISTSAN=0 or 1.

  XPINP(J,L) = value (m) of the x-coordinate of $z_p(x)$ at the point J.

  ZPINP(J,L) = value (m) of the z-coordinate of $z_p(x)$ of the point J. The vertical thickness of the permeable or sediment layer is given by $h_p = (z_b - z_p)$. If $z_p(x)$ includes a vertical step or wall, it should be replaced by a steep slope.

  Add the third column if ICLAY=0, IULSTE=0, and ISTSAN=2

  ZBSINP(J,L) = value (m) of the buried stone surface elevation only for ISTSAN=2.

  Add the third and fourth columns if ICLAY=1 or IULSTE=1

  RCINP(J,L) = clay resistance parameter for ICLAY=1 or the underlayer stone resistance parameter for IULSTE=1. The order of clay resistance is 10 m^2/s^2.

  FCINP(J,L) = sand volume per unit cohesive sediment f_c for ICLAY=1 or the armor stone fraction in the underlayer for IULSTE=1. For ICLAY=1, the sand fraction f_c should be in the range of 0 to $(1-n_p)$.

Vegetation Characteristics if IVEG=1 or 2

- VEGCD = vegetation drag coefficient of order of unity where vegetation input is required only if IVEG=1 or 2.

Input four columns if IVEG=1

- VEGN(J,L), VEGB(J,L), VEGD(J,L), and VEGRD(J,L) = number of vegetation ($1/m^2$) per unit horizontal area for segment J along cross-shore line, width (m) of each vegetation stand, height (m) of each vegetation stand above sand, and root depth (m) below sand for no vegetation uprooting. If there is no vegetation in segment J, VEGN(J,L), VEGB(J,L), VEGD(J,L), and VEGRD(J,L) (no input for IVEG=2) are specified as zero.

Input three columns of VEGN(J,L), VEGB(J,L), and VEGD(J,L) if IVEG=2.

Dike Grass and Soil Characteristics if IPROFL=2

Input three columns if IPROFL=2

- GDINP(J,L), GRINP(J,L), and GRDINP(J,L) = thickness (m) of grass cover for segment J along cross-

shore line L, grass surface resistance parameter (m^2/s^2), resistance parameter (m^2/s^2) below grass cover. GDINP(J,L)=0 if no grass cover in segment J. The grass resistance is assumed to decrease linearly downward in grass cover and become positive constant below the grass cover.

This is the end of the bottom profile input for L = 1, 2, …, ILINE.

Wind Speed and Direction if IWIND=1

- NWIND = number of data points in the time series of wind speed and direction data only if IWIND=1 where the wind data is read in the same way as the wave and water level data for ILAB=0.

- TWIND(I), WIND10(I) and WINDAN(I) for I = 1, 2, …, (NWIND+1) only for IWIND=1.
  TWIND(I) = time (s) for the I-th wind data where TWIND(1) = 0.0 and TWIND (NWIND+1) must be the same as the end time of the wave and water level data.
  WIND10(I) = wind speed W_{10} (m/s) at the elevation of 10 m above the sea surface at time = TWIND(I).
  WINDAN(I) = wind direction θ_w in degrees (see Fig. 1) at time = TWIND(I).
  After the wind data is read, Subroutine 19 TSINTP is called to create the stepped time series corresponding to ILAB=1. The input wind speed and direction are the same for the multiple cross-shore lines with ILINE $\geq$ 2.

Landward Still Water Level if IWTRAN=1

The following input is required only for the option of IWTRAN=1. ISWLSL=0 or 1 assumes that water exists landward of an emerged dune or coastal structure. ISWLSL=2 assumes no water landward of the crest of a structure or dune.

- ISWLSL=0 or 1 for the same or different still water levels on the seaward and landward sides. If ISWLSL=0, no additional input is required because the landward still water level is taken as the seaward still water level specified at the seaward boundary $x = 0$.
- NSLAN = number of data points in the time series of the landward still water level only if ISWLSL=1.
- TSLAND(I) and SLANIN(I) for I = 1, 2, …, (NSLAN+1) only if ISWLSL=1 where
  TSLAND(I) = time (s) for the I-th water level data where TSLAND(1) = 0.0 and TSLAND(NSLAN+1) must be the same as the end time of the wave and seaward water level data.
  SLANIN(I) = landward still water level (m) above the datum $z = 0$ at time = TSLAND(I).
  After the water level data is read, Subroutine 19 TSINTP is called to create the stepped time series corresponding to ILAB=1. ISWLSL=2 for no water in the landward zone is created to allow overflow (IOFLOW=1) over the submerged crest of a dike for the prediction of dike breaching.

Alongshore Water Level Gradient if ITIDE=1

If ITIDE=1, the time series of the alongshore water level gradient associated with the alongshore tidal

current must be specified in the same way as the wave and water level data for ILAB=0.

- NTIDE = number of data points in the time series of the alongshore water level gradient.
- TTIDE(I) and DEDYIN(I) for I = 1, 2, …, (NTIDE+1)

  TTIDE(I) = time(s) for the I-th alongshore water level gradient data where TTIDE(1) = 0.0 and TTIDE(NTIDE+1) must be the same as the end time of the wave and water level data.

  DEDYIN(I) = alongshore water level gradient at time = TTIDE(I) where the term associated with the alongshore water level gradient has been added to the alongshore momentum equation (23) by Farhadzadeh et al. (2012) and Miranda and Kobayashi (2022).

If ITIDE=1 and ILAB=0, the cross-shore volume flux associated with the temporal variation of the still water level S specified as input has been included in Eq. (19) by Do et al. (2012) and Miranda and Kobayashi (2022).

11.4 Output

A user of CSHORE must examine the contents of the output file **ODOC** (unit=20 for the WRITE statement) to ensure that the input file has been prepared and read correctly. The contents of this file created in Subroutine 8 **OUTPUT** and at the end of Subroutine 10 **QORATE** if IOVER=1 are self-explanatory.

First, **ODOC** stores the input parameters and variables. The following notations have not been explained:

BEDLM = bedload and suspended sediment volume reduction factor m in Eq. (146) where BEDLM=1.0 is specified in Subroutine 2 **INPUT** if ISEDAV=1.

RBZERO = lower limit of the wave-front slope β_r in Eq. (10) where RBZERO = 0.1 is specified in Subroutine 2 **INPUT.** This typical value has been used to reduce the number of calibration parameters.

JCREST = crest node of the maximum bottom elevation for the input bottom profile $z_b(x)$. If the crest is horizontal, JCREST corresponds to the landward end of the horizontal crest located at $x = x_c$ in Figs. 5 and 6. If IPROFL=1, the nodal location of JCREST may change with the evolution of the bottom profile.

RCREST = input bottom elevation (m) at the node JCREST corresponding to the maximum value of the input $z_b(x)$.

AWD = parameter α in Eqs. (92) and (131) which expresses the horizontal velocity U as a function of the water depth h in the wet and dry zone where $\alpha = 1.6$ or 2.0 is specified in Subroutine 4 **PARAM**.

EWD = exceedance probability e used in Eq. (143) for the comparison with measured values corresponding to 2% of incident irregular waves where e = EWD = 0.01 or 0.015 depending on IPERM=1 or 0 in Subroutine 4 **PARAM**.

ZW = initial ponded water level (m) if IOVER=1 and IPOND=1.

WMU = water kinematic viscosity (m^2/s) in Eqs. (68) and (121).

WPM = maximum seepage velocity in Eq. (127).

It is noted that JCREST, RCREST, AWD, and EWD are stored only if IOVER=1.

Second, **ODOC** stores the computed quantities for each cross-shore line at time = TIMEBC(2), …, TIMEBC(NTIME+1) for ILAB=1. For ILAB=0, the computed quantities are stored at specified storage time levels and at the last time level. The stored quantities at given time for the cross-shore line L include

JR = most landward node reached by the landward marching computation using the wet model in Section 4 if IPERM=0 and in Section 6 if IPERM=1.

XR = x-coordinate (m) of the node JR where XR = x_r shown in Figs. 5 and 6 for an emerged structure or beach.

ZR = z-coordinate (m) of the node JR corresponding to the bottom elevation above the datum.

H(JR) = mean water depth $\overline{h}$ (m) at the node JR which must be very small for an emerged structure or beach if the landward marching computation does not encounter numerical difficulties.

CSHORE estimates the wave reflection coefficient, assuming that the cross-shore wave energy flux F_x defined in Eq. (37) is reflected from the node JSWL at the still water shoreline located at $x = x_{SWL}$ in Fig. 5 and propagates seaward if JR > JSWL (the landward marching computation has reached above the still water shoreline) and JSWL < JMAX with JMAX = most landward node of the computation domain based on the input bottom geometry. If JSWL = JMAX, the computation domain is submerged and some of the cross-shore wave energy flux is transmitted landward. The wave reflection coefficient REFCOF is estimated as the ratio between σ_{ref} and σ_η at $x = 0$ where σ_{ref} is the free surface standard deviation due to the wave energy flux propagating seaward at $x = 0$. The wave reflection coefficient is estimated only for IOVER=0 because wave overtopping accompanies onshore wave energy flux. The estimated wave reflection coefficient may not be very accurate (Kobayashi et al. 2005, 2007a) but is useful in assessing the applicability of CSHORE which neglects reflected waves in its governing equations.

If IOVER=1, Subroutine OUTPUT calls Subroutine 10 **QORATE** with ICALL=1 to store the quantities associated with wave runup, overtopping and transmission in the file **ODOC**. The stored quantities include the following:

JWD = most seaward node of the landward marching computation in the wet and dry zone as explained in relation to Eqs. (100) and (137).

H1 = mean water depth $\overline{h}_1(m)$ at the node JWD.

JDRY = most landward node in the wet and dry zone which is less than and equal to the maximum node number JMAX in the computation domain.

POTF = wave overtopping probability P_o estimated using the wet probability P_c at the node JCREST as explained below Eqs. (102) and (141).

QOTF = wave overtopping rate q_o (m^2/s) above the bottom computed using Eq. (102) for an impermeable bottom. For a permeable bottom, QOTF = ($q_o - q_p$) in Eq. (141).

QP = seepage rate q_p (m^2/s) calculated using Eq. (123) at the node JCREST. The total overtopping rate is given by q_o = (QOTF + QP) in Eq. (141). QP = 0.0 for an impermeable bottom.

ITEQO = number of iterations performed to compute the wave overtopping rate q_o.

In addition, the following quantities for wave runup in Section 7 are stored in the file **ODOC** at the specified time levels:

SLPRUN = representative bottom slope S_r in the swash zone given in Eq. (76)

ERMEAN = mean shoreline elevation (m) above the datum $z = 0$ measured by the runup wire where ERMEAN = $\left(\overline{\eta}_r + S\right)$ and $\overline{\eta}_r$ given in Eq. (76) is the mean shoreline elevation above SWL. The still water level S above the datum $z = 0$ at $x = 0$ is specified as input.

SIGRUN = standard deviation σ_r (m) of the shoreline oscillation measured by the runup wire where σ_r is estimated using Eq. (76).

R13 = significant runup height (m) above the datum $z = 0$ corresponding to $\left(R_{1/3} + S\right)$ where $R_{1/3}$ above SWL is estimated using Eq. (78) or (84).

R2P = runup height (m) above the datum $z = 0$ for the 2% exceedance probability where R2P = $\left(R_{2\%} + S\right)$ and $R_{2\%}$ is estimated using Eq. (81) or (85).

R1P = runup height (m) above the datum $z = 0$ for the 1% exceedance probability where R1P = $\left(R_{1\%} + S\right)$ and $R_{1\%}$ is estimated using Eq. (82) or (86).

If IWTRAN=1, the following quantities related to wave transmission are stored in the file **ODOC** in Subroutine 10 **QORATE**:

JSL = most seaward wet node in the zone of wave transmission where its cross-shore location $x =$ XB(JSL), wave setup $\overline{\eta} =$ WSETUP(JSL), and standard deviation σ_η = SIGMA(JSL) are stored.

JMAX = most landward wet zone in the zone of wave transmission where its cross-shore location, wave setup $\overline{\eta}$, and standard deviation σ_η are stored.

Wave transmission coefficient = ratio between σ_η at the node JMAX and σ_η at the seaward boundary $x = 0$. An emerged structure can become submerged if the structure crest is lowered by wave action. For the submerged structure, the wave transmission coefficient is calculated in Subroutine 8 **OUTPUT**.

If IPOND=1 and NOPOND=0, the water in the runnel landward of the ridge is ponded and the following quantities related to the ponded runnel are stored in the file **ODOC** in Subroutine 10 **QORATE**:

JCREST = nodal location of the ridge crest

JXW = most seaward node in the ponded runnel

JX2 = most landward node in the ponded runnel

ZW = ponded water level (m) in the runnel

QD = wave-induced water volume flux (m^2/s) into the runnel

QM = wave overtopping rate (m^2/s) at the landward end node JMAX which is the water outflow from the ponded runnel.

If IPROFL=1 and IANGLE=1 (obliquely incident waves), Subroutine OUTPUT integrates the sum of the

longshore suspended sediment transport rate q_{sy} (m^2/s) and the longshore bedload transport rate q_{by} (m^2/s) from $x = 0$ to the landward limit of the wet and dry zone where q_{sy} and q_{by} are predicted using Eqs. (52) and (57), respectively, where Eqs. (52) and (57) have been extended to the wet and dry zone (Farhadzadeh et al. 2012). The integrated total longshore sediment transport rate (m^3/s) and the corresponding value of K in the CERC formula (Coastal Engineering Manual 2003) are stored in the file **ODOC**. The breaker location is taken at the cross-shore location of the maximum root-mean-square wave height and the value of K in the CERC formula is supposed to be of the order of 0.8 for sands. The value of $\sin\theta_B$ with θ_B = incident wave angle at the breaker location is also stored to interpret the calculated value of K.

If IPROFL=1 and IPERM=1, the profile evolution of a permeable beach or structure is computed. The computed bottom profile $z_b(x)$ at the given time t is compared with the initial bottom profile $z_i(x) = z_b(x)$ at $t = 0$. The eroded area A_e is defined as the area of $[z_i(x) - z_b(x)] > 0$. The maximum vertical erosion depth d_e is defined at the maximum value of $[z_i(x) - z_b(x)] > 0$. The damage S_e is defined as $S_e = A_e / D_{n50}^2$ and the normalized erosion depth E is defined as $E = d_e / D_{n50}$ where D_{n50} is the nominal stone or gravel diameter. The stability number N_{mo} is defined as $N_{mo} = H_{mo} / [(s-1) D_{n50}]$ where $H_{mo} = \sqrt{2}\, H_{\rm rms}$ = spectral significant wave height at $x = 0$ and s = specific gravity of the stone or gravel. The values of S_e, E, and N_{mo} are stored at the specified time levels in the **ODOC** file in Subroutine 8 OUTPUT.

The rest of the output files store the cross-shore variations of computed variables at the specified time levels TIMEBC(I) with I = 2, …, (NTIME+1) for ILAB=1. For ILAB=0, the cross-shore variations are stored at specified storage time levels and at the last time level. Each output file stores the cross-shore line number L, the number of nodes, and the output time level TIMOUT immediately before the computed variables are stored at the given number of nodes. This will facilitate displaying the computed variables using the output files. It is noted that the CSHORE computer program does not contain any plotting routine.

Other Output Files

The file **OBPROF** (unit=21) contains the bottom profile variables at all the nodes with J = 1, 2, …, JMAX. These variables are also stored at the initial time TIMEBC(1) = 0.0 to record the initial smoothed profile used for the computation. This output consists of two, three, or four columns.

XB(J) = cross-shore coordinate x (m) of node J where XB(J) = (J–1) Δx. [First column].

ZB(J) = vertical coordinate z_b (m) of the bottom elevation at the output time level where the bottom elevation evolves with time if IPROFL=1 or 2. [Second column].

ZP(J) = vertical coordinate z_p (m) of the lower boundary of the permeable layer (IPERM=1) or the fixed bottom below the sand layer (ISEDAV=1). [Third column except for ISEDAV=2].

ZMESH(J) = fixed wire mesh elevation for z_b (m) for ISEDAV=2. [Third column].

ZBSTON(J) = buried stone surface elevation (m) for ISTSAN=2 and TIME=0.0. [Fourth column].

UPROOT(J) = 0.0 (uprooted) or 1.0 (buried) for IVEG=1 [Last column].

VDSAND(J) = deposited sand height (m) inside porous structure above filter for ISTSAN=1 or 2 and TIME > 0.0 [Fourth column].

The file **OSETUP** (unit=22) stores the quantities related to the mean and standard deviation of the free surface elevation η for nodes J = 1, 2, …, JR using four columns

XB(J) = cross-shore coordinate x (m) of node J for the plotting convenience.

(H(J)+ZB(J)) = sum of the wave setup $\bar{\eta}$ (m) above SWL and storm tide S (m) above the datum at node J [see Eq. (1)].

H(J) = mean water depth $\bar{h}$ (m) at node J.

SIGMA(J) = free surface standard deviation σ_η (m) related to the root-mean-square wave height $H_{rms} = \sqrt{8}\sigma_\eta$.

If IOVER=1, these variables are also stored at nodes J = (JR+1), …, JDRY in the wet and dry zone.

If IWTRAN=1, these variables are also stored at nodes J = (JR+1), …, JMAX.

The file **OPARAM** (unit =23) stores XB(J) with nodes J = 1, 2, …, JR and the following parameters:

WT(J) = intrinsic wave period $T = 2\pi / \omega$ (s) where the angular frequency ω is computed using Eq. (2) and $T = T_p$ specified as input if IWCINT=0.

QBREAK(J) = fraction Q of breaking waves computed using Eq. (38).

SIGSTA(J) = ratio $\sigma_* = \sigma_\eta / \bar{h}$ in Eq. (31) whose upper limit is unity in the wet zone.

The file **OXMOME** (unit=24) stores XB(J) with J = 1, 2, …, JR and the following terms in the x-momentum equation (22):

SXXSTA(J) = $[S_{xx} / (\rho g) + Q_x^2 / (g\bar{h})]$ (m^2) where S_{xx} and Q_x are given in Eqs. (24) and (19), respectively.

TBXSTA(J) = $\tau_{bx} / (\rho g)$ (m) where τ_{bx} is given in Eq. (33).

If IANGLE=1 (obliquely incident waves), the file **OYMOME** (unit=25) stores XB(J) with J = 1, 2, …, JR and the following terms in the *y*-momentum equation (23):

SXYSTA(J) = $[S_{xy} / (\rho g) + Q_x Q_y / (g\bar{h})]$ (m^2) where S_{xy}, Q_x, and Q_y are defined in Eqs. (24), (19) and (20).

TBYSTA(J) = $\tau_{by} / (\rho g)$ (m) where τ_{by} is given in Eq. (33).

The file **OENERG** (unit=26) stores XB(J) with J = 1, 2, …, JR and the following terms in the wave action equation (36) or (66) with ω being replaced by T^{-1}:

EFSTA(J)/WT(J) = $\left[\mathrm{E}\left(C_g \cos\theta + Q_x / \bar{h} \right) \right] / (\rho g)$ (m^3/s) where E and C_g are given in Eqs. (25) and (3).

DBSTA(J) = $D_B / (\rho g)$ (m^2/s) where D_B is given by Eq. (38).

DFSTA(J) = $D_f / (\rho g)$ (m^2/s) where D_f is given by Eq. (40).

The file **OXVELO** (unit=27) stores XB(J) with J = 1, 2, …, JR and the following cross-shore velocity statistics:

UMEAN(J) = mean velocity $\overline{U}$ (m/s) of the depth-averaged cross-shore velocity U .

USTD(J) = standard deviation σ_U (m/s) of U .

UPMEAN(J) = mean discharge velocity $\overline{U}_p$ (m/s) in the permeable layer computed using Eqs. (73) and (120) if IPERM=1.

If IOVER=1, these variables are also stored at nodes J = (JR+1), …, JDRY in the wet and dry zone. If IWTRAN=1, these variables are also stored at nodes J = (JR+1), …, JMAX.

If IANGLE=1, the file **OYVELO** (unit=28) stores XB(J) with J = 1, 2, …, JR and the following longshore velocity statistics:

STHETA(J) = $\sin\theta$ with θ = wave angle as defined in Fig. 1 where $\sin\theta$ is computed using Eq. (21).

VMEAN(J) = mean velocity $\overline{V}$ (m/s) of the depth-averaged longshore velocity V .

VSTD(J) = standard deviation σ_V of V .

If IOVER=1, these variables are also stored at nodes J = (JR+1), …, JDRY in the wet and dry zone. If IWTRAN=1, these variables are assumed to be zero in the landward wet zone.

If IROLL=1, the file **OROLLE** (unit=29) stores XB(J) with J = 1, 2, …, JR and

RQ(J) = roller volume flux q_r (m^2/s) computed using Eq. (41).

If IROLL=0, $q_r = 0$ and $D_r = D_B$ in Eq. (41).

If IPROFL=1, the file **OBSUSL** (unit=30) stores XB(J) with J = 1, 2, …, JR and the following variables related to sediment transport:

PB(J) = probability P_b of sediment movement given by Eqs. (49) and (107) – (109).

PS(J) = probability P_s of sediment suspension given by Eqs. (50) and (110) – (112).

VS(J) = suspended sediment volume V_s (m) per unit horizontal bottom area given by Eqs. (51) and (113).

If IOVER=1, these variables are also stored at nodes J = (JR+1), …, JDRY in the wet and dry zone. If IWTRAN=1, these variables are also stored at nodes J = (JR+1), …, JMAX.

If IPERM=1, the file **OPORUS** (unit=31) stores XB(J) with J = 1, 2, …, JR and the following variables related to the permeable layers in the wet zone:

UPSTD(J) = standard velocity σ_p (m/s) of the discharge velocity computed using Eq. (75).

DPSTA(J) = $D_p / (\rho g)$ (m^2/s) where the energy dissipation rate D_p due to flow resistance in the permeable layer is computed using Eq. (71).

If IPROFL=1, the file **OCROSS** (unit=32) stores XB(J) with J = 1, 2, …, JMAX and the following cross-shore sediment transport rates explained in Sections 5, 8.2 and 9.2:

QBX(J) = cross-shore bedload transport rate q_{bx} (m^2/s).

QSX(J) = cross-shore suspended sediment transport rate q_{sx} (m^2/s).

(QBX(J) + QSX(J)) = cross-shore total sediment transport rate q_x (m^2/s).

It is noted that the transport rates are stored at all the nodes but the rates are zero in the completely dry zone.

If IPROFL=1 and IANGLE=1, the file **OLONGS** (unit=33) stores XB(J) with J = 1, 2, …, JMAX and the following longshore sediment transport rates explained in Sections 5, 8.2, and 9.2:

QBY(J) = longshore bedload transport rate q_{by} (m^2/s).

QSY(J) = longshore suspended sediment transport rate q_{sy} (m^2/s).

(QBY(J) + QSY(J)) = longshore total sediment transport rate q_y (m^2/s).

If IOVER=1, the file **OSWASH** (unit=34) stores XB(J) with J = 1, 2, …, JDRY or JMAX (if IWTRAN=1) and the following quantities related to the wet and dry zone:

PWET(J) = wet probability P_w at node J corresponding to the ratio between the wet duration and the total duration at this node where P_w = 1.0 in the wet zone.

QP(J) = water flux inside the permeable layer in Eqs. (65) and (123) if IPERM=1.

If IOVER=1, the file **OSWASE** (unit=35) stores XB(J) with J = JWD, …, JDRY and the following quantities in Eqs. (143) and (144):

HEWD(J) = water depth h_e (m) corresponding to the exceedance probability e = EWD.

UEWD(J) = cross-shore velocity U_e (m/s) corresponding to the exceedance probability *e*

QEWD(J) = cross-shore volume flux q_e (m^2/s) corresponding to the exceedance probability *e*.

If IOVER=1, the file **OTIMSE** (unit = 36) stores the following time series with time $t = 0$ at the beginning of the computation:

TIMID = time t (s) in the middle between TIMEBC(I) and TIMEBC(I+1) for I = 1, 2, …, NTIME.

TSQO(I) = average wave overtopping rate q_o (m^2/s) during TIMEBC(I) to TIMEBC(I+1).

TSQBX(I) = average cross-shore bedload transport rate q_{bx} (m^2/s) at the landward end of the computation domain during TIMEBC(I) to TIMEBC(I+1).

TSQSX(I) = average cross-shore suspended sediment transport rates q_{sx} (m^2/s) at the landward end of the computation domain during TIMEBC(I) to TIMEBC(I+1).

These computed time series have been compared with the measured wave overtopping and overwash rates obtained from the water and sand volumes collected during a burst of irregular waves.

If IPROFL=1, the file **OCRVOL** (unit 37) stores XB(J) with J = 1, 2, …, JMAX and the following cumulative cross-shore sediment transport volumes per unit width which are obtained by integrating q_{bx} and q_{sx} from time $t = 0$ to the output time TIMOUT:

VBX(J) = cross-shore bedload transport volume (m^3/m) which is positive (onshore).

VSX(J) = cross-shore suspended sediment transport volume (m^3/m) which is negative (offshore).

(VBX(J) + VSX(J)) = cross-shore net sediment transport volume (m^3/m).

Kobayashi and Jung (2012) used the computed values of VBX(J) and VSX(J) to explain the erosion and recovery of Rehoboth and Dewey Beaches in Delaware.

If IPROFL=1 and IANGLE=1, the file **OLOVOL** (unit 38) stores XB(J) with J =1, 2, …, JMAX and the following cumulative longshore sediment transport volumes per unit width which are obtained by integrating q_{by} and q_{sy} from time $t = 0$ to the output time TIMOUT:

VBY(J) = longshore bedload transport volume (m^3/m) which is positive in the downwave (downdrift) direction.

VSY(J) = longshore suspended sediment transport volume (m^3/m) which is positive in the downwave direction.

(VBY(J) + VSY(J)) = longshore total sediment transport volume (m^3/m).

If IPROFL=2, or ICLAY=1, or IULSTE=1 the file **ODIKER** (unit 39) stores XB(J) [first column] with J = 1, 2, …, JMAX and the following variables related to dike or clay erosion

EDIKE(J) = downward dike erosion depth (m). [Second column if IPROFL=2].

EPCLAY(J) = downward clay erosion depth (m). [Second column if ICLAY=1 and IPROFL=1].

DSTA(J) = variable (m^2/s) related to energy dissipation and dike or clay erosion forcing at Time = TIMOUT. [Third column].

DSUM(J) = cumulative forcing (m^2) obtained by integrating DSTA(J) from Time=0.0 to Time = TIMOUT. [Fourth column if IPROFL=2].

For IUSTE=1, EPCLAY(J) and DSTA(J) are used for underlayer stone erosion in three columns.

The file **OMESSG** (unit=40) stores warning and error messages generated during the computation. This file has been used to find input errors and improve the numerical iteration methods adopted in CSHORE. A user of CSHORE may not be interested in the computed results in all the output files but should examine all the appropriate output files and ensure that the computed results are realistic physically. This is especially true if CSHORE is applied to new problems where the previous applications of CSHORE have been summarized in Sections 2 and 10.

The file **OMAXEU** (unit 41) stores XB(J) with J = 1, 2, …, JMAX and the following cross-shore variables of maximum free surface elevation and onshore velocity based on the formulas by Quan and Kobayashi (2015):

ETMAX(J) = maximum free surface elevation (m) above datum. [Second column].

ETMAXM(J) = maximum ETMAX(J) from TIME=0. [Third column].

UMAX(J) = maximum onshore velocity (m/s). [Fourth column].

UMAXM(J) = maximum UMAX(J) from TIME=0. [Fifth column].

ETMAX(J) and UMAX(J) computed for each time interval TIMEBC(ITIME)

If IPROFL=1, the file **OFOPEU** (unit 42) stores XB(J) with J = 1, 2, …, JMAX and the following

probabilistic variables (Quan and Kobayashi 2015):

EFIVEP(J) = free surface elevation (m) of 5% exceedance. [Second column].

EONEP(J) = free surface elevation (m) of 1% exceedance. [Third column].

UFIVEP(J) = onshore velocity (m/s) of 5% exceedance. [Fourth column].

UONEP(J) = onshore velocity (m/s) of 1% exceedance. [Fifth column].

If IHOUSE=1 or 2, the file **OHOUSE** (unit 43) stores XB(J) with J = 1, 2, …, JMAX and the following probabilities related to damage on house during each time interval (maximum values during each interval)

CHOUS(J) = house clearance (m) above evolving ground. [Second column].

PFHOUS(J) = house floating probability. [Third column].

PSHOUS(J) = house sliding probability. [Fourth column].

PIHOUS(J) = house immersion probability. [Fifth column].

If ITRACE=1, the file **OPBSDO** (unit 44) stores XB(J) with J = 1, 2, …, JMAX and the following probabilities of Discrete Objects (DO) varying in the onshore (x) direction

PBDO(J) = probability of DO movement as bedload. [Second column].

PSDO(J) = probability of DO suspension as suspended load. [Third column].

If ITRACE=1, the file **OXYBDO** (unit 45) stores the traced DO locations at time = TIMOUT for I-th DO with I = 1, 2, …, IDO (number of DO)

XDO(I) = cross-shore location of I-th DO. [Second column after the value of I].

YDO(I) = alongshore location of I-th DO. [Third column].

BDO(I) = burial depth of I-th DO below sediment surface. [Fourth column].

ZDO(I) = elevation of I-th DO = (ZB-BDO(I)) above the datum. [Fifth column].

If IPROFL=1, and IMUD=1, the file **OMUDVQ** (unit 46) stores XB(J) with J = 1, 2, …, JMAX and the following mud variables at time = TIMOUT

FMUDX(J) = mud portion of solid (sand and mud) volume. [Second column].

VMUD(J) = suspended mud volume per unit area (m). [Third column].

QMUDX(J) = cross-shore suspended mud transport rate (m^2/s). [Fourth column].

QMUDY (J) = longshore mud transport rate (m^2/s) if IANGLE=1. [Fifth column].

12. Conclusions

The horizontally two-dimensional model C2SHORE and the cross-shore model CSHORE are presented. The numerical model C2SHORE is based on the spectral wave model STWAVE (Smith et al. 2001) for the prediction of the directional wave transformation, radiation stresses, and wave-induced volume fluxes as well as the circulation model, which is a simplified version of SHORECIRC (Svendsen et al. 2002) for irregular waves, for the prediction of the wave setup and depth-averaged current velocities. The combined wave current model CSHORE based on the time-averaged continuity, cross-shore momentum, longshore momentum, wave action or energy and roller energy equations predicts the cross-shore variations of the mean and standard deviation of the free surface elevation and depth-averaged cross-shore and longshore velocities under normally or obliquely incident irregular breaking waves. Both models use the same sediment transport formulas for the cross-shore and longshore transport rates of suspended sediment and bedload on sand beaches. These formulas are relatively simple and require the hydrodynamic input variables which can be predicted efficiently and fairly accurately using existing wave and current models. The numerical model C2SHORE has been compared only with very limited data partly because of its complexity and partly because of the lack of benchmark data. The much simpler model CSHORE has been compared with a number of small-scale and large-scale laboratory data and field data. CSHORE has been extended to the intermittently wet and dry zone for the prediction of wave overwash of dunes and deformation of low-crested stone structures and gravel beaches.

The improvement of CSHORE requires the simultaneous measurements of hydrodynamics and sediment dynamics because of the interactions among waves, sediment, and bottom elevation changes in the surf and swash zones. The simplicity and computational efficiency of CSHORE should allow its application to various coastal engineering problems that tend to occur in the vicinity of the shoreline. The development of CSHORE up to 2013 was focused on common coastal engineering applications in the U.S. such as dune erosion and overwash; beach erosion and recovery; wave runup, overtopping, and transmission over coastal structures; and damage to rubble mound breakwaters. CSHORE 2013 was limited to cohesionless sediments (sand, gravel, and stone). The CSHORE extensions during 2014 – 2022 were aimed at other specific applications such as the use of woody plants and piles to reduce dune erosion; the erosion of grassed dike and consolidated cohesive sediment; wave overtopping and overwash of a barrier beach; sand transport on and inside a porous stone structure; and intertidal mudflat profile evolution. Additional empirical formulas and parameters were introduced for these extensions and calibrated using small-scale laboratory experiments conducted for specific CSHORE extensions or available large-scale laboratory data and scarce field data. The next stage of CSHORE evolution may be the utilization of CSHORE in devising innovative solutions for coastal engineering problems. In addition, the predictive accuracy of CSHORE should be improved. The capabilities and shortcomings of CSHORE and XBEACH (Roelvink et al. 2009) were evaluated in the comparison with beach profile evolution data during storms in southern California (Kalligeris et al. 2020) and in Duck, North Carolina (Cohn et al. 2021). Both models were not very accurate.

References

Ahrens, J.P. (1989). "Stability of reef breakwaters." J. Waterway, Port, Coastal, Ocean Eng., 115(2), 221-234.

Anderson, D.A., Tannehill, J.C., and Pletcher, R.H. (1984). Computational fluid mechanics and heat transfer. Hemisphere, New York.

Apotsos, A., Raubenheimer, B., Elgar, S., and Guza, R.T. (2008). "Testing and calibrating parametric wave transformation models on natural beaches." Coastal Eng., 55, 224-235.

Ayat, B., and Kobayashi, N. (2015). "Vertical cylinder density and toppling effects on dune erosion and overwash." J. Waterway, Port, Coastal, Ocean Eng., 141(1), 04014026.

Bagnold, R.A. (1966). "An approach to the sediment transport problem from general physics." U.S. Geol. Surv., Prof. Paper 422-I.

Bailard, J.A. (1981). "An energetics total load sediment transport model for a plane sloping beach." J. Geophys. Res., 86, 10,938-10,954.

Battjes, J.A., and Stive, M.J.F. (1985). "Calibration and verification of a dissipation model for random breaking waves." J. Geophys. Res., 90(C5), 9159-9167.

Baquerizo, A., Losada, M., Smith, J., and Kobayashi, N. (1997). "Cross-shore variation of wave reflection from beaches." J. Waterway, Port, Coastal, Ocean Eng., 123(5), 274-279.

Becker, J.M., Firing, Y.L., Aucan, J., Holman, R., Merrifield, M., and Pawlak, G. (2007). "Video-based observations of nearshore sand ripples and ripple migration." J. Geophys. Res., 112, C01007, doi10.1029/2005JC003451.

Booij, N., Ris, R. C., and Holthuijsen, L. H. (1999). "A third-generation wave model for coastal regions: 1. Model description and validation." J. Geophys. Res., 104(C4), 7649-7666.

Burcharth, H. F., Kramer, M., Lamberti, A., and Zanuttigh, B. (2006). "Structural stability of detached low crested breakwaters." Coastal Eng., 53(4), 381-394.

Cárdenas, C.X., and Kobayashi, N. (2017). "Cross-shore damage variation of wooden blocks in swash zone on sand beach." Coastal Eng. J., 59(1), 175001, 1-22.

Chaudhry, M.H. (1993). Open-channel Flow. Prentice Hall, Englewood Cliffs, NJ.

Coastal Engineering Manual. (2003). Coastal and Hydraulics Lab, US Army Engineer Research and Development Center, Vicksburg, Miss.

Cohn, N., Brodie, K.L., Johnson, B., and Palmsten, M.L. (2021). "Hotspot dune erosion on an intermediate beach." Coastal Eng., 170, 103998.

Cox, D., and Kobayashi, N. (1997). "Kinematic undertow model with logarithmic boundary layer." J. Waterway, Port, Coastal, Ocean Eng., 123(6), 354-360.

Cox, D. T., and Kobayashi, N. (1998). "Application of an undertow model to irregular waves on plane and barred beaches." J. Coastal Res., 14(4), 1314-1324.

Cox, D. T., and Kobayashi, N. (2000). "Identification of intense, intermittent coherent motions under shoaling and breaking waves." J. Geophys. Res., 105(C6), 14223-14236.

Cox, D. T., Kobayashi, N., and Okayasu, A. (1996). "Bottom shear stress in the surf zone." J. Geophys. Res., 101(C6), 14337-14348.

Dalrymple, R.A. (1988). "Model for refraction of water waves." J. Waterway, Port, Coastal, Ocean Eng., 114(4), 423-435.

Damgaard, J.S., and Dong, P. (2004). "Soft cliff recession under oblique waves: Physical model tests." J. Waterway, Port, Coastal, Ocean Eng. 130(5): 234-242.

Dean, R.G. (1991). "Equilibrium beach profile: Characteristics and applications." J. Coastal Res., 7, 53-84.

Do, K., Kobayashi, N., and Suh, K.-D. (2012). "Erosion and accretion on curved beach." Proc. 32nd Coastal Eng. Conf., Sediment 11, 1-12.

Do, K., Kobayashi, N., and Suh, K.-D. (2014). "Erosion of nourished Bethany Beach in Delaware, USA." Coastal Eng. J., 56(1), 1450004, 1-17.

Do, K., Kobayashi, N., Suh, K.-D., and Jin, J.-Y. (2016). "Wave transformation and sand transport on a macrotidal pocket beach." J. Waterway, Port, Coastal, Ocean Eng., 142(1), 04015009, 1-8.

Dohmen-Janssen, C.M., and Hanes, D.H. (2002). "Sheet flow dynamics under monochromatic nonbreaking waves." J. Geophys. Res., 107(C10), 3149, doi:10.1029/2001JC001045.

Dohmen-Janssen, C.M., Kroekenstoel, D.F., Hassan, W.N., and Ribberink, J.S. (2002). "Phase lags in oscillatory sheet flow: Experiments and bed load modeling." Coastal Eng., 47, 295-327.

EurOtop Manual (2007). "Wave overtopping of sea defenses and related structures: Assessment manual." www.overtopping-manual.com.

Farhadzadeh, A., Kobayashi, N., and Gravens, M.B. (2012). "Effect of breaking waves and external current on longshore sediment transport." J. Waterway, Port, Coastal, Ocean Eng., 138(3), 256-260.

Feddersen, F., Guza, R.T., Elgar, S., and Herbers, T.H.C. (2000). "Velocity moments in alongshore bottom stress parameterization." J. Geophys. Res., 105(C4), 8673-8686.

Figlus, J., Kobayashi, N., Gralher, C., and Iranzo, V. (2011). "Wave overtopping and overwash of dunes." J. Waterway, Port, Coastal, Ocean Eng., 137(1), 26-33.

Figlus, J., Kobayashi, N., and Gralher, C. (2012). "Onshore migration of emerged ridge and ponded runnel." J. Waterway, Port, Coastal, Ocean Eng., 138(5), 331-338.

Garcia, R., and Kobayashi, N. (2015). "Trunk and head damage on a low crested breakwater." J. Waterway, Port, Coastal, Ocean Eng., 141(2), 04014037.

Gallagher, E.L., Elgar, S., and Guza, R.T. (1998). "Observations of sand bar evolution on a natural beach." J. Geophys. Res., 103, 3203-3215.

Henderson, S.M., Allen, J.S., and Newberger, P.A. (2004). "Nearshore sandbar migration predicted by an eddy-diffusive boundary layer model." J. Geophys. Res., 109, C06024, doi:10.1029/2003JC02137.

Hoefel, F., and Elgar, S. (2003). "Wave-induced sediment transport and sandbar migration." Science, 299, 1885-1887.

Holland, K.T., Holman, R.A., and Sallenger, A.H., Jr. (1991). "Estimation of overwash bore velocities using video techniques." Proc. Coastal Sediments'91, ASCE, Reston, Va., 489-497.

Jiménez, J.A., and Madsen, O.S. (2003). "A simple formula to estimate settling velocity of natural sediments." J. Waterway, Port, Coastal, Ocean Eng., 129(2), 70-78.

Johnson, B. D., Kobayashi, N., and Gravens, M. B. (2012). "Cross-shore numerical model CSHORE for waves, currents, sediment transport and beach profile evolution." Final Rep. No. ERDC/CHL TR-12-22, U.S. Army Corps of Engineers, Coastal and Hydraulics Laboratory, Vicksburg, MS.

Kalligeris, N., Smit, P.B., Ludka, B.C., Guza, R.T., and Gallien, T.W. (2020). "Calibration and assessment of process-based numerical models for beach profile evolution in southern California." Coastal Eng., 158, 103650.

Kamphuis, J.S. (1991). "Alongshore sediment transport rate." J. Waterway, Port, Coastal, Ocean Eng., 117(6), 624-640.

Kobayashi, N. (1982). "Sediment transport on a gentle slope due to waves." J. Waterway, Port, Coastal, Ocean Eng., 108(3), 254–271.

Kobayashi, N. (1999). "Wave runup and overtopping on beaches and coastal structures." Advances in Coastal and Ocean Engineering, World Scientific, Singapore, 5, 95-154.

Kobayashi, N. (2009). "Documentation of cross-shore numerical model CSHORE 2009." Res. Rep. No. CACR-09-06, Center for Applied Coastal Research, Univ. of Delaware, Newark, DE.

Kobayashi, N. (2013). “Cross-shore numerical model CSHORE 2013 for sand beaches and coastal structures.” Res. Rep. No. CACR-13-01, Center for Applied Coastal Research, Univ. of Delaware, Newark, DE.

Kobayashi, N. (2016). “Coastal sediment transport modeling for engineering applications.” J. Waterway, Port, Coastal, Ocean Eng. 142 (6), 03116001.

Kobayashi, N., and de los Santos, F.J. (2007). “Irregular wave seepage and overtopping of permeable slopes.” J. Waterway, Port, Coastal, Ocean Eng., 133(4), 245-254.

Kobayashi, N., and Johnson, B.D. (2001). “Sand suspension, storage, advection, and settling in surf and swash zones.” J. Geophys. Res., 106, 9363-9376.

Kobayashi, N., and Jung, H. (2012). “Beach erosion and recovery.” J. Waterway, Port, Coastal, Ocean Eng., 138(6), 473-483.

Kobayashi, N., and Kim, H. D. (2017). “Rock seawall in the swash zone to reduce wave overtopping and overwash of a sand beach.” J. Waterway, Port, Coastal, Ocean Eng. 143(6): 04017033.

Kobayashi, N., and Otta, A.K. (1987). “Hydraulic stability analysis of armor units.” J. Waterway, Port, Coastal, Ocean Eng., 113(2), 171-186.

Kobayashi, N., and Tega, Y. (2002). “Sand suspension and transport on equilibrium beach.” J. Waterway, Port, Coastal, Ocean Eng., 128(6), 234-248.

Kobayashi, N., and Weitzner, H. (2015). “Erosion of a seaward dike slope by wave action.” J. Waterway, Port, Coastal, Ocean Eng., 141(2), 04014034.

Kobayashi, N., and Wurjanto, A. (1990). “Numerical model for waves on rough permeable slopes.” J. Coastal Res., SI(7), 149-166.

Kobayashi, N., and Wurjanto, A. (1992). “Irregular wave setup and run-up on beaches.” J. Waterway, Port, Coastal, Ocean Eng., 118(4), 368-386.

Kobayashi, N., and Zhu, T. (2017). “Bay flooding through tidal inlet and by wave overtopping of barrier beach.” J. Waterway, Port, Coastal, Ocean Eng. 143(5): 04017024.

Kobayashi, N., and Zhu, T. (2020). “Erosion by wave action of consolidated cohesive bottom containing cohesionless sediment.” J. Waterway, Port, Coastal, Ocean Eng. 146(2): 04019041.

Kobayashi, N., Agarwal, A., and Johnson, B.D. (2007a). “Longshore current and sediment transport on beaches.” J. Waterway, Port, Coastal, Ocean Eng., 133(4), 296-304.

Kobayashi, N., Buck, M., Payo, A., and Johnson, B.D. (2009a). “Berm and dune erosion during a storm.” J. Waterway, Port, Coastal, Ocean Eng., 135(1), 1-10.

Kobayashi, N., de los Santos, F.J., and Kearney, P.G. (2008a). “Time-averaged probabilistic model for irregular wave runup on permeable slopes.” J. Waterway, Port, Coastal, Ocean Eng., 134(2), 88-96.

Kobayashi, N., DeSilva, G.S., and Watson, K.D. (1989). “Wave transformation and swash oscillation on gentle and steep slopes.” J. Geophys. Res., 94(C1), 951-966.

Kobayashi, N., Farhadzadeh, A., and Melby, J.A. (2010a). “Wave overtopping and damage progression of stone armor layer.” J. Waterway, Port, Coastal, Ocean Eng., 136(5), 257-265.

Kobayashi, N., Farhadzadeh, A., Melby, J., Johnson, B., and Gravens, M. (2010b). “Wave overtopping of levees and overwash of dunes.” J. Coastal Res., 26(5), 888-900.

Kobayashi, N., Gralher, C, and Do, K. (2013a). “Effects of woody plants on dune erosion and overwash.” J. Waterway, Port, Coastal, Ocean Eng., 139(6), 466-472.

Kobayashi, N., Herrman, M.N., Johnson, B.D., and Orzech, M.D. (1998). “Probability distribution of surface elevation in surf and swash zones.” J. Waterway, Port, Coastal, Ocean Eng., 124(3), 99-107.

Kobayashi, N., Hicks, B.S., and Figlus, J. (2011). “Evolution of gravel beach profiles.” J. Waterway, Port, Coastal, Ocean Eng., 137(5), 258-262.

Kobayashi, N., Meigs, L.E., Ota, T., and Melby, J.A. (2007b). “Irregular breaking wave transmission over

submerged porous breakwater." J. Waterway, Port, Coastal, Ocean Eng., 133(2), 104-116.

Kobayashi, N., Payo, A., and Johnson, B.D. (2009b). "Suspended sand and bedload transport on beaches." Handbook of Coastal and Ocean Engineering, World Scientific, Singapore, Chapter 28, 807-823.

Kobayashi, N., Payo, A., and Schmied, L. (2008b). "Cross-shore suspended sand and bedload transport on beaches." J. Geophys. Res., 113, C07001, doi:10.1029/2007JC004203.

Kobayashi, N., Pietropaolo, J.A., and Melby, J.A. (2013b). "Wave transformation and runup on dikes and gentle slopes." J. Coastal Research, 29(3),615-623.

Kobayashi, N., Pietropaolo, J.A., and Melby, J.A. (2013c). "Deformation of reef breakwaters and wave transmission." J. Waterway, Port, Coastal, Ocean Eng., 139(4), July 1, 336-340.

Kobayashi, N., Pozueta, B., and Melby, J.A. (2003). "Performance of coastal structures against sequences of hurricanes." J. Waterway, Port, Coastal, Ocean Eng., 129(5), 219-228.

Kobayashi, N., Raichle, A., and Asano, T. (1993). "Wave attenuation by vegetation." J. Waterway, Port, Coastal, Ocean Eng., 119(1), 30-48.

Kobayashi, N., Zhao, H., and Tega, Y. (2005). "Suspended sand transport in surf zones." J. Geophys. Res., 110, C12009, doi:10.1029/2004JC002853.

Kobayashi, N., Zhu, T., and Mallavarapu S. (2018). "Equilibrium beach profile with net cross-shore sand transport." J. Waterway, Port, Coastal, Ocean Eng. 144(6): 04018016.

Kramer, M., and Burcharth, H. (2003). "DELOS: Wave basin experiment final form: 3D stability tests at AAU." Rep. EVK-CT-2000-0004, Hydraulics and Coastal Engineering Group, Dept. of Civil Engineering, Aalborg Univ., Aalborg, Denmark.

Kriebel, D.L., and Dean, R.G. (1985). "Numerical simulation of time-dependent beach and dune erosion." Coastal. Eng., 9, 221-245.

Large, W.G., and Pond, S. (1981). "Open ocean momentum flux measurements in moderate to strong winds." J. Phys. Oceanography, 11, 324-336.

Lentz, S., Guza, R.T., Elgar, S., Feddersen, F., and Herbers, T.H.C. (1999). "Momentum balances on the North Carolina inner shelf." J. Geophys. Res., 104(C8), 18,205-18,226.

Losada, I.J., Lara, J.L., Guanche, R., and Gonzalez-Ondina, J.M. (2008). "Numerical analysis of wave overtopping of rubble mound breakwaters." Coastal Eng., 55, 47-62.

Madsen, O.S., and Grant, W.D. (1976). "Quantitative description of sediment transport by waves." Proc. 15th Coastal Engineering Conf., ASCE, Reston, Va., 1093-1112.

Madsen, O.S., Chisholm, T.A., and Wright, L.D. (1994). "Suspended sediment transport in inner shelf waters during extreme storms." Proc. 24th Coastal Engineering Conf., ASCE, Reston, Va., 1849-1864.

Mase, H. (1989). "Random wave runup height on gentle slope." J. Waterway, Port, Coastal, Ocean Eng., 115(5), 649-661.

Masselink, G., Austin, M.J., O'Hare, T.J., and Russell, P.E. (2007). "Geometry and dynamics of wave ripples in the nearshore zone of a coarse sandy beach." J. Geophys. Res., 112, C10022, doi:10.1029/2006JC003839.

Mei, C.C. (1989). The applied dynamics of ocean surface waves. World Scientific, Singapore.

Melby, J.A., and Kobayashi, N. (1998). "Progression and variability of damage on rubble mound breakwaters." J. Waterway, Port, Coastal, Ocean Eng., 124(6), 286-294.

Melby, J.A., and Kobayashi, N. (2011). "Stone armor damage initiation and progression based on maximum momentum flux." J. Coastal Res., 27(1), 110-119.

Melby, J.A., Nadal-Caraballo, N.C., and Kobayashi, N. (2012). "Wave runup prediction for flood mapping." Proc. 32nd Coastal Eng. Conf., Management 79, 1-15.

Miranda, P.S., and Kobayashi, N. (2022). "Numerical modeling of intertidal mudflat evolution under waves and currents." Coastal Eng. J. (accepted).

Nairn, R.B., and Southgate, H.N. (1993). "Deterministic profile modeling of nearshore processes. Part 2. Sediment transport and beach profile development." Coastal Eng., 19, 57-96.

Neves, M.G., Reis, M.T., Losada, I.J., and Hu, K. (2008). "Wave overtopping of Póvoa de Varzim breakwater: Physical and numerical simulations." J. Waterway, Port, Coastal, Ocean Eng., 134(4), 226-236.

Norton, P.A., and Holmes, P. (1992). "Armor displacements on reshaping breakwaters." Proc. 23rd Coastal Engineering Conf., ASCE, Reston, Va., 1448-1460.

Ota, T., Kobayashi, N., and Kimura, A. (2006). "Irregular wave transformation over deforming submerged breakwater." Proc., 30th Coastal Engineering Conf., World Scientific, Singapore, 4945-4956.

Payo, A., Kobayashi, N., and Yamada, F. (2009). "Suspended sand transport along pier depression." J. Waterway, Port, Coastal, Ocean Eng., 135(5), 245-249.

Phillips, O.M. (1977). The dynamics of the upper ocean. Cambridge Univ. Press, Cambridge, U.K.

Powell, M.D., Vickery, P.J., and Reinhold, T.A. (2003). "Reduced drag coefficient for high wind speeds in tropical cyclones." Nature, 422, 279-283.

Press, W.H., Flannery, B.P., Teukolsky, S.A., and Vettering, W.T. (1989). Numerical recipes. The art of scientific computing. Cambridge Univ. Press, New York, NY.

Quan, R., and Kobayashi, N. (2015). "Pile fence to reduce wave overtopping and overwash of dune." J. Waterway, Port, Coastal, Ocean Eng., 141(6), 04015005.

Ribberink, J.S. (1998). "Bed-load transport for steady flow and unsteady oscillatory flows." Coastal Eng., 34, 59-82.

Ribberink, J.S., and Al-Salem, A.A. (1994). "Sediment transport in oscillatory boundary layers in cases of rippled beds and sheet flow." J. Geophys. Res., 99, 12,707-12,727.

Roelvink, D., Reniers, A., Van Dongeren, A.P., De Vries, J.V.T., McCall, R., and Lescinski, J. (2009). "Modelling storm impacts on beaches, dunes and barrier islands." Coastal Eng., 56(11-12), 1133-1152.

Ruessink, B.G., Miles, J.R., Feddersen, F., Guza, R.T., and Elgar, S. (2001). "Modeling the alongshore current on barred beaches." J. Geophys. Res., 106(C10), 22,451-22,463.

Saitoh, T., and Kobayashi, N. (2012). "Wave transformation and crossshore sediment transport on sloping beach in front of vertical wall." J. Coastal Res., 28(2), 354-359.

Seymour, R., Guza, R.T., O'Reilly, W., and Elgar, S. (2005). "Rapid erosion of a small southern California beach fill." Coastal Eng., 52, 151-158.

Shi, F., Kirby, J.T., and Hanes, D.M. (2007). "An efficient model-splitting method for a curvilinear nearshore circulation model." Coastal Eng., 54, 811-824.

Shi, F., Johnson, B., and Kobayashi, N. (2008). "2DH modeling of waves, currents and sediment transport at FRF during Hurricane Isabel." 2008 Ocean Sciences Meeting, American Geophysical Union, Orlando, Florida.

Skafel, M.G. 1995. "Laboratory measurement of nearshore velocities and erosion of cohesive sediment (till) shorelines." Coastal Eng. 24 (3-4): 343-349.

Smith, G.M., Seijffert, J.W.W., and Van der Meer, J.W. (1994). "Erosion and overtopping of a grass dike: large scale model tests." Coastal Eng. Proc., 24(1994), 2639-2652.

Smith, J.M., Sherlock, A.R., and Resio, D.T. (2001). "STWAVE: Steady-state spectral wave model user's manual for STWAVE, version 3.0." ERDC/CHL SR-01-1, Coastal and Hydraulics Laboratory, US Army Corps of Engineers, Vicksburg, Miss.

Schüttrumpf, H., and Oumeraci, H. (2005). "Layer thickness and velocities of wave overtopping flow at seadikes." Coastal Eng., 52, 473-495.

Steendam, G. J., Provoost, Y., and van der Meer, J. (2012). "Destructive wave overtopping and wave run-up tests on grass covered slopes of real dikes." Coastal Eng. Proc., 33(2012), 1-14.

Steendam, G. J., van der Meer, J., Hardeman, B., and van Hoven, A. (2010). “Destructive wave overtopping tests on grass covered landward slopes of dikes and transitions to berms.” Coastal Eng. Proc., 32(2010), 1-14.

Svendsen, I.A., Haas, K., and Zhao, Q. (2002). “Quasi-3D nearshore circulation model SHORECIRC version 2.0.” Res. Rep. No. CACR-02-01, Center for Applied Coastal Research, Univ. of Delaware, Newark, Del.

Tega, Y. and Kobayashi, N. (1996). “Wave overwash of subaerial dunes.” Proc. 25th Coastal Engineering Conf., ASCE, Reston, Va., 4148-4160.

Thornton, E.G., Humiston, R.T., and Birkemeier, W. (1996). “Bar/trough generation on a natural beach.” J. Geophys. Res., 101, 12,097-12,110.

Tørum, A. (1989). “Wave forces on pile in surface zone.” J. Waterway, Port, Coastal, Ocean Eng., 115(4), 547-565.

Trowbridge, J., and Young, D. (1989). “Sand transport by unbroken water waves under sheet flow conditions.” J. Geophys. Res., 94, 10,971-10,991.

van Gent, M.R.A. (1995). “Porous flow through rubble-mound material.” J. Waterway, Port, Coastal, Ocean Eng., 121(3), 176-181.

van Gent, M.R.A. (2001). “Wave runup on dikes with shallow foreshores.” J. Waterway, Port, Coastal, Ocean Eng., 127(5), 254-262.

van Gent, M.R.A. (2002a). “Wave overtopping events at dikes.” Proc. 28th Coastal Engineering Conf., World Scientific, Singapore, 2203-2215.

van Gent, M.R.A. (2002b). “Low-exceedance wave overtopping events: Measurements of velocities and the thickness of water-layers on the crest and inner slope of dikes.” Delft Cluster Report DC030202/H3803, Delft Hydraulics, Delft, The Netherlands.

van Gent, M.R.A., Coeveld, E.M., Walstra, D.J.R., van de Graaff, J., Steetzel, H.J., and Boers, M. (2006). “Dune erosion tests to study the influence of wave periods.” Proc. 30th Coastal Engineering Conf., World Scientific, Singapore, 2779-2791.

van Rijn, L.C., Walstra, D.J.R., Grasmeijer, B., Sutherland, J., Pan, S., and Sierra, J.P. (2003). “The predictability of cross-shore bed evolution of sandy beaches at the time scale of storms and seasons using process-based Profile models.” Coastal Eng., 47, 295-327.

Vidal, C., and Mansard, E. P. D. (1995). “On the stability of reef breakwaters.” Tech. Rep., National Research Council of Canada, Ottawa.

Wolters, G., Nieuwenhuis, J. W., van der Meer, J., and Klein Breteler, M. (2008). “Large scale tests of boulder clay erosion at the Wieringermeer dike (Ijsselmeer).” Proc., 31st Coastal Engineering Conf., World Scientific, Singapore, 3263-3275.

Wurjanto, A., and Kobayashi, N. (1993). “Irregular wave reflection and runup on permeable slopes.” J. Waterway, Port, Coastal, Ocean Eng., 119(5), 537-557.

Yamada, F. and Kobayashi, N., (2004). “Annual variations of tide level and mudflat profile.” J. Waterway, Port, Coastal, Ocean Eng., 130(3), 119-126.

Yuksel, Z. T., and Kobayashi, N. (2020). “Comparison of revetment and sill in reducing shore erosion and wave overtopping.” J. Waterway, Port, Coastal, Ocean Eng., 146(1): 04019028.

Zhu, T., and Kobayashi, N. (2021a). “Modeling of soft cliff erosion by oblique breaking waves during a storm.” J. Waterway, Port, Coastal, Ocean Eng., 147(4): 04021009.

Zhu, T., and Kobayashi, N. (2021b). “Rock mound to reduce wave overwash and crest lowering of a sand barrier.” Coastal Eng. J., 63(3), 1-13.

Appendix A Input and Output for Wave Overtopping of Barrier Beach

The input file (***infile***), output file (**ODOC**), and output figures of the cross-shore line L14 for the case of SandyPlus are shown in this Appendix as an example. The details refer to Kobayashi and Zhu (2017) and the CACR research report No. CACR-17-01, as explained concisely in Section 10.3.

A.1 Input file (*infile*)

Line14_500 year storm tide_infile — Monday, March 28, 2022

```
3                                                       --> NLINES
------------------------------------------------------------
Line 14: 500-year Storm Tide
------------------------------------------------------------
1                                                       --> ILINE
0                                                       --> IQYDY
1                                                       --> IPROFL
0                                                       --> ISEDAV
0                                                       --> IPERM
1                                                       --> IOVER
1                                                       --> IWTRAN
0                                                       --> INFILT
0                                                       --> IWCINT
0                                                       --> IROLL
0                                                       --> IWIND
0                                                       --> ITIDE
0                                                       --> IVEG
0                                                       --> IHOUSE
0                                                       --> ITRACE
3.00                                                    --> DX
0.7000                                                  --> GAMMA
0.3300      0.0500      2.6000                          --> D50,WF,SG
0.0050      0.0100      0.2000      0.1000              --> EFFB,EFFF,SLP,SLPOT
0.6300      0.0020                                      --> TANPHI,BLP
0.1000                                                  --> RWH
1                                                       --> ILAB
72                                                      --> NWAVE
72                                                      --> NSURGE
3600.0      13.2200     1.8102      0.0000      0.3090      36.3800
7200.0      13.1300     1.8526      0.0000      0.2960      35.3800
10800.0     12.9800     1.8950      0.0000      0.4180      34.3800
14400.0     12.7400     1.9375      0.0000      0.6680      33.3800
18000.0     12.3000     1.9940      0.0000      0.9620      32.3800
21600.0     12.1900     2.0365      0.0000      1.3180      32.3800
    .           .           .           .           .           .
    .           .           .           .           .           .      } 72 lines
    .           .           .           .           .           .
241200.0    9.0500      2.2981      0.0000      0.4150      68.3800
244800.0    9.0200      2.2840      0.0000      0.7390      69.3800
248400.0    9.1100      2.2274      0.0000      0.9680      69.3800
252000.0    10.8100     2.1213      0.0000      1.0130      68.3800
255600.0    10.9400     2.0011      0.0000      0.9930      67.3800
259200.0    10.9700     1.8880      0.0000      0.7910      66.3800
300                                                     --> NBINP
    0.00    -20.0000        0.020
10901.87    -12.1350        0.020
10909.98    -12.1820        0.020
10918.08    -12.2300        0.020
10926.19    -12.2770        0.020
10934.29    -12.3240        0.020
    .           .           .
    .           .           .       } 300 lines
    .           .           .
13276.48     -1.1220        0.020
13284.58     -1.1490        0.020
13292.69     -1.1750        0.020
13300.79     -1.2010        0.020
13308.90     -1.2280        0.020
13317.00     -1.2540        0.020
0                                                       --> ISWLSL
```

A.2 Output file (ODOC)


```
 2022 CSHORE: Tingting ; 2022 January 1
 ---------------------------------------------------------------
 Line 14: 500-year Storm Tide
 ---------------------------------------------------------------
COMPUTATION OPTION ILINE=  1
Alongshore gradient IQYDY=  0
ILINE cross-shore lines are computed together

COMPUTATION OPTION IPROFL =  1
Profile evolution is computed from Time = 0.0
to Time =      259200.0  for NTIME =   72

NO ROLLER is included in computation

NO wave and current interaction included

WAVE OVERTOPPING, OVERFLOW AND SEEPAGE
Runup wire height (m)               RWH=    0.100
Initial crest location for L=1      JCREST=  4208
Initial crest height (m) for L=1    RCREST=    3.262
Swash velocity parameter            AWD=    1.600
Output exceedance probability       EWD=    0.015

IMPERMEABLE BOTTOM assumed

NO wind shear stresses included

NO vegetation in computation domain


BREAKER RATIO PARAMETER
Input Gamma = 0.70

SEDIMENT PARAMETERS if IPROFL=1
Median diameter (mm)                D50=       0.33
Fall velocity (m/s)                  Wf=    0.0500
Specific gravity                     Sg=    2.60
Suspension efficiency                eB=    0.005
Suspended load parameter               =    0.20
Tangent(friction angle)                =    0.63
Bedload parameter                     b=    0.0020
Susp.load para. (IOVER=1)              =    0.10


INPUT WAVE AND WATER LEVEL:NTIME=    72 from TIME=0.0
Output lines are limited to first and last    10 lines
End Time(sec) Tp (sec)  Hrms(m) Wave Setup(m)Storm tide(m) ANGLE(deg)

      3600.0    13.2200     1.8102     0.0000     0.3090    36.3800
      7200.0    13.1300     1.8526     0.0000     0.2960    35.3800
     10800.0    12.9800     1.8950     0.0000     0.4180    34.3800
     14400.0    12.7400     1.9375     0.0000     0.6680    33.3800
     18000.0    12.3000     1.9940     0.0000     0.9620    32.3800
     21600.0    12.1900     2.0365     0.0000     1.3180    32.3800
     25200.0    12.2200     2.0718     0.0000     1.5770    32.3800
     28800.0    12.3400     2.1001     0.0000     1.7170    34.3800
     32400.0    12.5000     2.1355     0.0000     1.7190    35.3800
     36000.0    12.7200     2.1708     0.0000     1.5530    36.3800
    226800.0     9.0600     2.4254     0.0000    -0.0760    67.3800
    230400.0     9.1000     2.3900     0.0000    -0.1440    67.3800
    234000.0     9.1200     2.3476     0.0000    -0.0390    67.3800
    237600.0     9.1000     2.3193     0.0000     0.1680    67.3800
    241200.0     9.0500     2.2981     0.0000     0.4150    68.3800
    244800.0     9.0200     2.2840     0.0000     0.7390    69.3800
```

```
    248400.0     9.1100     2.2274     0.0000     0.9680    69.3800
    252000.0    10.8100     2.1213     0.0000     1.0130    68.3800
    255600.0    10.9400     2.0011     0.0000     0.9930    67.3800
    259200.0    10.9700     1.8880     0.0000     0.7910    66.3800

 INPUT BEACH AND STRUCTURE GEOMETRY
 Cross-shore line number                    L=     1
 Alongshore coordinate                  YLINE=          0.0000
 Line angle(degrees)                   AGLINE=          0.0000
 Depth at seaward boundary (m)              =       20.000000
 Number of input points                 NBINP=        300
 Output lines are limited to first and last 5 lines
 Node spacing (m)                         DX=          3.000000
 Shoreline location (m) of Zb=0           Xs=     12546.896838
 Maximum landward node                  JMAX=     4440

 X  (m)       Zb  (m)  Fric.factor  Wire mesh
      0.000   -20.000
  10901.870   -12.135      0.020
  10909.980   -12.182      0.020
  10918.080   -12.230      0.020
  10926.190   -12.277      0.020
  13284.580    -1.149      0.020
  13292.690    -1.175      0.020
  13300.790    -1.201      0.020
  13308.900    -1.228      0.020
  13317.000    -1.254      0.020

 INPUT LANDWARD STILL WATER LEVEL for IWTRAN=1 and ISWLSL=0
 same as input seaward still water level


 **********COMPUTED CROSS-SHORE VARIATIONS**********
 on bottom profile computed at TIME (s) =      3600.0  Line L=  1

 LANDWARD WET COMPUTATION LIMIT
 Most landward node of wet zone computation    JR=     4185
 X-coordinate at JR (m)                        XR=    12552.000000
 Bottom elevation at JR (m)                    ZR=        0.592532
 Mean water depth at this node (m)          H(JR)=        0.252789

 COMBINED WAVE OVERTOPPING AND OVERFLOW
 Still water level above Z=0 (m)              SWL=        0.309000
 Cross-shore line number                        L=     1
 Structure or dune crest elevation (m)      RCREST=        3.261521
 Node number at SWL                           JSWL=     4185
 Wet and dry transition node                   JWD=     4185
 Mean water depth H1(m) at node JWD             H1=        0.224204
 End node of wet and dry zone                 JDRY=     4206
 Wave overtopping probability at JCREST       POTF=        0.000000
 Comb. overtopping and overflow rate(m*m/s)   QOTF=     0.000000000
 Seepage rate(m*m/s) at JCREST                  QP=     0.000000000
 Total rate (QOTF+QP)(m*m/s)                     =     0.000000000
 QO iteration number                         ITEQO=     1

 EMPIRICAL WAVE RUNUP
 Cross-shore line number                        L=     1
 Swash zone bottome slope                   SLPRUN=        0.133246
 Mean runup elevation above Z=0 (m)         ERMEAN=        0.865136
 Runup standard deviation (m)               SIGRUN=        0.316352
 Significant runup height above Z=0 (m)        R13=        2.131475
 2 percent runup height above Z=0 (m)          R2P=        2.638011
 1 Percent runup height above z=0 (m)          R1P=        2.789972
```

```
Line14_500 year storm tide_ODOC                                  Monday, March 28, 2022
  129   WAVE TRANSMISSION DUE TO OVERTOPPING
  130   Cross-shore line number                          L=     1
  131   Starting node for wave transmission            JSL=     4336
  132   X-coordinate (m) at node JSL                    XB=    13005.000000
  133   Wave setup (m) above SWL at node JSL         WSETUP=       0.000000
  134   Standard deviation (m) at node JSL           SIGMA=        0.000000
  135   X-coordinate (m) at landward end node JMAX       =    13317.000000
  136   Wave setup (m) above SWL at landward end node JMAX=       0.000000
  137   Standard dev. (m) at landward end node JMAX      =        0.000000
  138   Wave transmission coefficient at JMAX            =        0.000000
  139
  140   LONGSHORE SUSPENDED AND BEDLOAD SAND TRANSPORT RATE
  141   Transport Rate (m**3/s) =    0.98809E-01
  142   CERC Formula K=       0.073
  143   sin(breaker angle)=     0.59314
  144
  145
  146   Computed Cross-shore Varations for TIME=7200.0-259200.0 are omitted.
```


A.3 Output figures

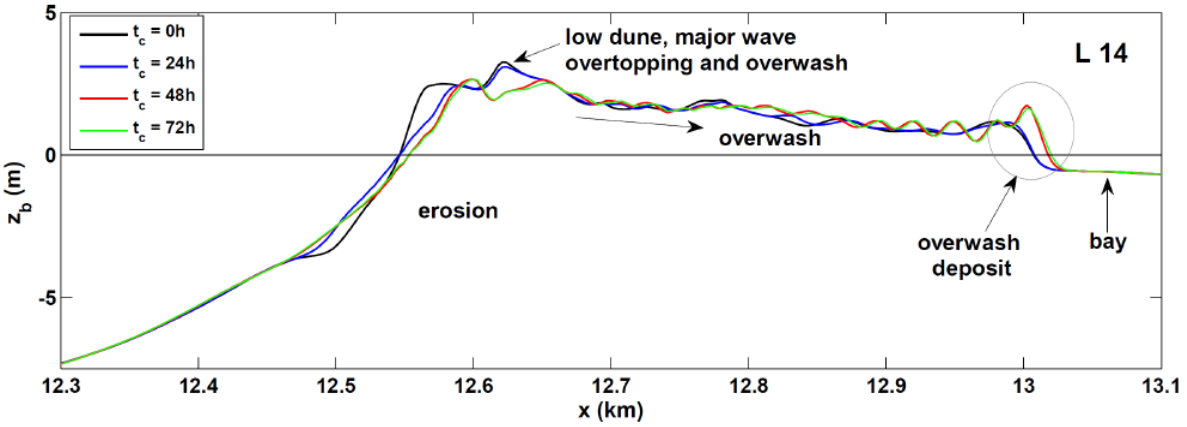

Figure A.1 Initial (t_c = 0) and computed beach profiles at computation time t_c = 24, 48, and 72 h along cross-shore line L14 for Hurricane Sandy. [Results from the file **OBPROF**].

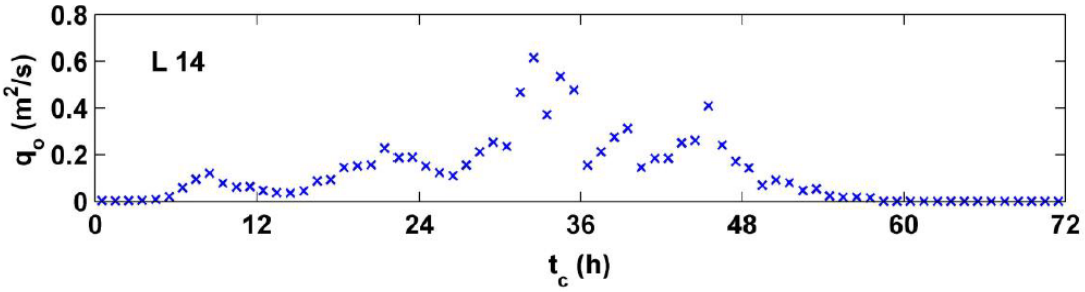

Figure A.2 Computed temporal variation of hourly wave overtopping rate q_o per unit width along cross-shore line L14 for SandyPlus. [Results from the file **OTIMSE**].

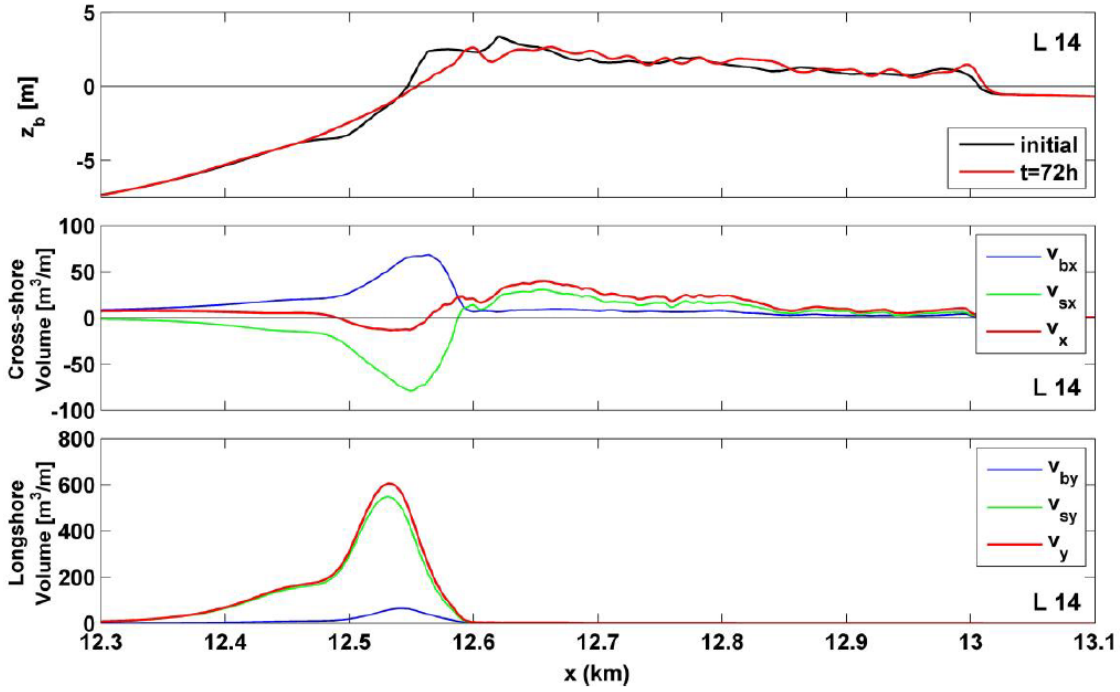

Figure A.3 Initial and final profiles z_b, cumulative cross-shore sand transport volumes v_{bx}, v_{sx}, and v_x per unit width and cumulative longshore sand transport volumes v_{by}, v_{sy}, and v_y per unit width along cross-shore line L14 for SandyPlus. [Results from the files **OBPROF**, **OCRVOL**, and **OLVOL**, respectively].

Appendix B Input and Output for Consolidated Cohesive Bottom Erosion

The input files (***infile***) and output figures for S75 and S85 tests are shown in this Appendix as examples. The details refer to Kobayashi and Zhu (2020) and the CACR research report No. CACR-19-01, as explained concisely in Section 10.2.

B.1 Input file (Infile)

Skafel 75 cm_infile — Monday, March 28, 2022

```
3                                                       --> NLINES
-----------------------------------------------------------
Skafel(1995): 0.75m water depth; GAMMA=0.7; fb=0.0034; Rc=30
-----------------------------------------------------------
1                                                       --> ILINE
0                                                       --> IQYDY
1                                                       --> IPROFL
1                                                       --> ISEDAV
0                                                       --> IPERM
1                                                       --> IOVER
0                                                       --> IWTRAN
0                                                       --> IPOND
0                                                       --> INFILT
0                                                       --> IWCINT
1                                                       --> IROLL
0                                                       --> IWIND
0                                                       --> ITIDE
0                                                       --> IVEG
0                                                       --> IHOUSE
1                                                       --> ICLAY
0                                                       --> ITRACE
0.02                                                    --> DX
0.7000                                                  --> GAMMA
0.5100      0.0730      2.6000                          --> D50,WF,SG
0.0050      0.0100      0.2000      3.3000              --> EFFB,EFFF,SLP,SLPOT
0.6300      0.0020                                      --> TANPHI,BLP
0.0200                                                  --> RWH
0.0002      0.0100                                      --> DEEB,DEEF
1                                                       --> ILAB
4                                                       --> NWAVE
4                                                       --> NSURGE
3600        3.1000      0.1838      0.0000   0.0000     0.0000
36000       3.1000      0.1838      0.0000   0.0000     0.0000
54000       3.1000      0.1838      0.0000   0.0000     0.0000
108000      3.1000      0.1838      0.0000   0.0000     0.0000
436                                                     --> NBINP
436                                                     --> NPINP
0.00    -0.7500     0.0034   ┐
2.54    -0.4105     0.0034   │
2.56    -0.4099     0.0034   │
2.58    -0.4073     0.0034   │
  .         .         .      ├ 436 lines
  .         .         .      │
  .         .         .      │
11.18    0.1519     0.0034   │
11.20    0.1518     0.0034   │
13.60    0.6000     0.0034   ┘
2.54    -0.4105     1000.0      0.0000   ┐
2.56    -0.4099     1000.0      0.0000   │
2.58    -0.4073     1000.0      0.0000   │
2.60    -0.4054     1000.0      0.0000   │
2.62    -0.4031       30.0      0.2100   │
2.64    -0.4009       30.0      0.2100   │
  .         .         .           .      │
  .         .         .           .      ├ 435 lines
9.16    -0.0629       30.0      0.2100   │
9.18    -0.0620       30.0      0.2100   │
9.20    -0.0612     1000.0      0.0000   │
9.22    -0.0605     1000.0      0.0000   │
  .         .         .           .      │
  .         .         .           .      │
11.20    0.1518     1000.0      0.0000   │
13.60    0.6000     1000.0      0.0000   ┘
```

```
3                                                       --> NLINES
-------------------------------------------------------------
Skafel(1995):0.85m water depth; GAMMA=0.7; fb=0.0034; Rc=30
-------------------------------------------------------------
1                                                       --> ILINE
0                                                       --> IQYDY
1                                                       --> IPROFL
1                                                       --> ISEDAV
0                                                       --> IPERM
1                                                       --> IOVER
0                                                       --> IWTRAN
0                                                       --> IPOND
0                                                       --> INFILT
0                                                       --> IWCINT
1                                                       --> IROLL
0                                                       --> IWIND
0                                                       --> ITIDE
0                                                       --> IVEG
0                                                       --> IHOUSE
1                                                       --> ICLAY
0                                                       --> ITRACE
0.02                                                    --> DX
0.7000                                                  --> GAMMA
0.5100      0.0730      2.6000                          --> D50,WF,SG
0.0050      0.0100      0.2000      3.3000              --> EFFB,EFFF,SLP,SLPOT
0.6300      0.0020                                      --> TANPHI,BLP
0.0200                                                  --> RWH
0.0002      0.0100                                      --> DEEB,DEEF
1                                                       --> ILAB
4                                                       --> NWAVE
4                                                       --> NSURGE
3600        3.1000      0.1838      0.0000   0.0000     0.0000
36000       3.1000      0.1838      0.0000   0.0000     0.0000
54000       3.1000      0.1838      0.0000   0.0000     0.0000
108000      3.1000      0.1838      0.0000   0.0000     0.0000
436                                                     --> NBINP
436                                                     --> NPINP
0.00    -0.8500     0.0034   ┐
2.54    -0.5105     0.0034   │
2.56    -0.5099     0.0034   │
2.58    -0.5073     0.0034   │
  .         .         .      ├ 436 lines
  .         .         .      │
11.18    0.0519     0.0034   │
11.20    0.0518     0.0034   │
13.60    0.5000     0.0034   ┘
2.54    -0.5105     1000.0      0.0000   ┐
2.56    -0.5099     1000.0      0.0000   │
2.58    -0.5073     1000.0      0.0000   │
2.60    -0.5054     1000.0      0.0000   │
2.62    -0.5031       30.0      0.2100   │
2.64    -0.5009       30.0      0.2100   │
  .         .         .           .      │
  .         .         .           .      ├ 435 lines
10.42    0.0112       30.0      0.2100   │
10.44    0.0146       30.0      0.2100   │
10.46    0.0177     1000.0      0.0000   │
10.48    0.0201     1000.0      0.0000   │
  .         .         .           .      │
  .         .         .           .      │
11.20    0.0518     1000.0      0.0000   │
13.60    0.5000     1000.0      0.0000   ┘
```

B.2 Output figures

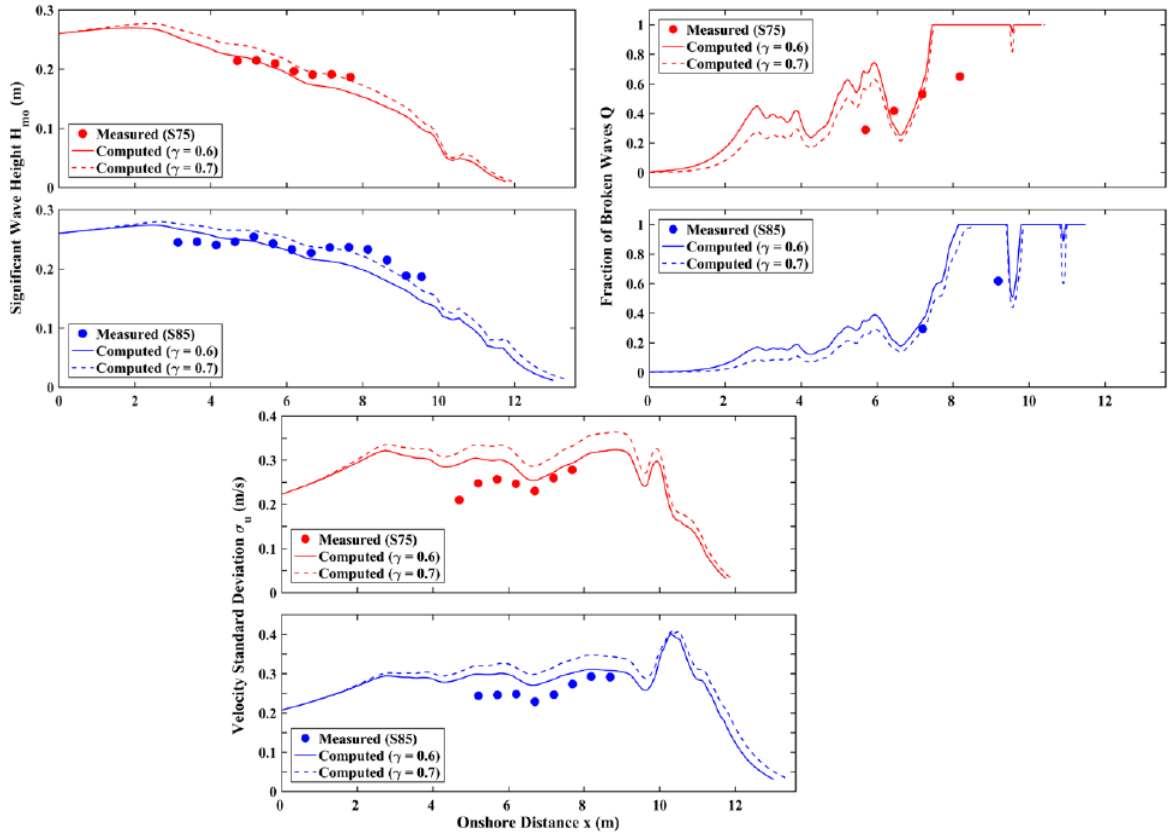

Figure B.1 Measured and computed (γ = 0.6 and 0.7, t = 1 h) significant wave height H_{mo}, fraction of broken waves Q, and velocity standard deviation σ_u for S75 and S85 tests. [Results from the files **OSETUP**, **OPARAM**, and **OXVELO**, respectively].

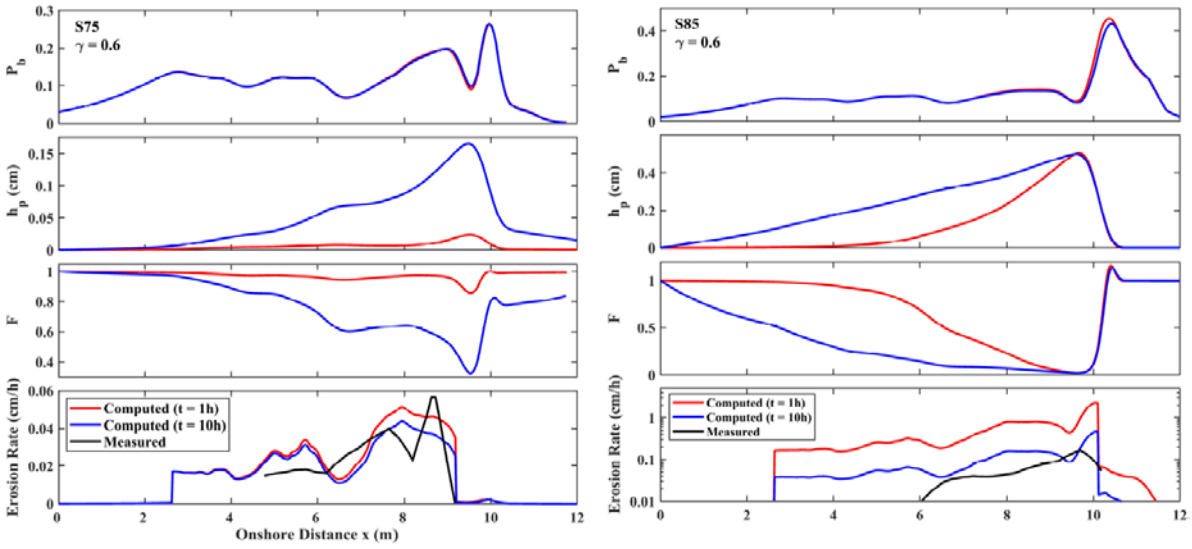

Figure B.2 Computed (t = 1 h and 10 h, γ = 0.6) sand movement probability P_b, sand layer thickness h_p, abrasion and protection function F, and measured and computed erosion rates for S75 and S85 tests. [Results from the files **OBSUSL**, **OBPROF**, and **ODIKER**, respectively].

Appendix C Input and Output for Soft Cliff Erosion

The input files (***infile***) and output figures for four cases are shown in this Appendix: Test 5 with IQYDY=0 and 1 (neglecting or including the alongshore gradient of the longshore sediment transport rate), and Test 16 with ICLAY=0 and 1 (absence or presence of clay). The details refer to Zhu and Kobayashi (2021a) and the CACR research report No. CACR-19-05, as explained concisely in Section 10.2.

C.1 Input file (*infile*)

Damgaard_Test5_IQYDY0_infile Monday, March 28, 2022

```
3                                                       --> NLINES
------------------------------------------------------------
Damgarrd (1999): Test 5, Tp, dx=0.02, IQYDY=0
------------------------------------------------------------
1                                                       --> ILINE
0                                                       --> IQYDY
1                                                       --> IPROFL
1                                                       --> ISEDAV
0                                                       --> IPERM
1                                                       --> IOVER
0                                                       --> IWTRAN
0                                                       --> IPOND
0                                                       --> INFILT
0                                                       --> IWCINT
1                                                       --> IROLL
0                                                       --> IWIND
0                                                       --> ITIDE
0                                                       --> IVEG
0                                                       --> IHOUSE
0                                                       --> ICLAY
0                                                       --> ITRACE
0.02                                                    --> DX
0.6000                                                  --> GAMMA
0.2330      0.0280      2.6400                          --> D50,WF,SG
0.0050      0.0100      0.2000      3.3000              --> EFFB,EFFF,SLP,SLPOT
0.6300      0.0020                                      --> TANPHI,BLP
0.0100                                                  --> RWH
1                                                       --> ILAB
30                                                      --> NWAVE
30                                                      --> NSURGE
360     1.4400      0.0672      0.0000      0.0000      30.0000
720     1.4400      0.0672      0.0000      0.0000      30.0000
1080    1.4400      0.0672      0.0000      0.0000      30.0000
1440    1.4400      0.0672      0.0000      0.0000      30.0000
1800    1.4400      0.0672      0.0000      0.0000      30.0000
2160    1.4400      0.0672      0.0000      0.0000      30.0000
  .       .           .           .           .           .        } 30 lines
  .       .           .           .           .           .
  .       .           .           .           .           .
9360    1.4400      0.0672      0.0000      0.0000      30.0000
9720    1.4400      0.0672      0.0000      0.0000      30.0000
10080   1.4400      0.0672      0.0000      0.0000      30.0000
10440   1.4400      0.0672      0.0000      0.0000      30.0000
10800   1.4400      0.0672      0.0000      0.0000      30.0000
4                                                       --> NBINP
4                                                       --> NPINP
0.00    -0.38
7.00    -0.18   0.02
7.80     0.22   0.02
9.03     0.22   0.02
7.00    -0.18
9.02    -0.18
9.03     0.22
```

```
3                                                       --> NLINES
-------------------------------------------------------------
Damgarrd (1999): Test 5, dx=0.02, IQYDY=1, ye=10
-------------------------------------------------------------
1                                                       --> ILINE
1                                                       --> IQYDY
1                                                       --> IPROFL
1                                                       --> ISEDAV
0                                                       --> IPERM
1                                                       --> IOVER
0                                                       --> IWTRAN
0                                                       --> IPOND
0                                                       --> INFILT
0                                                       --> IWCINT
1                                                       --> IROLL
0                                                       --> IWIND
0                                                       --> ITIDE
0                                                       --> IVEG
0                                                       --> IHOUSE
0                                                       --> ICLAY
0                                                       --> ITRACE
0.02                                                    --> DX
0.6000                                                  --> GAMMA
0.2330      0.0280      2.6400                          --> D50,WF,SG
0.0050      0.0100      0.2000      3.3000              --> EFFB,EFFF,SLP,SLPOT
0.6300      0.0020                                      --> TANPHI,BLP
0.0100                                                  --> RWH
1                                                       --> ILAB
30                                                      --> NWAVE
30                                                      --> NSURGE
360     1.4400      0.0672      0.0000      0.0000      30.0000
720     1.4400      0.0672      0.0000      0.0000      30.0000
1080    1.4400      0.0672      0.0000      0.0000      30.0000
1440    1.4400      0.0672      0.0000      0.0000      30.0000
1800    1.4400      0.0672      0.0000      0.0000      30.0000
2160    1.4400      0.0672      0.0000      0.0000      30.0000
  .       .           .           .           .           .        } 30 lines
  .       .           .           .           .           .
  .       .           .           .           .           .
9360    1.4400      0.0672      0.0000      0.0000      30.0000
9720    1.4400      0.0672      0.0000      0.0000      30.0000
10080   1.4400      0.0672      0.0000      0.0000      30.0000
10440   1.4400      0.0672      0.0000      0.0000      30.0000
10800   1.4400      0.0672      0.0000      0.0000      30.0000
10                                                      --> YEADIS
4                                                       --> NBINP
4                                                       --> NPINP
0.00    -0.38
7.00    -0.18   0.02
7.80     0.22   0.02
9.03     0.22   0.02
7.00    -0.18
9.02    -0.18
9.03     0.22
```

```
3                                                       --> NLINES
-------------------------------------------------------------
Damgarrd (1999): Test 16, Tp, dx=0.02, IQYDY=1, ye=10, ICLAY=0
-------------------------------------------------------------
1                                                       --> ILINE
1                                                       --> IQYDY
1                                                       --> IPROFL
1                                                       --> ISEDAV
0                                                       --> IPERM
1                                                       --> IOVER
0                                                       --> IWTRAN
0                                                       --> IPOND
0                                                       --> INFILT
0                                                       --> IWCINT
1                                                       --> IROLL
0                                                       --> IWIND
0                                                       --> ITIDE
0                                                       --> IVEG
0                                                       --> IHOUSE
0                                                       --> ICLAY
0                                                       --> ITRACE
0.02                                                    --> DX
0.6000                                                  --> GAMMA
0.2330      0.0280      2.6400                          --> D50,WF,SG
0.0050      0.0100      0.2000      3.3000              --> EFFB,EFFF,SLP,SLPOT
0.6300      0.0020                                      --> TANPHI,BLP
0.0100                                                  --> RWH
1                                                       --> ILAB
30                                                      --> NWAVE
30                                                      --> NSURGE
360     1.4400      0.0672      0.0000      0.0000      30.0000
720     1.4400      0.0672      0.0000      0.0000      30.0000
1080    1.4400      0.0672      0.0000      0.0000      30.0000
1440    1.4400      0.0672      0.0000      0.0000      30.0000
1800    1.4400      0.0672      0.0000      0.0000      30.0000
2160    1.4400      0.0672      0.0000      0.0000      30.0000
  .       .           .           .           .           .        } 30 lines
  .       .           .           .           .           .
  .       .           .           .           .           .
9360    1.4400      0.0672      0.0000      0.0000      30.0000
9720    1.4400      0.0672      0.0000      0.0000      30.0000
10080   1.4400      0.0672      0.0000      0.0000      30.0000
10440   1.4400      0.0672      0.0000      0.0000      30.0000
10800   1.4400      0.0672      0.0000      0.0000      30.0000
10                                                      --> YEADIS
4                                                       --> NBINP
4                                                       --> NPINP
0.00    -0.38
7.00    -0.18   0.02
7.80     0.22   0.02
9.03     0.22   0.02
7.00    -0.18
9.02    -0.18
9.03     0.22
```

```
3                                                       --> NLINES
-------------------------------------------------------------
Damgarrd(1999): Test 16,IQYDY=1,ye=10,ICLAY=1,Rc=1,fc=0.545
-------------------------------------------------------------
1                                                       --> ILINE
1                                                       --> IQYDY
1                                                       --> IPROFL
1                                                       --> ISEDAV
0                                                       --> IPERM
1                                                       --> IOVER
0                                                       --> IWTRAN
0                                                       --> IPOND
0                                                       --> INFILT
0                                                       --> IWCINT
1                                                       --> IROLL
0                                                       --> IWIND
0                                                       --> ITIDE
0                                                       --> IVEG
0                                                       --> IHOUSE
1                                                       --> ICLAY
0                                                       --> ITRACE
0.02                                                    --> DX
0.6000                                                  --> GAMMA
0.2330      0.0280      2.6400                          --> D50,WF,SG
0.0050      0.0100      0.2000      3.3000              --> EFFB,EFFF,SLP,SLPOT
0.6300      0.0020                                      --> TANPHI,BLP
0.0100                                                  --> RWH
0.0002      0.0100                                      --> DEEB,DEEF
1                                                       --> ILAB
30                                                      --> NWAVE
30                                                      --> NSURGE
360     1.4400      0.0672      0.0000      0.0000      30.0000
720     1.4400      0.0672      0.0000      0.0000      30.0000
1080    1.4400      0.0672      0.0000      0.0000      30.0000
1440    1.4400      0.0672      0.0000      0.0000      30.0000
1800    1.4400      0.0672      0.0000      0.0000      30.0000
2160    1.4400      0.0672      0.0000      0.0000      30.0000
  .       .           .           .           .           .        } 30 lines
  .       .           .           .           .           .
  .       .           .           .           .           .
9360    1.4400      0.0672      0.0000      0.0000      30.0000
9720    1.4400      0.0672      0.0000      0.0000      30.0000
10080   1.4400      0.0672      0.0000      0.0000      30.0000
10440   1.4400      0.0672      0.0000      0.0000      30.0000
10800   1.4400      0.0672      0.0000      0.0000      30.0000
10                                                      --> YEADIS
4                                                       --> NBINP
4                                                       --> NPINP
0.00    -0.38
7.00    -0.18   0.02
7.80     0.22   0.02
9.03     0.22   0.02
7.00    -0.18   1000    0.0
7.80     0.22   1   0.545
9.03     0.22   1   0.545
```

C.2 Output figures

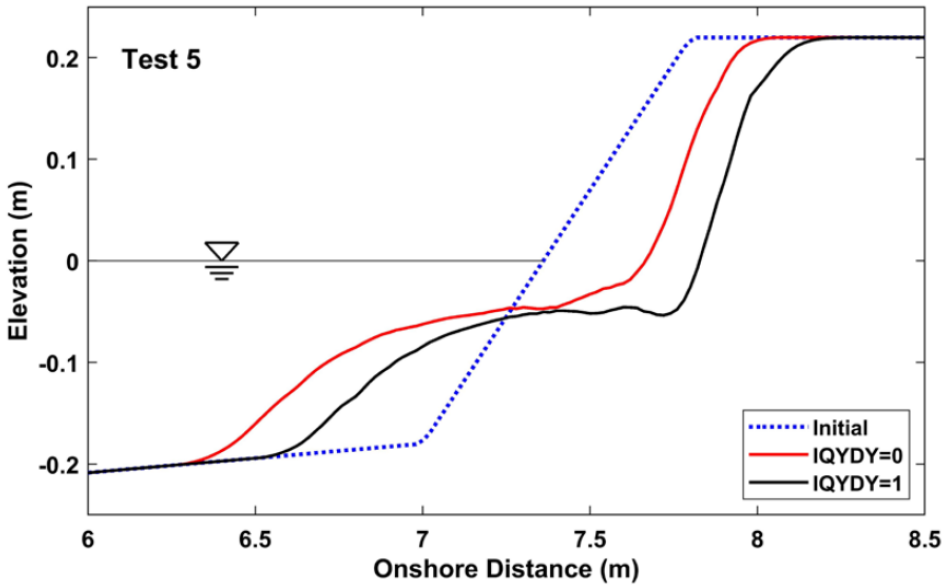

Figure C.1 Initial profile and computed profile of IQYDY=0 and 1 at time t = 3 h for Test 5 (oblique wave angle α = 30°). [Results from the file **OBPROF**].

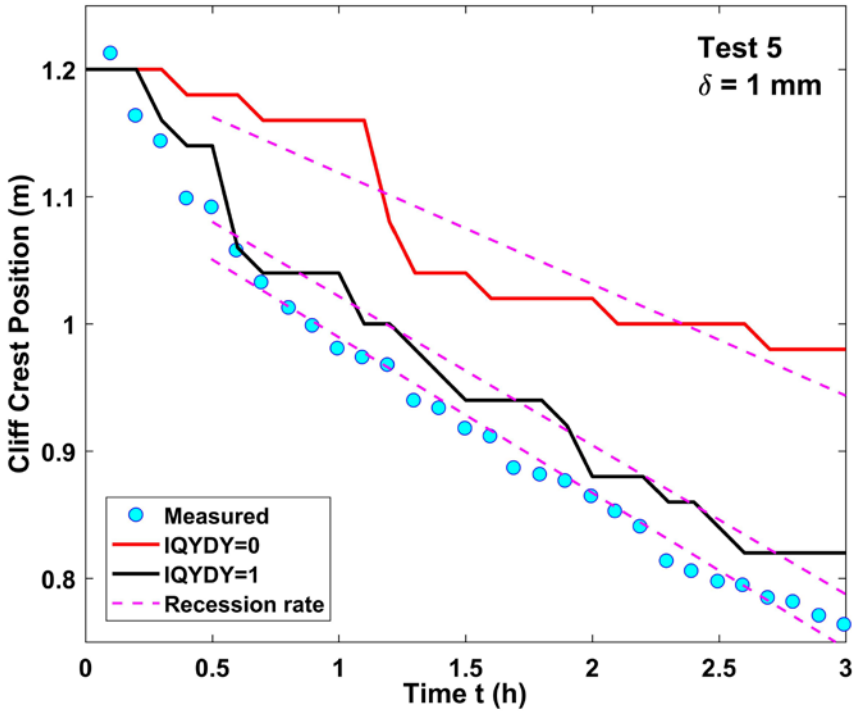

Figure C.2 Measured cliff crest position during Test 5 in comparison with computed positions (δ = 1 mm) for IQYDY=0 and IQYDY=1 with equivalent longshore distance y_e = 10 m. [Results analyzed based on the file **OBPROF**].

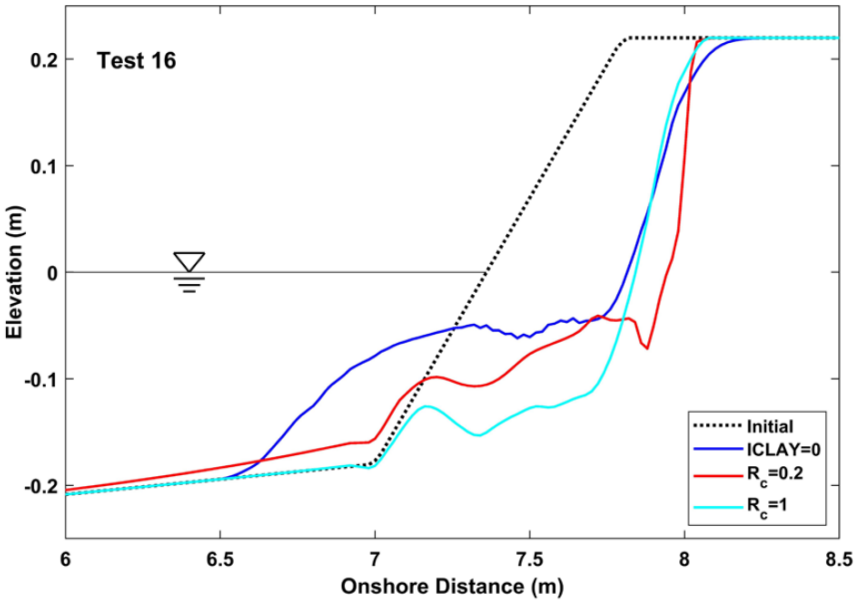

Figure C.3 Initial and computed sand profiles z_b at t = 3 h for Test 16 with ICLAY=0 (no clay) and ICLAY=1 (sand/clay mixture and erosion resistance parameter R_c = 0.2 and 1 m^2/s^2) . [Results from the file **OBPROF**].

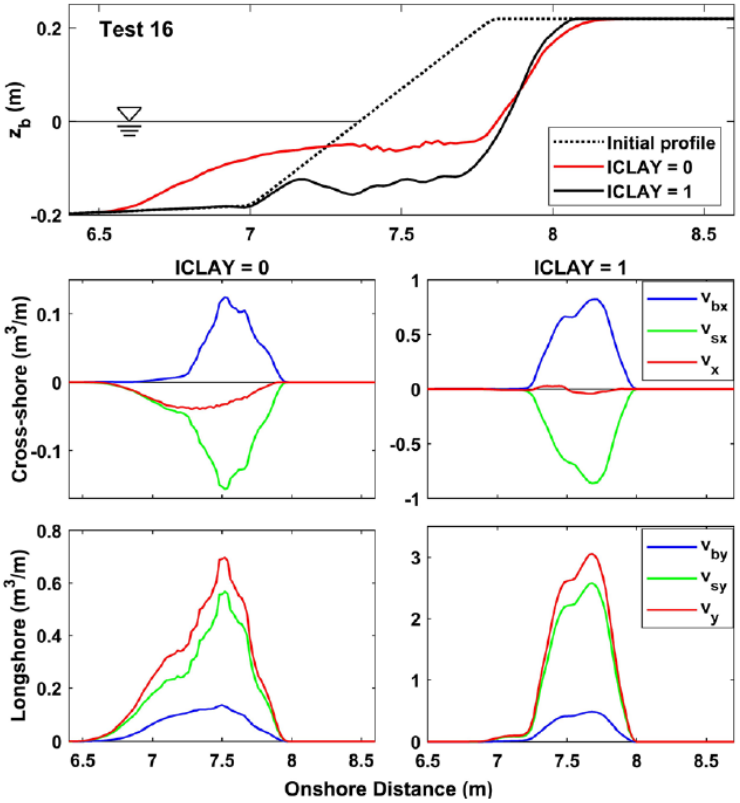

Figure C.4 Comparison of computed sand profiles, cumulative cross-shore and longshore sand transport volumes at t = 3 h for Test 16 with ICLAY=0 and ICLAY=1 (R_c = 1 m^2/s^2) . [Results from the files **OBPROF**, **OCRVOL**, and **OLVOL**, respectively].

Appendix D Input and Output for Rock Mound on Sand Barrier

The input file (***infile***) and output figures for Test R are shown in this Appendix as an example. The details refer to Zhu and Kobayashi (2021b) and the CACR research report No. CACR-21-01, as explained concisely in Section 10.4.

D.1 Input file (Infile)

Test R_infile Monday, March 28, 2022

```
3                                                          --> NLINES
------------------------------------------------------------
Rock mound (R) test: IWTRAN=1,ISWLSL=1,SLPOT=1.8,BLP=0.01
------------------------------------------------------------
1                                                          --> ILINE
0                                                          --> IQYDY
1                                                          --> IPROFL
0                                                          --> ISEDAV
1                                                          --> IPERM
1                                                          --> IOVER
1                                                          --> IWTRAN
0                                                          --> IWCINT
1                                                          --> IROLL
0                                                          --> IWIND
0                                                          --> ITIDE
0                                                          --> IVEG
0                                                          --> IHOUSE
1                                                          --> ISTSAN
0                                                          --> IFTLTR
0                                                          --> ITRACE
0.02                                                       --> DX
0.6000                                                     --> GAMMA
0.1800      0.0200      2.6000                             --> D50,WF,SG
0.0050      0.0100      0.2000      1.8000                 --> EFFB,EFFF,SLP,SLPOT
0.6300      0.0100                                         --> TANPHI,BLP
0.0200                                                     --> RWH
0.4400      0.0365      0.7000                             --> SNP,SDP,CSTABN
1                                                          --> ILAB
30                                                         --> NWAVE
30                                                         --> NSURGE
400     2.6200      0.1387      -0.0034     0.0000      0.0000
800     2.6200      0.1400      -0.0040     0.0000      0.0000
1200    2.6200      0.1417      -0.0036     0.0000      0.0000
  .       .           .           .           .           .      } 30 lines
  .       .           .           .           .           .
11200   2.6200      0.1426      -0.0040     0.0000      0.0000
11600   2.6200      0.1420      -0.0040     0.0000      0.0000
12000   2.6200      0.1418      -0.0041     0.0000      0.0000
931                                                        --> NBINP
931                                                        --> NPINP
0.00    -0.8300
0.02    -0.8280     0.015
0.04    -0.8260     0.015
  .       .           .     } 931 lines
  .       .           .
18.58   -0.1813     0.015
18.60   -0.1813     0.015
0.02    -0.8280
0.04    -0.8260
  .       .       } 930 lines
  .       .
18.58   -0.1813
18.60   -0.1813
1                                                          --> ISWLSL
30                                                         --> NSLAN
0       0.0000
400     0.0287
800     0.0310
  .       .       } 30 lines
  .       .
11200   0.0376
11600   0.0382
12000   0.0382
```

D.2 Output figures

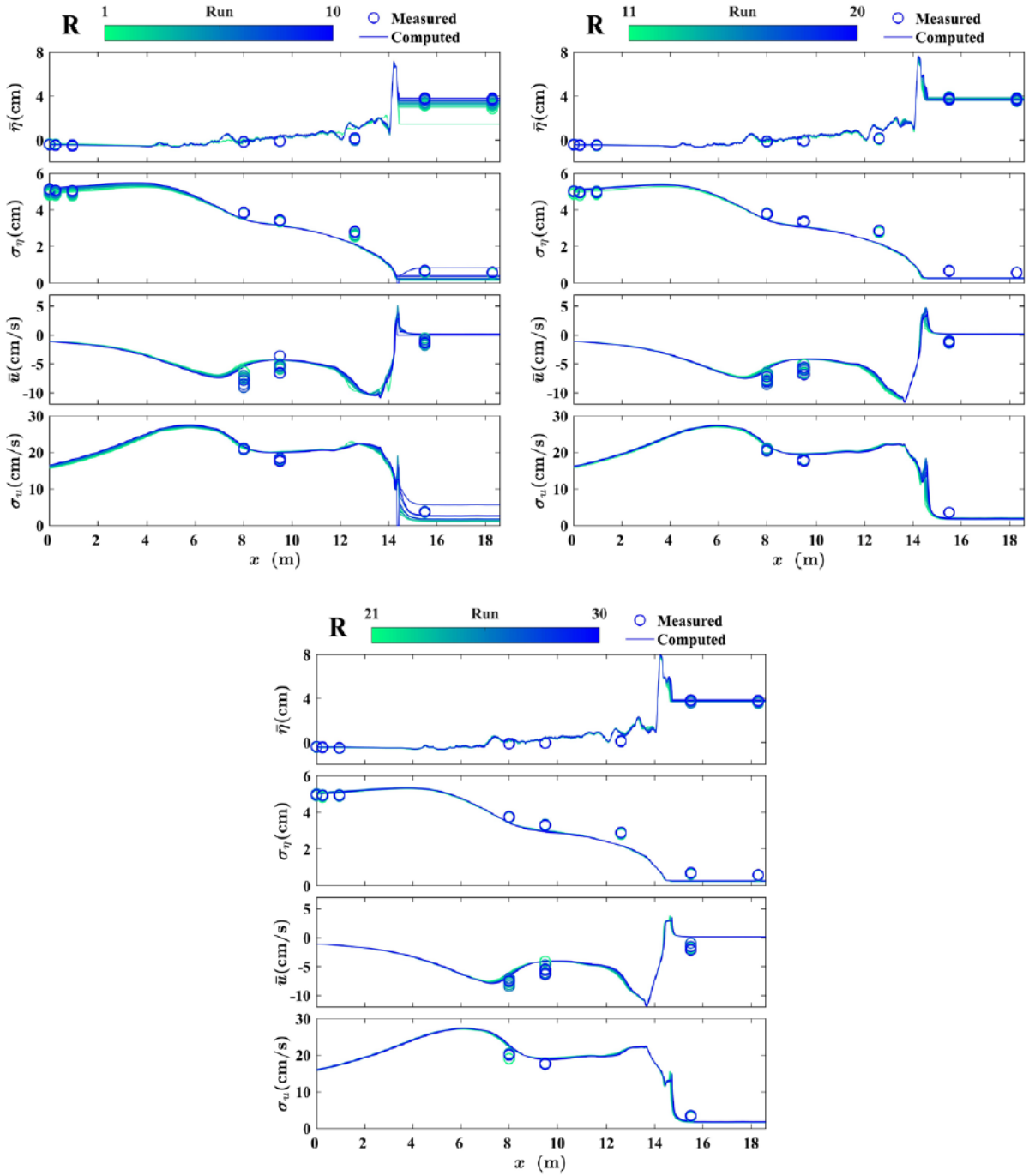

Figure D.1 Computed and measured mean and standard deviation of free surface elevation η and cross-shore velocity u for 30 runs in Test R. [Results from the files **OSETUP** and **OXVELO**, respectively].